UNIVERSITY OF BIRMINGHAM

DESIGN, SYNTHESIS, AND REACTIVITY OF A BORON-BASED LEWIS SUPERACID: A COMBINED COMPUTATIONAL AND EXPERIMENTAL STUDY

by

KIMBERLEY ELLIS

A thesis submitted to the University of Birmingham for the degree of

MSC BY RESEARCH

School of Chemistry

College of Engineering and Physical Sciences

University of Birmingham

August 2024

ABSTRACT

In today's chemical industry, many organic transformations rely on the employment of catalysts to enhance reaction performance and provide pathways to products that may be otherwise inaccessible without providing large quantities of thermal energy. Unfortunately, these catalysts often consist of scarcely abundant transition metals which pose environmental concerns. Given this, there has been a paradigm shift towards more sustainable regimes that focus on utilising the Lewis acidity of *p*-block elements, such as those that sit in group III of the periodic table. In particular, boron-centred complexes are of wide interest to many organometallic chemists. The seminal innovation of the Lewis acid *tris*(pentafluorophenyl)borane in the 1960s paved the way for the burgeoning field of Lewis superacids that far surpass the activity of classic antimony pentafluoride and as such, these superacids are being investigated for their catalytic properties. This thesis will focus on the background of these unique compounds, the measurement of them against well-established forerunners and detail the development and testing of a novel Lewis superacidic borane through computational and experimental means.

ACKNOWLEDGEMENTS

I would like to acknowledge the University of Birmingham for allowing me to carry out this project by providing DTP funding. All works pertaining to this project are my own aside from the Fluoride Ion Affinity and Hydride Ion Affinity calculations for the novel borane which were performed by Dr Andrew Jupp.

DEDICATIONS

I dedicate this thesis to all of the people who have made this project and my time at UoB as enjoyable as it has been. Firstly, thanks goes to Dr Andrew Jupp for his supervision and guidance throughout this project. The time and patience taken to introduce me into an unfamiliar field is very much appreciated. I really liked his “no such thing as a stupid question” policy although I feel I definitely put that to the test a couple of times when my mouth overtook my brain occasionally.

Next, credit goes to Dr Laura English who spent many long days with me helping me become a competent Schlenk line chemist as well providing a supporting shoulder to cry on when things inevitably got frustrating. I owe her more than a few pints for the above and definitely for bringing us all baked goods in as often as she did. Her unparalleled baking skills still continue to amaze me – although I appreciate her beating me at various board games a lot less!

To Emma Jordan, Alastair Littlewood and Ethan Calder – it’s been a blast working alongside them. I have spent many hours talking rubbish (with them all politely listening to me) and I will miss the camaraderie we all have. Those daily crosswords and Wordles just aren’t the same on my own…I wish them all the best of luck with their theses and success in whatever they decide to pursue.

Thank you to the analytical staff, in particular Drs Louise Male, Christopher Williams and Cécile Le Duff who gave me training in the analytical techniques needed for my work. They were always very helpful and provided me with solutions when I couldn’t get one myself.

To my family - I think they are all glad that I’m finally getting a “real job”. We’ve had multiple jokes that they’re running out of formal wear for my graduations because I keep collecting degrees…On a serious note though, they have been the backbone of why I’ve been able to pursue higher education to such an extent. My parents and their dog George have an uncanny ability to cheer me up on a bad

day and encourage me to carry on so I can achieve my dreams. Even though I'm choosing to study medicine, which is quite a change from my original plans, they still remain supportive in whatever I choose to do. For that, I will be eternally grateful.

Last but not least, to my partner Jake Richard. I'm not sure I can entirely summarise how I feel about the kindness, love and support I've felt from him. The constant laughing at silly things and unwavering patience has really helped keep me afloat. I do however want to apologise for the amount of money he spent on buying coffee so I could finish all of my work…it'll all be worth it when I eventually become rich and famous from my zany ideas.

Although I'm sad to be leaving UoB, I will always remember the people in the chemistry department who became my friends over the last 2 years. There's something to be said about the closeness and strange humour you develop with people when undertaking a research degree. Our Friday night pub tradition will be one I'll keep with me, and I hope our paths will continue to cross in the future.

I'll end this with one of my favourite quotes that's pretty reflective of my experience in research so far; "*Dude, sucking at something is the first step towards being good at something*".

TABLE OF CONTENTS

1. LEWIS ACIDS 1

1.1 Introduction 1

1.1.1 Applications within catalysis 2

1.1.2 Small molecule activation by Frustrated Lewis Pairs 8

1.1.3 Computational studies of small molecule activation mechanisms 11

1.2 Measuring Lewis acidity 12

1.2.1 Substituent effects on Lewis acidity 13

1.2.2 Fluoride ion affinity 15

1.2.3 Other methods 17

1.3 Lewis superacids 19

1.3.1 Boron-based Lewis superacids 21

1.3.2 Catalytic applications 22

2. AIMS 26

3. COMPUTATIONAL RESULTS AND DISCUSSION 27

3.1 DFT studies 27

3.1.1 Exploring adduct and FLP formation 30

3.1.2 Activation of H_2 35

4. EXPERIMENTAL RESULTS AND DISCUSSION 39

4.1 Precursor synthesis 39

*4.1.1 Sodium 2-methyl-2-propanethiolate (**22**)* 40

*4.1.2 1,3-bis(tert-butylthio)-5-bromobenzene (**23**)* 41

*4.1.3 5-bromobenzene-1,3,-dithiol (**24**)* 43

4.2 Borane synthesis 44

4.2.1 Solution state reaction for tris[(3,5-bis(trifluoromethyl)phenyl]borane 44

4.2.2 Solid state reaction for tris[(3,5-bis(trifluoromethyl)phenyl]borane 45

*4.2.3 Tris[(3,5-bis(pentafluorosulfanyl)phenyl]borane (**1**)* 46

5. CONCLUSIONS AND FUTURE WORK **50**

6. EXPERIMENTAL **52**

6.1 Computational details 52

6.2 Materials and general experimental details 52

6.3 Precursor synthesis 53

*6.3.1 Sodium 2-methyl-2-propanethiolate (**22**)* 53

*6.3.2 5-bromobenzene-1,3-dithiol (**24**)* 55

6.4 Synthesis of Tris[3,5-bis(pentafluorosulfanyl)phenyl]borane (1) 56

6.4.1 Using $BF_3.OEt_2$ 56

6.4.2 Using BCl_3 (0.98 M in heptane) 57

7. REFERENCES **59**

8. APPENDIX **67**

8.1 Computational data 67

8.2 Experimental data 72

ABBREVIATIONS

AN	Acceptor-Number Scale
ASI-MS	Atmospheric Solid Ionisation-Mass Spectrometry
DFT	Density Functional Theory
EDA	Energy Decomposition Analysis
eLA	Effective Lewis acidity
FIA	Fluoride Ion Affinity
FLP	Frustrated Lewis Pair
GEI	Global Electrophilicity Index
gLA	Global Lewis Acidity
GLC	Gas-Liquid Chromatography
HF	Hartree-Fock
HIA	Hydride Ion Affinity
HOMO	Highest Occupied Molecular Orbital
ICR	Ion Cyclotron Resonance
iLA	Intrinsic Lewis Acidity
LUMO	Lowest Unoccupied Molecular Orbital
NBO	Natural Bonding Orbital
SIE	Self-Interaction Errors
TS	Transition State
WCA	Weakly Coordinating Anion

1. LEWIS ACIDS

1.1 Introduction

In 1923, physical chemist Gilbert. N. Lewis presented the notion of Lewis acids and Lewis bases.[1] The former refers to a molecular species with a vacant orbital capable of accepting an electron pair, while the latter describes a species that can donate an electron pair to form a dative bond. This interaction between the two forms a Lewis adduct as described in Figure 1.[2] In a general sense, both of these terms are often interchanged with electrophile and nucleophile. However, both electrophilicity and nucleophilicity emphasises the kinetic aspect of reactivity whereas Lewis acidity and basicity more specifically refer to the thermodynamic properties of Lewis adduct formation. Lewis acidity is formally defined by IUPAC as '*the thermodynamic tendency of a substance to act as a Lewis acid*'.[3] Lewis adduct formation is reversible; the stronger the Lewis acid, the more the equilibrium shifts towards forming an adduct with a Lewis base.

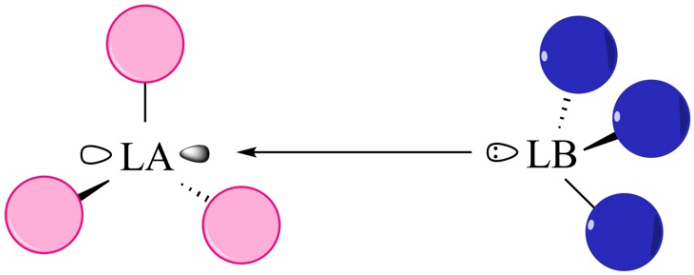

Figure 1. Donation of electron pair from Lewis base to empty *p*-orbital of Lewis acid to form a dative bond.

1.1.1 Applications within catalysis

Due to these chemical properties, Lewis acids can be used as catalysts. This involves the Lewis acid accepting electron donation from lone pair bearing atoms in substrates. Upon adduct formation, the electrophilicity of the substrate is increased due to partial charge transfer. This ultimately activates the substrate towards reactions such as nucleophilic attack, cycloaddition with 1,3-dienes and 1,3-dipoles and heterolytic bond cleavage (Scheme 1a). Notable examples of this chemistry includes the use of metal centres such as titanium, with one of the earliest reports by Teruaki *et al*. in 1973.[4] They introduced a water-stable titanium tetrachloride-mediated aldol reaction of trimethylsilyl enol ethers with ketones or aldehydes to give β-hydroxyketones. Equally, zinc and aluminium salts have been popular choices in facilitating asymmetric catalysis through the addition of enantiomerically pure ligands.[5] For instance, BINOL (1,1'-binaphthyl-2,2'-diol) coordinated to aluminium has been shown to catalyse the desymmetrising asymmetric ring expansion of cyclohexanones with α-Diazoacetates (Scheme 1b).[6]

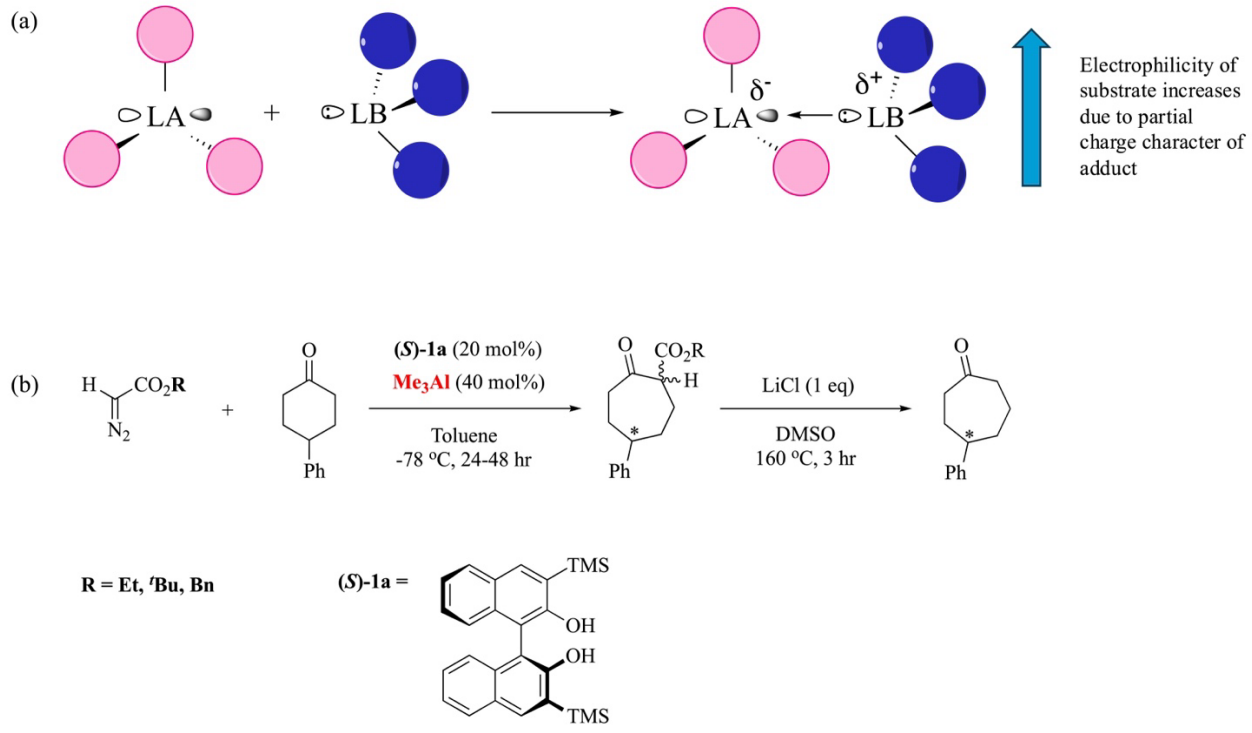

Scheme 1. (a) General scheme showing how Lewis acid catalysis works; (b) General reaction scheme for the desymmetrising asymmetric ring expansion of cyclohexanones with α-Diazoacetates. Lewis acid highlighted in red. Adapted from ref. 6.

Metalloids such as boron have also garnered significant interest with various boranes being applied within catalysis.[7, 8] One of the simplest examples are the archetypal boron trihalides, BX_3 (X = F, Cl, Br) whose vacant boron *p*-orbitals lie perpendicular to their trigonal planar structure. These are highly efficient at driving reactions forward; however, substantial drawbacks include moisture sensitivity and volatility, making them difficult to manipulate. This stimulated further research into derivatives with perfluoroalkyl boranes, $B(Rf)_3$ (Rf = perfluoroalkyl) being investigated in the 1950s.[9] The highly electronegative Rf ligand was expected to increase Lewis acidity on the tricoordinate boron centre and the B–C bonds were predicted to be less hydrolytically sensitive. Whilst this was true, perfluoroalkyl boranes are unfortunately thermally unstable owing to fluorine migration to boron with the elimination of a perfluoroalkene or difluorocarbene.[9] In 1964, Massey *et al*. shifted the focus to

halogenated triaryl boranes and published the synthesis of *tris*(pentafluorophenyl)borane ($B(C_6F_5)_3$).[10] Remarkable at the time, its Lewis acidity was reviewed several times but its capabilities remained largely unexplored until the 1980s where it was used by Naumann as a C_6F_5 transfer agent in the synthesis of pentafluorophenyl-xenon compounds (Scheme 2).[11]

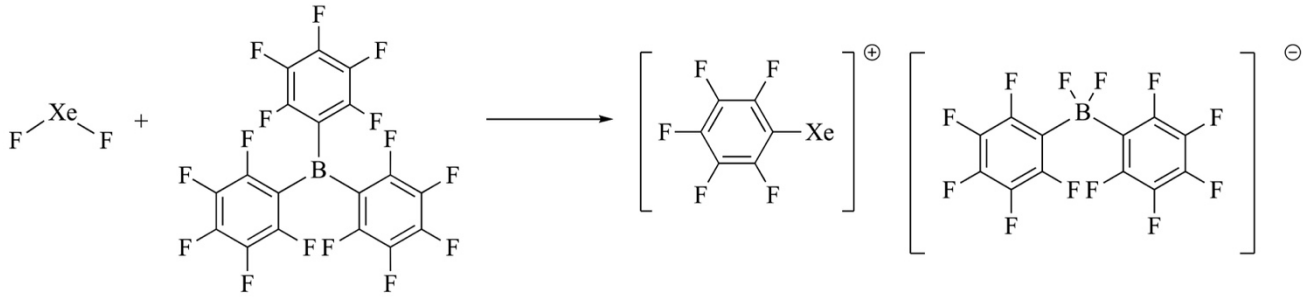

Scheme 2. Formation of pentafluorophenyl-xenon compounds using $B(C_6F_5)_3$. Adapted from ref. 11.

Since then, $B(C_6F_5)_3$ has returned to prominence with a notable example being when Marks *et al.* utilised it as a co-catalyst for the polymerisation of olefins with zirconocene alkyls.[12, 13] This area of chemistry was not new with species such as aluminium alkyls and methyl-aluminoxane being common Lewis acid components within zirconocene and titanocene catalysts.[13] Previous to this work, it was theorised that the role of the Lewis acid is to promote the formation of unsaturated active centres such as Cp_2MR^+, however the exact structural relationship between co-catalyst and catalyst remained elusive due to stability issues. The authors discovered that through using $B(C_6F_5)_3$, its strong Lewis acidic properties meant that it could abstract an alkyl group from the zirconocene alkyl complex which forms a cationic zirconocene species. Subsequently, they were able to isolate it and characterise it through x-ray crystallography for the first time.

Piers and co-workers then built upon that work and revealed that it could also catalyse the hydrosilylation of carbonyl compounds (Scheme 3).[14] Its Lewis acidity is comparable to that of BF_3

and BCl_3, however it offers the advantage of having stronger B–C and C–F bonds, making it easier to handle.

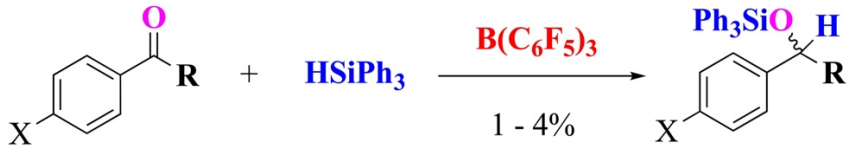

R = H, Me, OEt

Scheme 3. $B(C_6F_5)_3$-catalysed hydrosilylation of carbonyl compounds. Adapted from ref. 14.

When 1 equivalent of silane reagents with $B(C_6F_5)_3$ was used, the reaction proceeded with no side products. Isolated yields of up to 96% of hydrosilylated products were seen with over 90% selectivity for acetal products. When an ester was used (R = OMe), reduction happened rapidly with the subsequent acetal products being converted to aldehydes which were also obtained in significant yields. Kinetic experiments to determine the mechanism were performed quantitatively using Gas-Liquid Chromatography (GLC). Upon plotting ln[Ph_3SiH] against time, it was ascertained that the reaction was first order with respect to silane as the plots were linear. The expected mechanism based on dogma at the time was one whereby the carbonyl is activated by complexation with $B(C_6F_5)_3$ followed by reaction with silane to form the products (Scheme 4a).

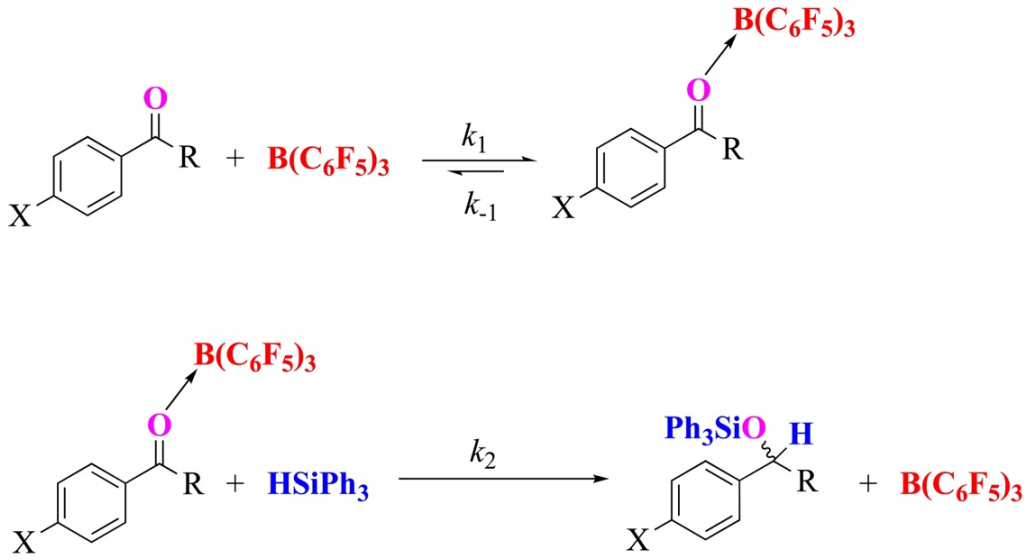

Scheme 4a. Activation of the carbonyl substrate by $B(C_6F_5)_3$ followed by addition of silane to form products. Adapted from ref. 14.

However, what was observed was the activation of the silane with $B(C_6F_5)_3$ and carbonyl in a concerted manner (Scheme 4b).

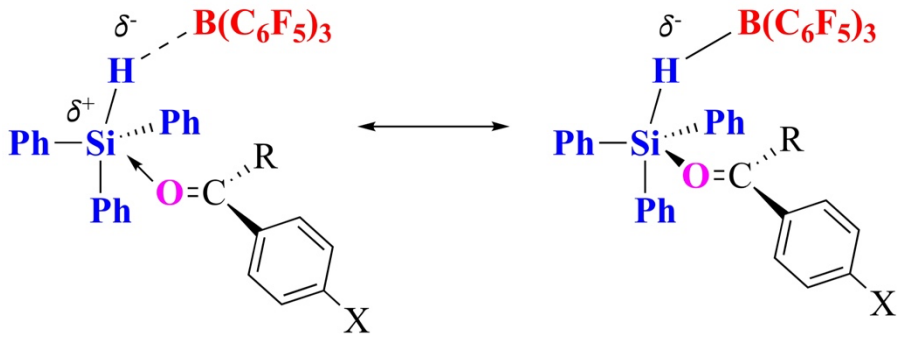

Scheme 4b. Reactivity between $B(C_6F_5)_3$ and carbonyl to activate the silane. Adapted from ref. 14.

These principle works then inspired investigations into $B(C_6F_5)_3$ derivatives for other applications, leading the same group to report the synthesis of $HB(C_6F_5)_2$ in 1995[15] and its hydroboration activities in 1998.[16] Previously hydroboration, a term which refers to the addition of a H–B bond to certain C–

C double and triple bonds, mostly relied upon the tetrahydrofuran (THF) adduct of BH_3 to facilitate the synthesis of organoboranes. Whilst this worked well, its applications were limited to simple substrates as more complex ones introduced regio- and diastereoselectivity issues. Upon synthesis of $HB(C_6F_5)_2$, Piers and co-workers sought to explore its application and found that it could be used in more challenging hydroboration transformations due to its high Lewis acidity induced by the electron-withdrawing C_6F_5 groups around the boron centre. This led to an increase in reaction rates compared to BH_3.THF and the elimination of regioselectivity issues as it favours anti-Markovnikov selectivity. It is also protected from dimerisation reactions, unlike BH_3 which can form diborane and undergo unwanted side reactions, as the C_6F_5 groups sterically hinder the boron atom. Aptly termed 'Piers' borane', this seminal discovery led to other researchers using this species in applications such as the dimerisation of arylallenes,[17] tetramerisation of arylacetylenes[18] and reactions with stable conjugated primary enamines to form 6-membered N,B heterocycles (Scheme 5).[19]

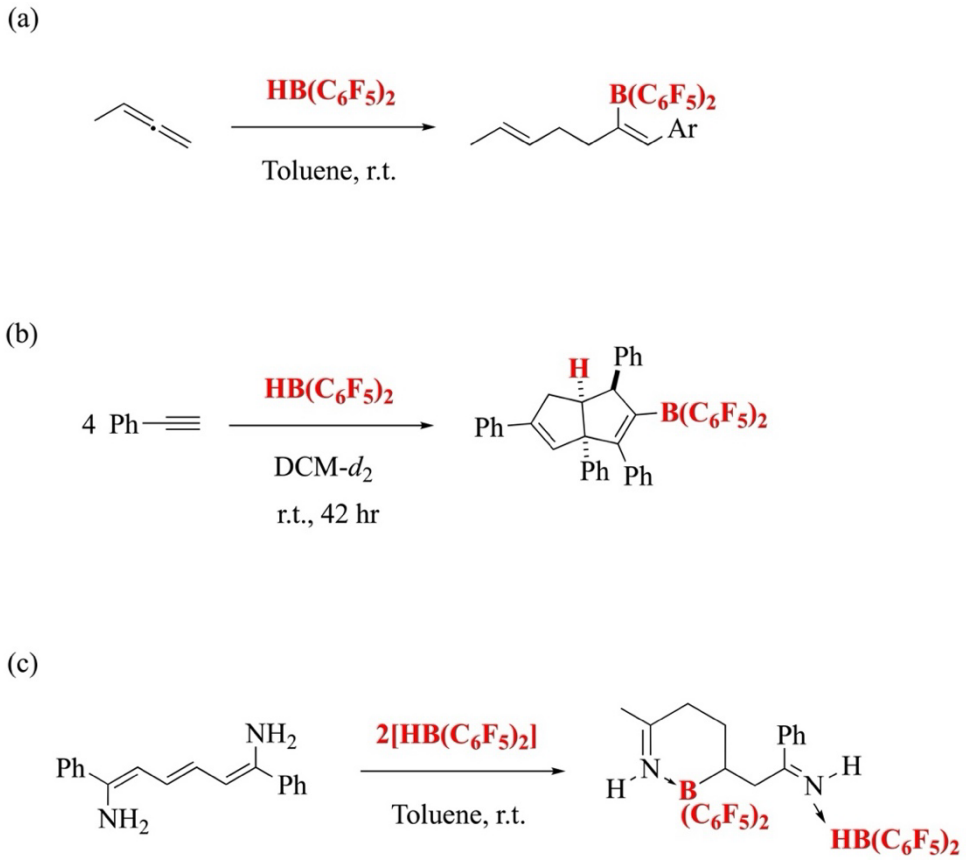

Scheme 5. (a) dimerisation of arylallenes; (b) tetramerisation of arylacetylenes; (c) formation of 6-membered heterocycles from conjugated primary amines. Adapted from refs. 17-19.

1.1.2 Small molecule activation by Frustrated Lewis Pairs

Intriguingly, if a Lewis acid and base pair possess enough steric bulk, they can form what is known as a Frustrated Lewis Pair (FLP). This term was introduced in 2007 by Stephan and co-workers[20] and the phenomenon can be observed when steric repulsion prevents formation of a typical Lewis adduct. Records suggest that the earliest example of an FLP was observed by Brown in 1942, who noted that a reaction occurred between BF_3 and lutidine but not between lutidine and BMe_3. This was attributed to the bulkier methyl groups of BMe_3 coinciding with lutidine's *ortho*-methyl groups.[21] This unique chemistry allows for transition metal-free splitting of small molecules, such as H_2, in a concerted fashion *via* an 'encounter complex' which is stabilised by dispersion interactions (Scheme 6).[22]

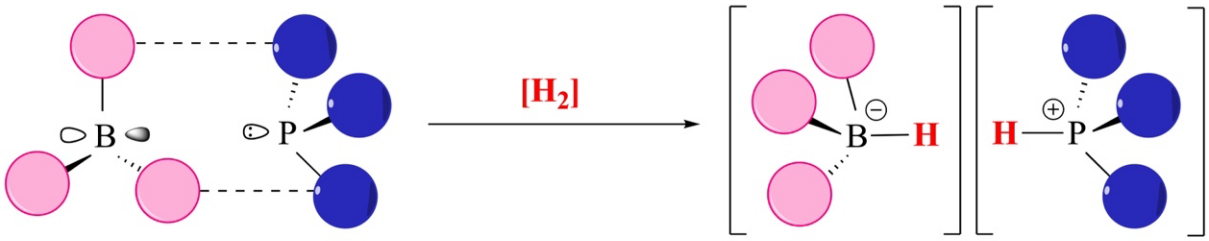

Scheme 6. Activation of H_2 by the encounter complex. Adapted from ref. 22.

In 2006, Stephan *et al.* demonstrated that H_2 could be cleanly cleaved using an intramolecular FLP system containing Lewis acidic boron and Lewis basic phosphorus (Scheme 7). They reported the facile uptake of H_2 by this system at only 25 °C with H_2 being released upon heating to over 100 °C allowing for re-uptake.[23]

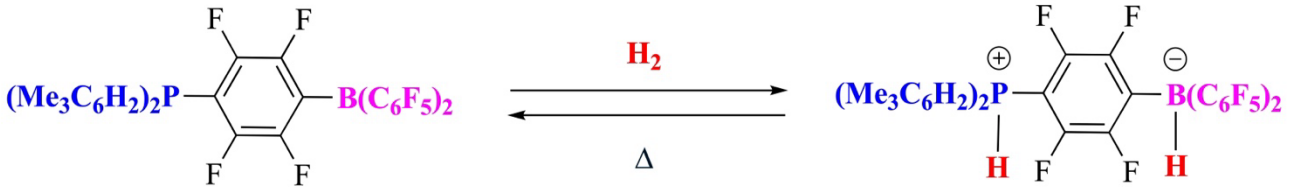

Scheme 7. Reaction between a phosphane borane FLP and H_2 to form a phosphonium borate. Adapted from ref. 23.

Whilst $B(C_6F_5)_3$ is well-known for its use within FLPs due to its bulk and high Lewis acidity (an early example including the aforementioned work by Piers and co-workers on the hydrosilylation of carbonyl compounds) research into other systems enabled new reactivity to be explored. A notable example is *tris*[3,5-bis(trifluoromethyl)phenyl]borane ($BArF_{18}$) presented by Ashley and co-workers.[24] The trifluoromethyl (CF_3) group is known to be one of the strongest electron-withdrawing groups, imparting increased stability and lipophilicity.[25, 26] Metal-halogen exchange with isopropyl magnesium chloride (^{i}PrMgCl) and 1-bromo-3,5-*bis*(trifluoromethyl)benzene generated the aryl Grignard reagent, which was subsequently reacted with boron trifluoride ($BF_3.OEt_2$) to produce

tris[3,5-bis(trifluoromethyl)phenyl]borane. This was determined to be a stronger Lewis acid than $B(C_6F_5)_3$ by Gutmann-Beckett measurements ($\Delta\delta$ $B(C_6F_5)_3$ = 26.6 ppm *vs.* $\Delta\delta$ $BArF_{18}$ = 78.9 ppm - see below for information on the Gutmann-Beckett method). Through reaction between *tris*[3,5-*bis*(trifluoromethyl)phenyl]borane, 2,2,6,6-tetramethylpiperidine (TMP) and H_2 (Scheme 8), they were able to demonstrate the heterolytic splitting of H_2.[27]

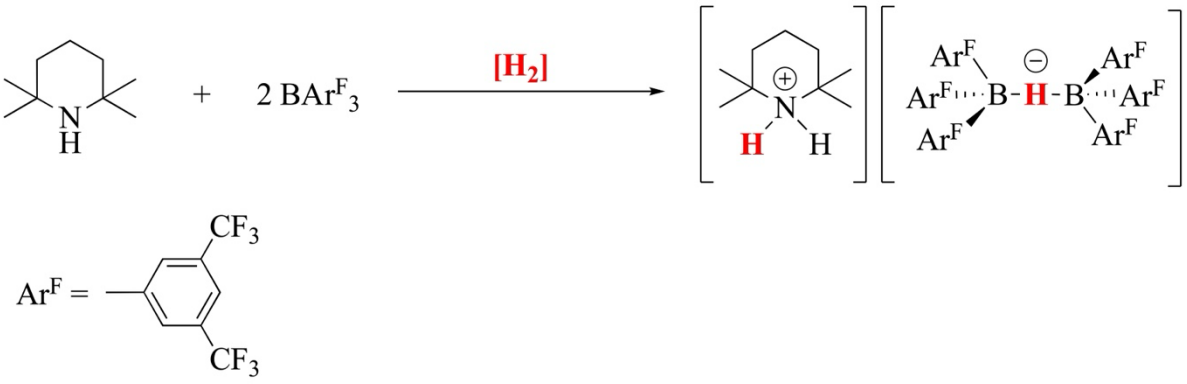

Scheme 8. Splitting of H_2 through FLP formation between $BArF_{18}$ and TMP. Adapted from ref. 27.

Successive to the splitting of H_2, the field of FLP-catalysed hydrogenation has advanced considerably. Such examples include hydrogenation of imines by using an intermolecular FLP[28] and alkene hydrogenation.[29] Other meaningful uses of FLPs also includes the capture of toxic gases such as NO, CO and SO_2 (Scheme 9) which has clear significant impact on the environment.[30]

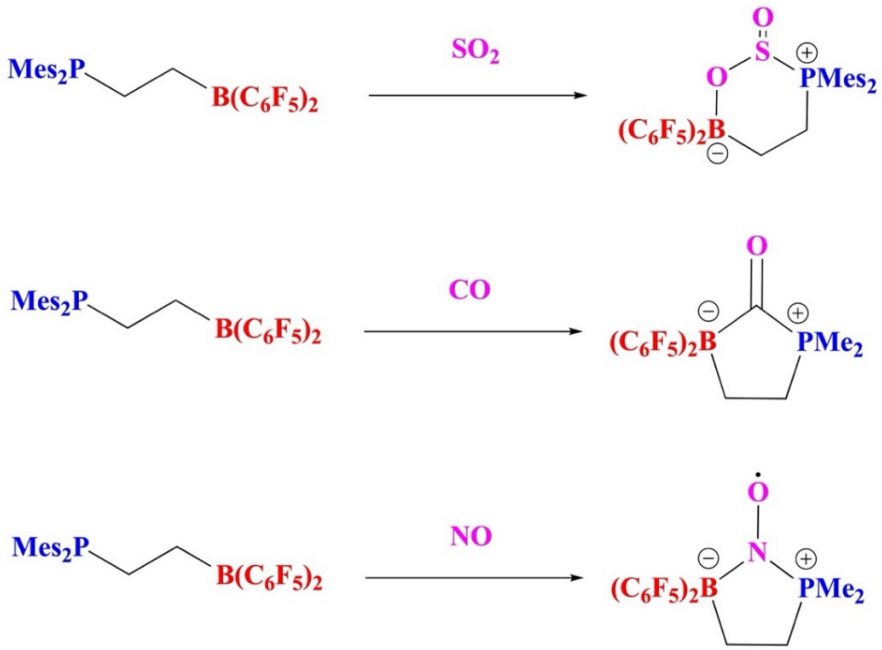

Scheme 9. Examples of FLPs capturing small molecules. Adapted from ref. 31.

1.1.3 Computational studies of small molecule activation mechanisms

In all chemistry, it is important to understand the mechanisms behind reactions. Computational methods, such as Density Functional Theory (DFT), are powerful tools that allow synthetic chemists to observe and rationalise experimental findings and in turn, guide future works. For example, in the activation of H_2, through the use of DFT it was proposed that these reactions can occur *via* two pathways. One way is through simultaneous donor-acceptor action of the Lewis base lone pair into the H_2 σ^*-orbital and from the H_2 σ-orbital into the Lowest Unoccupied Molecular Orbital (LUMO) of the Lewis acid (Scheme 10a), closely resembling the behaviour of transition metals. Alternatively, cleavage is also possible through the polarisation of H_2 by the acidic and basic components (Scheme 10b).[32]

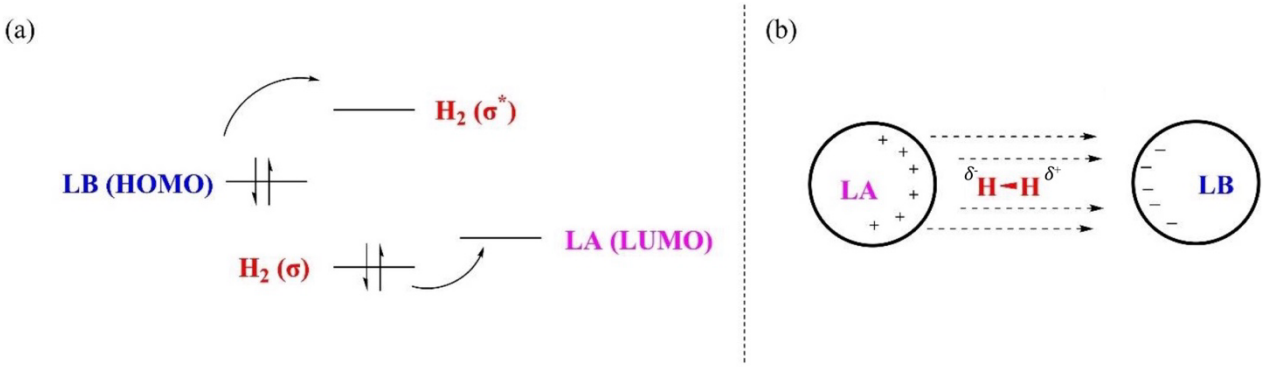

Scheme 10. Proposed H_2 activation modes. (a) electron transfer model; (b) electrostatic field model. Adapted from ref. 32.

Other publications have also shown how using quantum calculations can allow for rapid screening of substrates, making optimisation of reactions much faster.[33] For instance, Heshmat and Ensing explored 75 FLP combinations and concluded that splitting H_2 can be made more favourable by increasing the electrophilicity of the Lewis acid. It was also found that by increasing the nucleophilicity of the base, the barrier height for activation was decreased.[34] In a similar report from Pinter and co-workers, an in-depth look at the two low- and high-energy transition states involved in H_2 activation was described. It was revealed that within each transition state, a different mechanism was occurring, supporting the notion of both the electron transfer model and the electrostatic field model.[35]

1.2 Measuring Lewis acidity

Measuring Lewis acidity is somewhat difficult as there are different interactions such as covalent, dispersive and electrostatic forces to consider. In a review by Greb, it is mentioned that no universal reference has been established unlike for Brønsted acidity where the log of the acid dissociation constant (pK_a) is used to describe a molecule's ability to donate protons.[36, 37] Due to the Lewis base dependency of the donor-acceptor strength, no such unified scale for Lewis acidity can be created.[38] Pearson's principle of hard and soft acids and bases (HSAB) can however be used to quantify

experimental findings.[39] According to this principle, soft acids prefer to bind with soft bases and the same is true for hard acids and bases. The terms 'hard' and 'soft' refer to electrostatic and covalent interactions respectively. This can be used in conjunction with the ECW model from Drago *et. al* [40-42] (Equation 1), which predicts the enthalpies of adduct formation using electrostatic (E) and covalent (C) parameters and steric constants (W). The E and C parameters refer to the strength of the bond formed between the acid and base. Large E values were responsible for producing particularly strong Lewis adducts so Klopman[43] and Mulliken[44] provided speculative explanations for the basis of these interactions through the employment of perturbational molecular orbital theory. In his review however, Greb cited that these measurements alone were not enough to significantly quantify differing affinities so alternative methods must be employed. This prompted the creation of three definitions: global Lewis acidity (gLA), effective Lewis acidity (eLA) and intrinsic Lewis acidity (iLA). These measurements can accurately interpret reaction outcomes and in turn, help delineate the Lewis acids whose affinities far surpass classic species into their own superclass.

$$\Delta H = E_{LA}E_{LB} + C_{LA}C_{LB} + W \qquad (\mathbf{1})$$

E = Electrostatic influence

C = Covalent influence

W = Steric constant, derived from experimentally determined equilibrium constants

1.2.1 Substituent effects on Lewis acidity

The choice of substituent when creating new Lewis acids is a very important aspect to consider as this is part of what dictates the molecule's acidity. Whilst most examples are out of the scope of this thesis, the lesser explored SF_5 group is highly relevant. The so-called 'super trifluoromethyl group' has an octahedral geometry, is greatly electron-withdrawing ($\sigma_m = 0.61$ *vs*. $CF_3 = 0.43$),[45] possesses high chemical stability and high lipophilicity ($\pi = 1.51$) and is less water-soluble than CF_3.[46, 47]

Because of these properties, compounds containing this are particularly popular within biological sciences[48, 49] as well as reactions where stereochemical control can be influenced by the SF_5 groups dipolar effects and steric demand. Once such example where this is explored is with the Staudinger ketene-imine cycloaddition reaction.[50] These are also very useful building blocks for accessing other compounds such as drugs to treat tuberculosis,[51] luminescent materials[51] and complicated heterocycles.[52]

Given its usefulness in other areas of chemistry, it is fitting that this group was utilised within catalysis. In 2019, Mecking and co-workers devised *tetrakis* [3,5-bis(pentafluorosulfanyl)phenyl]borate (**S**-$BArF_4$)$^-$,[53] taking advantage of the SF_5 group. During synthesis it was noticed that attempts to access the SF_5-substituted aryl Grignard reagent resulted in unreacted starting material being recovered when tried *via* the heterogenous route with magnesium, as previously reported by Reger *et al*. in their work exploring the synthesis of a different borate.[54] Thus a modified approach *via* transmetallation with ^{i}PrMgCl followed by reaction with BCl_3 was used (Scheme 11a). The borate was then combined with a nickel(II) complex to form novel [Ni(allyl)(mesitylene)]$^+$[**S**-$BArF_4$]$^-$. This was noted to act as a catalytic precursor for the polymerisation of butadiene in heptane and showed high activity and 1,4-cis selectivity (≥93%) (Scheme 11b). In comparison to the related anion $[BArF_{24}]^-$, they were able to demonstrate twice as much polymerisation activity with **S**-$BArF_4$ which resulted in higher molecular weights of the polybutadiene product.

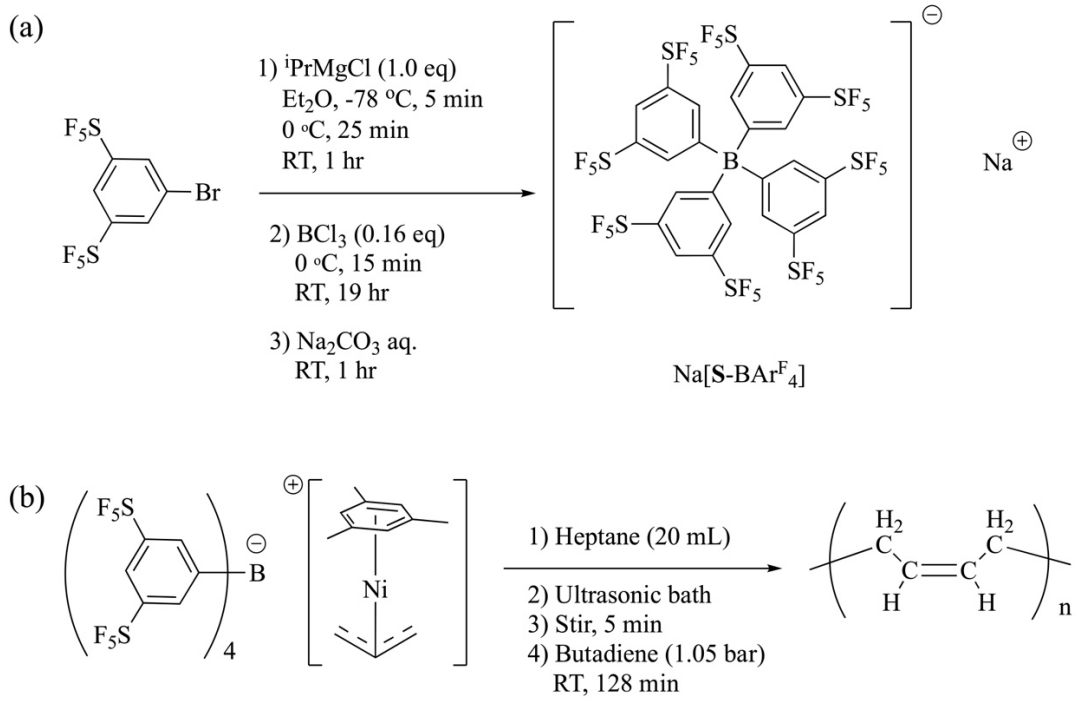

Scheme 11. (a) Synthesis of Na(**S**-BArF$_4$); (b) Polymerisation of butadiene using [Ni(allyl)(mesitylene)]$^+$[**S**-BArF$_4$]$^-$ in heptane. Adapted from ref. 53.

1.2.2 Fluoride ion affinity

Fluoride ion affinity (FIA) is a popular method for quantifying Lewis acidity which measures the negative enthalpy of a gas phase reaction between a Lewis acid with a fluoride ion (Equation 2).[55, 56] Taking advantage of the small size and strong basicity of fluoride ions, these chemical properties mean steric repulsion is diminished and effects such as charge transfer, dispersion and π-back bonding are negated.[56] First introduced by Haartz and McDaniel in 1973, they pioneered the use of ion cyclotron resonance (ICR) mass spectrometry which involves measuring the mass-charge ratio of fluoride ions based on the cyclotron frequency of the ions in a fixed magnetic field.[57] This method proceeded to be utilised in the measurement of many compounds such as main group oxides, alkyls, fluorides,[58, 59] silanes and boranes.[57] Since this technique requires specialised equipment and quite often, the absolute values were in systematic error due to incorrect anchor points[37, 60] this necessitated

the development of *in silico* analysis. Krespan and Dixon published the first reliable method using an isodesmic approach in 1996 where the known FIA value of carbonyl fluoride was used as an absolute value.[60] Isodesmic reaction is common terminology within theoretical chemistry defined as *'reactions where the bonds being broken in the reactants are the same as the ones formed in the product'*.[61] This methodology is often used due to the established difficulty of modelling the electron affinity of a lone fluoride ion.

$$LA + F^- \xrightarrow{\Delta H} [LA - F]^- \quad (\mathbf{2})$$

$$FIA = -\Delta H$$

Whilst *in silico* analysis is renowned for its diverse analytical power, its relatively easy steps and modelling hundreds of values to assess the stability of weakly coordinating anions for example,[62] it is not without its shortcomings. A key limitation of FIA is that the fluoride ion is considered a hard Lewis base and ergo only reflects hard Lewis acidity. This dismisses soft Lewis bases such as methide and hydride anions. A good example of this is that tris(pentafluorophenyl)aluminium ($Al(C_6F_5)_3$) is a Lewis superacid when judged by FIA whereas $B(C_6F_5)_3$ is not. However $B(C_6F_5)_3$ has a higher hydride ion affinity (HIA) than $Al(C_6F_5)_3$.[37] There have been various mentions of HIA over the past three decades,[63-65] with it working in a similar manner to FIA but utilising the hydride ion instead (Equation 3). Combining both practices allows for a more thorough depiction of a Lewis acidity scale.

$$LA + H^- \xrightarrow{\Delta H} [LA - H]^- \quad (\mathbf{3})$$

$$HIA = -\Delta H$$

Another issue to consider is the difference between experimental and theoretical findings. As the fluoride ion binds to the Lewis acid, this involves charged species which will inevitably be influenced by solvent interactions. FIA values are commonly calculated within a vacuum so are not necessarily reflective of experimental conclusions as these are performed in solution. This combined with the lack of experimental data means that calculated FIA values are not always the most reliable.

1.2.3 Other methods

Whilst the above methods are the most employed, there are other ways to measure Lewis acidity. These include the Gutmann-Beckett method which was introduced in 1976 by Viktor Gutmann.[66] Through using ^{31}P-NMR spectroscopy to track the downfield shift of triethyl phosphine oxide's (Et_3PO) phosphorus NMR spectroscopic resonance when bound to a Lewis acid (Figure 2), the strength of the acid can be determined.

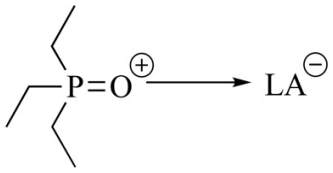

Figure 2. Triethylphosphine oxide probe bound to a Lewis acid.

The magnitude of the shift correlates to strength which can be quantified through using Equation 4. The acceptor-number (AN) scale is a metric that was devised using hexane which is not Lewis acidic (AN = 0) and antimony pentachloride (strong Lewis acid, AN = 100) as reference points and allows for a quantitative measurement of Lewis acidity.

$$\mathrm{AN} = 2.21\ (\partial_{\mathrm{sample}} - 41.0) \qquad (4)$$

Another way is the Child's method which involves recording the proton chemical shift of *trans*-crotonaldehyde when the carbonyl oxygen binds to a Lewis acid.[67, 68] Notably, Marks used this to

characterise a number of perfluoroaryl boranes relative to BBr_3 (1.00).[67] In a similar fashion, Hilt and Nödling utilised a novel quinolizidine as a ^2H NMR probe, recording the change in signals once bound to a Lewis acid (Scheme 12a).[69] An infra-red approach can also be taken as the –CN group within acetonitrile, when reacted with a Lewis acid, makes a good spectroscopic handle due to its symmetry.[37] It was noted that this method is generally limited to solid-state analysis of one compound class as attempting to compare different classes resulted in misleading results.[70-72] In 2019, Baumgartner and Caputo introduced using a fluorescent dithienophosphole oxide architecture, enabling correlation of optical response to the strength of a Lewis acid (Scheme 12b).[73] It emulates the structural motifs used within Gutmann-Beckett analysis however is independent of the base which allows for more direct measurements of strength.

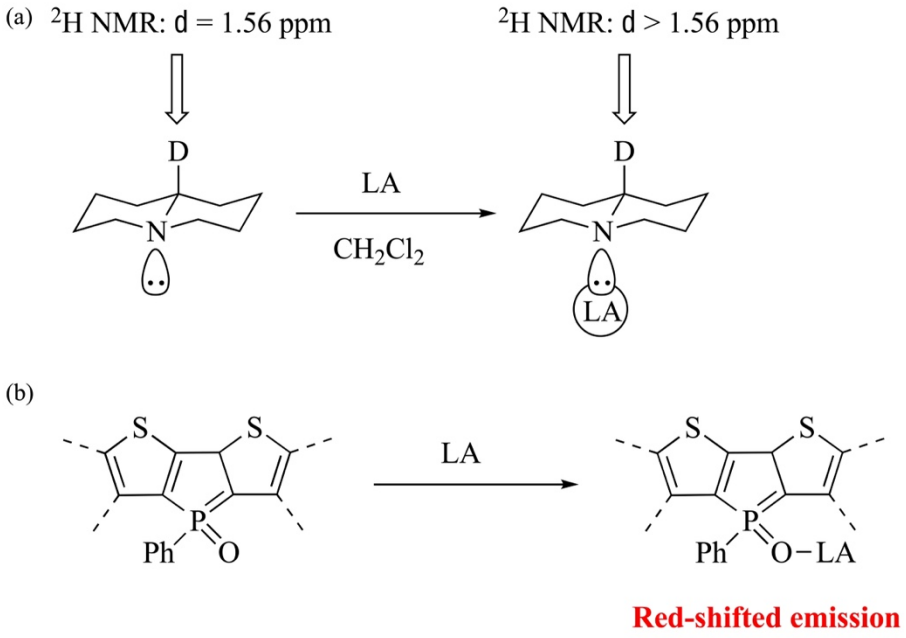

Scheme 12. (a) Novel quinolizidine which elicits a shift in deuterium signal once bound in ^2H NMR spectroscopy; (b) Fluorescent dithienophosphole oxide architecture which causes a bathochromic shift in emission. Adapted from refs. 69 and 73.

In the previous year, Stephan and co-workers suggested the use of the global electrophilicity index (GEI) as another computational metric.[74] Formally introduced in 1999 by Parr,[75] GEI (Equation 5a) is the measurement of a molecule's ability to uptake electrons. The chemical potential (μ) and hardness (η) can be derived from the energies of the HOMO and LUMO as demonstrated in Equation 5b.

$$\omega = \frac{\mu^2}{2\eta} \qquad \textbf{(5a)}$$

μ = chemical potential

η = chemical hardness

$$\mu = \frac{1}{2}(E_{HOMO} + E_{LUMO}) \qquad \eta = E_{LUMO} - E_{HOMO} \qquad \textbf{(5b)}$$

Like computational FIA methods, data collection is quicker than experimental methods however the key difference is that calculations are done independent of the base used. This avoids the impracticalities of producing numerous combinations of acids and bases, offering a more convenient way of scaling acidity.

1.3 Lewis superacids

Superacids have been described in the literature from as early as 1927 when Conant and Hall described the use of a chloranil electrode in glacial acetic acid and characterised certain weak bases.[76, 77] The term is generally applied to Brønsted (protic) acids, with the definition alluding to any species that is stronger than sulfuric acid[78] although there have been a few interesting references in literature to Lewis superacids. Noticing that there was no reasonable *a priori* distinction between Brønsted acids and Lewis acids, Olah *et al.* gave an early definition of '*those stronger than anhydrous $AlCl_3$ should be categorised as Lewis superacids*'.[79] However, the definition shifted when FIA was used as a benchmark for strength. Krossing and co-workers cited *'Molecular Lewis acids, which are stronger*

than monomeric antimony pentafluoride (SbF_5) in the gas phase are Lewis superacids'.[80] Until fairly recently, SbF_5 was considered the strongest Lewis acid known with its ability to form Lewis superacid fluoroantimonic acid with liquid hydrofluoric acid in a 1:1 ratio (Scheme 13).[81] Since the recording of its structure in 1958 by Hoffman and co-workers[82] there has been a plethora of research into its capabilities, ranging from utilising it within isobutane ionisation[83] to reduction chemistry with alkanes.[84] Despite its versatility however, many efforts have gone into discovering different Lewis superacids as SbF_5 is highly corrosive, toxic and oxidising in nature,[85] making it very challenging to handle.

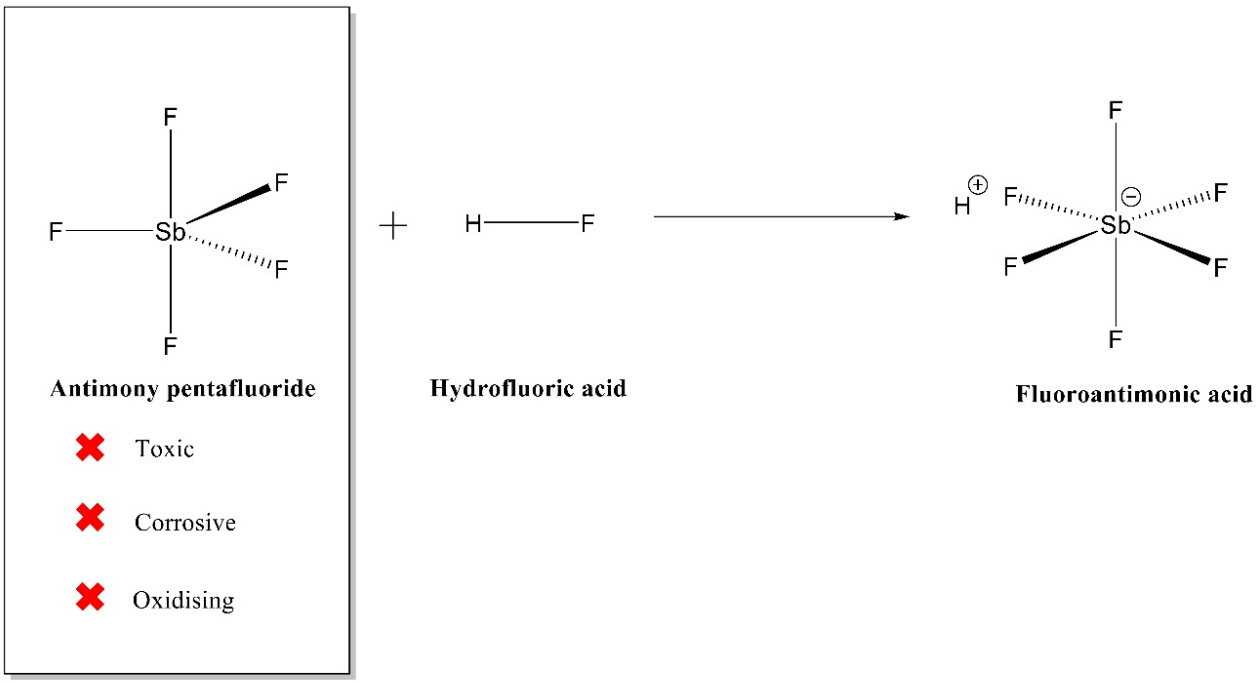

Scheme 13. Generation of superacid fluoroantimonic acid.

1.3.1 Boron-based Lewis superacids

When considering new structural designs for the ideal boron-centred Lewis superacid, there is a set of criteria that needs to be satisfied. Firstly, high thermal stability should be achieved with decomposition pathways kinetically and thermodynamically disfavoured. Secondly, ligands must be strongly bound to the boron centre to avoid scrambling and solvolysis. With this in mind, $B(CN)_3$ was isolated for the first time in 1954 by Chaigneau,[37] with a computational FIA value of 551 kJ mol^{-1} exceeding that of SbF_5 (477 kJ mol^{-1}).[86] Remarkably, it was shown that this could stabilise one negative charge when the related dianion $B(CN)_3^{2-}$ was isolated.[87] Since then, various substituents around the tricoordinate boron centre have been shown to give high computational FIA values. The triflate group (OTf) is one of the strongest electron withdrawing groups known and as such, $B(OTf)_3$ (FIA = 530 kJ mol^{-1}) was made in 1977 as part of a Brønsted acid system and then later isolated by Olah *et al.* in 1984.[88] They used it for the generation of stable carbocations with it possessing thermal stability of up to 100 °C and good solubility in polar solvents such as dichloromethane. As such, it possesses the highest catalytic activity within ring enlargement and Friedel-Crafts reactions[89] and went on to be used in applications such as an OTf ligand transfer agent, an initiator for phosphaacetylene cycloadditions[90] and the generation of supersilylating agents.[91]

A pertinent example of the fine balance between Lewis superacidity and synthetic design is $B(CF_3)_3$. From previous works, it was clear that the more inductive the substituents are, the better the compound performed as a Lewis acid and so investigation into trifluoromethyl (CF_3) groups was launched. $B(CF_3)_3$ was theoretically calculated to be a Lewis superacid possessing a much higher FIA value than SbF_5 (556 kJ mol^{-1} *vs.* 478 kJ mol^{-1}), with it being touted as the strongest neutral borane. However synthetic difficulties due to the favourable elimination of α-fluoride meant that it could not be isolated. Tris(perfluorotolyl)borane ($B(p\text{-}CF_3\text{-}C_6F_4)_3$) (FIA = 499 kJ mol^{-1}) is another example of sacrificing stability in favour of acidity. Many attempts at obtaining a pure sample of this superacid

were made with the most successful attempt being in 2017 when tetrameric perfluorotolyl copper ($F_3CC_6F_4$-Cu^I) and BBr_3 in 1,4-dioxane were reacted to form the 1,4-dioxane adduct.[92] The solvent could be removed through heating the crude solid gradually from 50 to 100 °C under high vacuum, however it was seen that minor product decomposition occurred when attempting to do so. To date, no one has successfully isolated a pure sample of this complex. Despite these problems however, a lot of progress has recently been made within the field, especially towards catalysis.

1.3.2 Catalytic applications

It stands to reason that if these complexes are more Lewis acidic than the standard benchmarks then they should display greater efficacies towards activating small molecules. However, there are few borane-based examples due to high reactivity and isolation issues. With this in mind, Martin and co-workers introduced a one-pot isolable halogen-free Lewis superacid capable of C–F bond functionalisation in 2022.[93] *Tris*(*ortho*-carboranyl)borane (B*o*Cb_3) has an FIA value of 605 kJ mol^{-1} and was investigated in typically challenging reactions to measure its potential reactivity. For example, through Friedel-Crafts reactions of 1-fluoroadamantane with benzene in the presence of B*o*Cb_3, 1-phenyladamantane was obtained in 90% isolated yield after only 30 minutes (Scheme 14). In comparison, it was noted that when $B(C_6F_5)_3$ was employed no conversion was seen, even after 4 hours. *Tris*(*ortho*-carboranyl)borane's superior performance was attributed to the electron-withdrawing effects of the *ortho*-carborane moiety and lack of LUMO π-delocalisation, meaning that it demonstrates unusually high Lewis acidity.

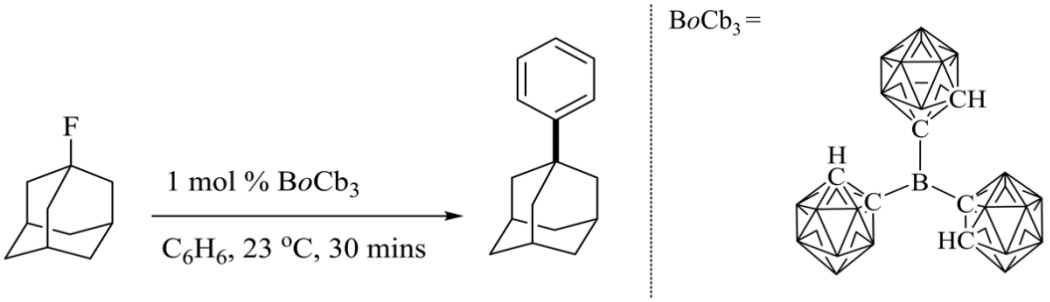

Scheme 14. Catalytic transformation of 1-fluoroadamantane to 1-phenyladamantane. Adapted from ref. 93.

Carrying on from this, the same group recently devised *bis*(1-methyl-ortho-carboranyl)borane, describing its role in the hydroboration of alkenes and alkynes (Scheme 15).[94] Once again, FIA calculations reveal that this is a Lewis superacid (527 kJ mol^{-1}), surpassing $B(C_6F_5)_3$ and $HB(C_6F_5)_2$ by almost 100 kJ mol^{-1}. Up to 90% and 98% conversions were seen within 10 minutes for alkynes and alkenes respectively. Impressively, this is the first Lewis superacidic secondary borane and most reactive neutral hydroboration reagent known to date.

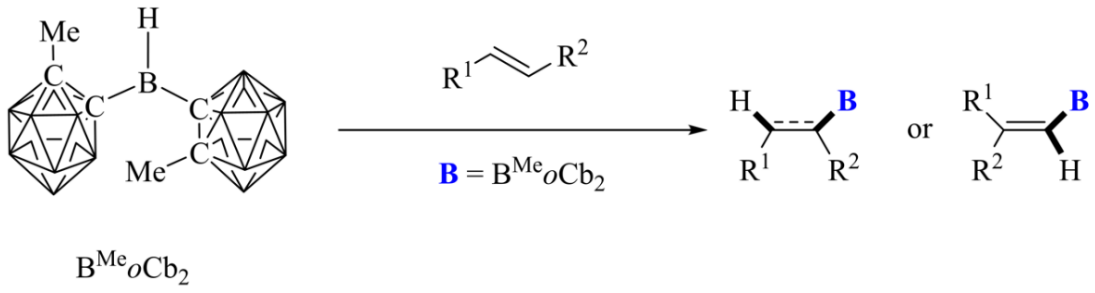

Scheme 15. Overall reaction for the hydroboration of alkenes and alkynes. Adapted from ref. 94.

In 2021, Berionni and Chardon took a different approach and tempered the reactivity of pyramidal 9-sulfonium-10-boratriptycene (Figure 3).[95] The strongly pyramidalised boron centre means it showed high Lewis acidity with an FIA value of 476 kJmol^{-1}. This allowed them to achieve difficult chemical transformations such as inert C–H bond activation through FLP formation with TMP and cleavage of

C–Si bonds. Whilst exploration into the boratriptycene family is still relatively new, it could provide yet further insight into how main group elements can mimic transition metal chemistry.

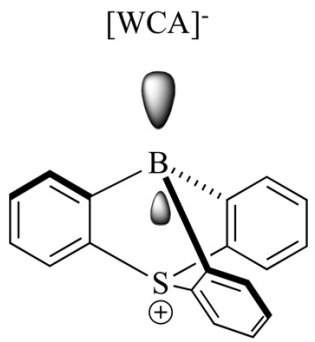

Figure 3. Structure of Lewis superacid 9-sulfonium-10-boratriptycene. Adapted from ref. 95.

In early 2023, Paradies and co-workers described the generation of ferrocenium-boranes through the oxidation of ferrocenyl-substituted boranes.[96] The reversible redox-active behaviour of ferrocene is well documented, with its use typically associated with medicinal and sensing applications.[97, 98] Due to this intrinsic behaviour, it was theorised that this could increase Lewis acidity as cationic boranes and those incorporating pendant cationic groups have been shown to possess high Lewis acidity.[95, 99] Through careful control of electrochemical processes, the handling of these LSAs became significantly easier and thus allowed precise measurements of catalytic activity towards the activation of C–F and S–F bonds. It was revealed that reaction with various compounds with CF_3 and SF_5 substituents, up to 93% isolated yields of product were seen (Scheme 16). Both of these groups are known for their strong bonds, so these works showed promise in successfully achieving activation of more challenging substituents.

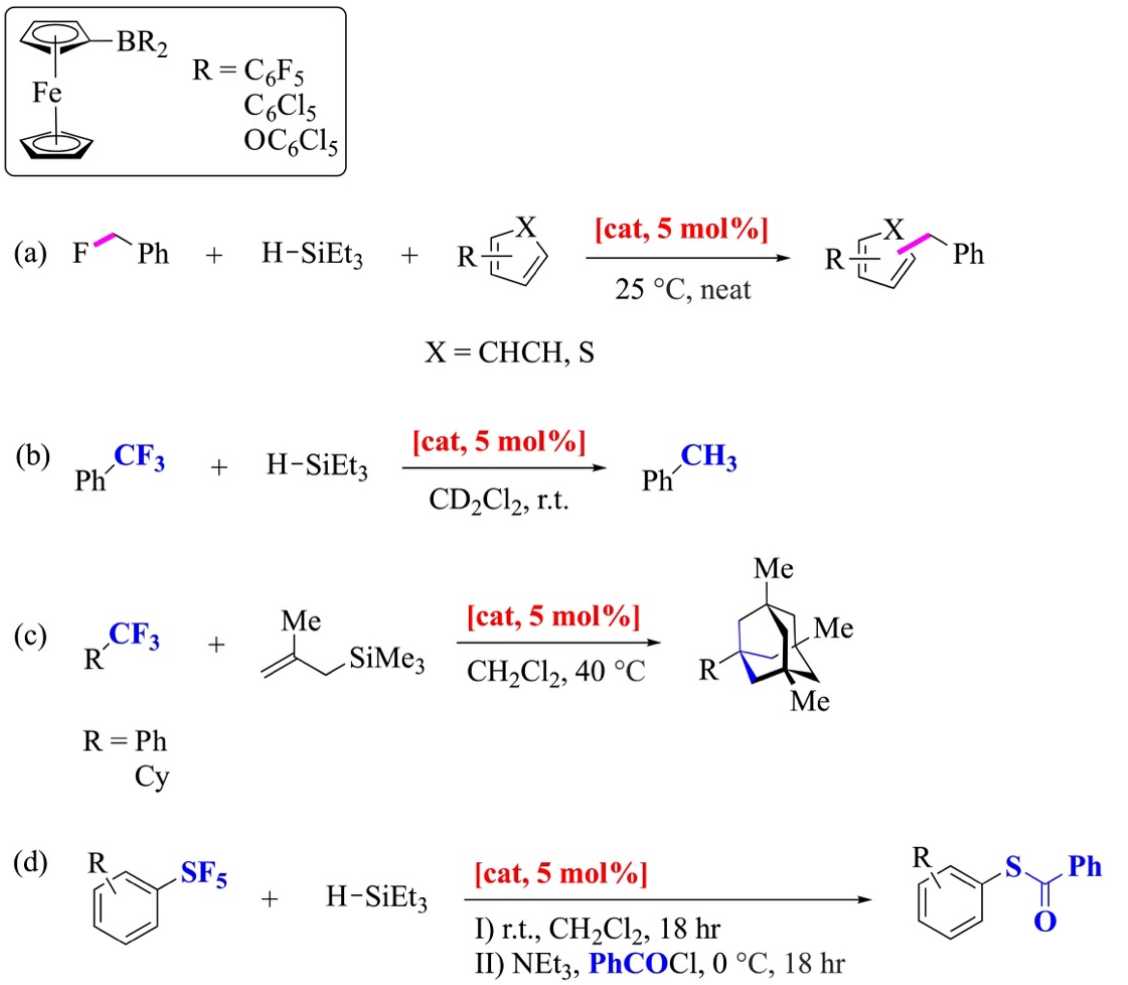

Scheme 16. Ferrocenyl-substituted borane catalyst. (a) C–F bond arylation; (b) C–F bond reduction; (c) C–F bond alkylation; (d) S–F bond functionalisation. Adapted from ref. 96.

2. AIMS

This project aims to add to the family of Lewis superacidic boranes by designing, synthesising and evaluating a new species, *tris*[3,5-bis(pentafluorosulfanyl)phenyl]borane (**1**) (Figure 4). Through incorporating SF_5 groups into its scaffold, it is hoped that the above discussed advantages that these groups impart will benefit this borane. Computational methods such as FIA and HIA calculations will probe whether it is a Lewis superacid and assess its hardness against other species. This will aid in evaluating its suitability within reactions such as H_2 activation mediated through FLP formation. DFT studies will help to back up discussions of this through the screening of 20 different Lewis bases in combination with **1**, ranging in basicity and size.

In addition to this, different experimental routes will be explored to see whether **1** is a feasible target. An improved synthetic route to access 1-bromo-3,5-bis(pentafluorosulfanyl)benzene (**26**), the precursor needed for the formation of **1**, is also going to be documented. Currently, this is expensive to purchase, with the cheapest supplier selling 100g at 95% purity for £224.93 before the price of delivery is considered. Given this, a cheaper alternative method is needed to be able to produce **1** on a greater scale (>500 g).

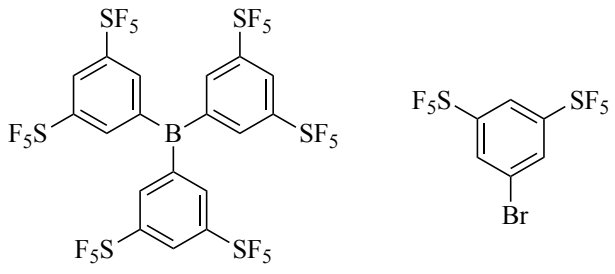

1

26

Figure 4. Novel borane **1** and precursor **26**.

3. COMPUTATIONAL RESULTS AND DISCUSSION

3.1 DFT studies

FIA and HIA results in Table 1 showed that **1** (Figure 4) is a soft Lewis superacid (FIA = 553.9 kJmol^{-1}, HIA = 556.8 kJmol^{-1}) as its FIA value is 76.4 kJmol^{-1} stronger than SbF_5. These were calculated using an isodesmic methodology as explained in the introduction. It is also stronger than the boron trihalides, $HB(C_6F_5)_2$ and $B(C_6F_5)_3$. It has similar strength to $B(OTeF_5)_3$, $B(CN)_3$ and $B(CF_3)_3$ which are Lewis superacids as well, however $B(CF_3)_3$ cannot be isolated due to instability (see above discussion). In comparison to the systems devised by Martin and co-workers, it is more acidic than $B^{Me}OCb_2$ (FIA = 527 kJmol^{-1}) but weaker than B*o*Cb_3 (FIA = 605 kJmol^{-1}). Due to the bulky *ortho*-carborane moieties however, small molecule activation such as those with H_2 and CO_2 could not be achieved with this.[93] So whilst its acidity is higher, it is not synthetically useful in this context. Borane **1** offers the advantage of having strong electron-withdrawing groups around the boron centre which are small enough that it is predicted they will not hinder reactivity.

Table 1. FIA and HIA values of known boranes and SbF_5. Adapted from refs. 100, 101, 102 and 103.

Compound	FIA/kJ mol^{-1} [a]	HIA/kJ mol^{-1} [a]
BF_3	342	299
BCl_3	405	391
BBr_3	438	441
BI_3	493	505
$B(OTeF_5)_3$	552	556
$B(CN)_3$	551	587
$B(CF_3)_3$ [c]	556	583
$B(C_6F_5)_3$	454	497
$HB(C_6F_5)_2$	429	- [b]
$B(OTf)_3$	530	- [b]
$B(OC_6F_5)_3$	431	411
B*o*Cb$_3$	605	622
B^{Me}*O*Cb$_2$	527	- [b]
SbF_5	477.5	530 (517) [d]
This work (borane 1)	**553.9**	**556.8**

[a] Calculated at PBEh-3c//M06-2X/def2-QZVPP level of theory. [b] Not calculated. [c] Cannot be isolated due to instability. [d] $[SbF_5H]^-$ is not stable and would decompose to SbF_4^- + HF, this value is given in brackets.

Based on these values for the Lewis acidity of **1**, we sought to explore how this borane would interact with a range of common bases used in FLP chemistry through computational methods. To probe interactions between **1** and the different Lewis bases (**2** – **21**) detailed in Figure 5, geometry

optimisations and reaction energies were calculated to see whether FLP formation would occur. Because of the predicted FIA of **1**, it was hypothesised that a weaker Lewis base could potentially be used for an FLP and still achieve the same small molecule activation as established systems.

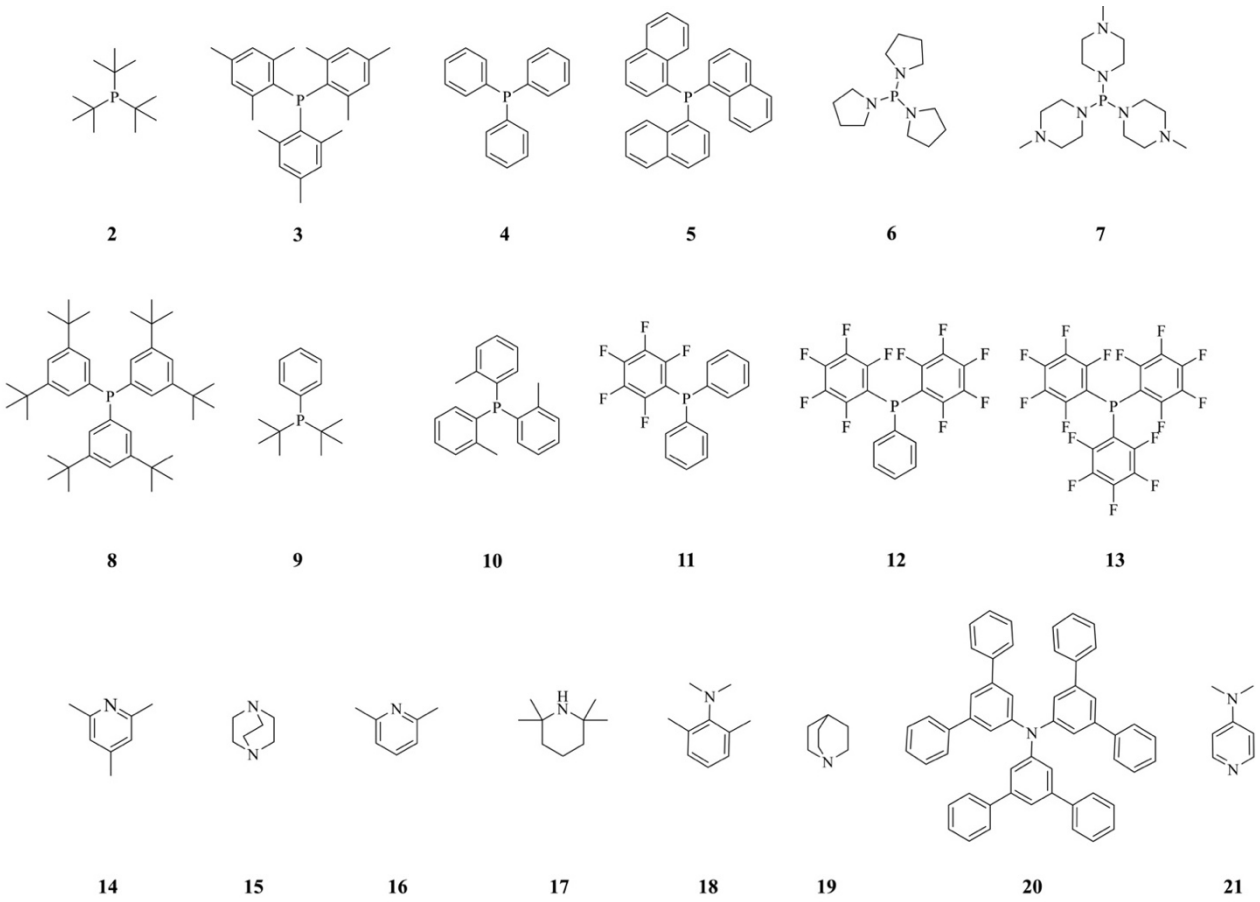

Figure 5. Lewis bases **2** – **21** tested in conjunction with **1**.

As a starting point, a suitable level of theory needed to be selected. When doing this, it is worth considering the complexity of the systems being studied. Quite often researchers refer to a Jacob's ladder where Hartree-Fock theory is at the bottom and on each successively higher rung there is a computational method. As you ascend the ladder, accuracy increases but so does computational cost.[104, 105] Because of this, hybrid functionals are a regular choice as they are a middle ground between the two parameters. Hybrid refers to the fact that Hartree-Fock (HF) exchange and exchange correlation functionals are combined. This is used to increase accuracy as Hartree-Fock calculates

exchange interactions using precise integrals (exact exchange) whereas when using exchange correlations, these interactions are approximated.

Since these are main group systems, the M06-2X hybrid functional was the best choice as it has been benchmarked against other main group systems with positive results.[106] Introduced in 2005 by Truhlar and co-workers, [106] it offers a relatively low computational cost whilst maintaining accuracy. There are more popular choices such as B3LYP from Becke, Lee, Yang and Parr which achieves the same outcome, however there is evidence to suggest that this functional degrades as the systems get larger.[107] M06-2X additionally includes a higher percentage of HF exchange (54%) *vs.* B3LYP (20%). This provides a better description of electronic correlation effects and reduces self-interaction errors between electrons (SIE). These are particularly important for systems where electron-electron interactions play a major role and reducing SIE means a more accurate electronic structure can be obtained.

3.1.1 Exploring adduct and FLP formation

Beginning with the individual optimisations of **1** and **2** – **21**, the total energies of the systems (E) were recorded as well as the sum of electronic and thermal enthalpies (H) and sum of electronic and thermal free energies (G). After this, to improve accuracy, single point energies (G_{BB}) were re-computed with a bigger basis set (BB) (see experimental section for more details). Geometry optimisations are less sensitive to basis set size than electronic energy calculations so performing them this way gave a better representation of the systems. As well as this, starting optimisation and frequency calculations with a smaller basis set saves time for large systems as it provides a close estimate to the true coordinates and requires less computational power. After these were completed, the value of G was corrected (G_{corr}) by adding the values of G and G_{BB} and subtracting the value of E for each system (Equation 6a). Following the conversion of these values from Hartrees (Ha) to kcal/mol, relative

energies (E_{rel}) were determined by subtracting the value of G_{corr} from the sum of the independent LSA and LB G_{corr} values as shown in Equation 6b. By calculating E_{rel}, the thermodynamic favourability of these systems could be determined.

$$G_{Corr} = (G + G_{BB}) - E \quad \textbf{(6a)}$$

$$E_{Rel} = G_{Corr} - (LSA\ G_{Corr} + LB\ G_{Corr}) \quad \textbf{(6b)}$$

Table 2 contains bond lengths as well as G_{corr} and E_{rel} values for systems **1** and **2** – **21**. These bond distances were compared to typical Lewis adducts such as $B(C_6F_5)_3/PPh_3$ (B–P bond length = 2.2 Å) and $B(C_6F_5)_3$/MeCN (B–N bond = 1.6 Å) to establish whether FLP formation was likely, *i.e.* if the bond distance is greater than these benchmarks then FLP formation can be considered.[108]

Table 2. Thermodynamic data and bond lengths for systems **1** and **2**-**21**. Systems that formed adducts are highlighted in yellow with those that could have possible FLP applications highlighted in blue. Those that are left are systems in which neither application is seen.

System	ΔG (kcal/mol)	B···P (Å)	B···N (Å)
1 + 2	-1.0	3.3	
1 + 3	2.3	4.9	
1 + 4	-14.8	2.1	
1 + 5	-10.3	3.5	
1 + 6	4.2	5.6	
1 + 7	-20.7	2.0	
1 + 8	-25.3	2.1	
1 + 9	4.8	4.5	
1 + 10	7.9	6.3	
1 + 11	2.5	4.1	
1 + 12	1.9	4.5	
1 + 13	8.1	3.5	
1 + 14	1.6		3.5
1 + 15	-10.9		1.6
1 + 16	1.2		3.8
1 + 17	5.8		6.2
1 + 18	4.6		3.9
1 + 19	-13.9		1.6
1 + 20	-4.2		4.2
1 + 21	-25.5		1.6

As demonstrated by values being equal or under the typical adduct lengths described above, combining **1** with bases **4**, **7**, **8**, **15**, **19** and **21** elicited adduct formation (Figure 6). In addition to the bond lengths, the E_{rel} values for each indicated this occurred readily with exergonic energies in the range of -10 to -25 kcal/mol.

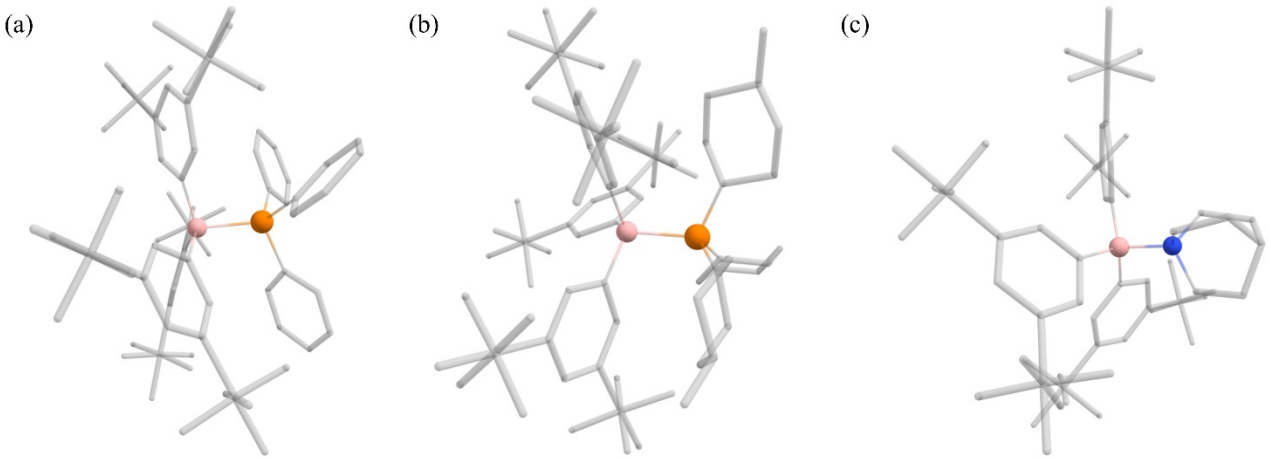

Figure 6. Selected optimised local geometries to demonstrate adducts. (a) **1** and **4**; (b) **1** and **7**; (c) **1** and **19**. Pink atom = B, orange atom = P, blue atom = N. H atoms are omitted, and all other substituents represented in wireframe for clarity.

These results were not unexpected given that most of these bases do not possess the steric bulk to prevent adduct formation. What was surprising however is that **8** forms an adduct but **9** does not. Upon first inspection, the opposite was inferred given that **8** possesses three phenyl rings adorned with *tert*-butyl groups in the *meta*-positions, increasing its steric bulk over **9** which possesses one phenyl ring and two *tert*-butyl groups. However, other features such as the basicity of **9** being less than that of **8** may be an influencing factor as thermodynamically, the association energy between **1** + **9** is endergonic at 4.8 kcal/mol *vs.* -25.3 kcal/mol for **8**.

For instances **1** + **3**, **6**, **9**, **10, 12** and **17** where bond lengths appear unusually long, these bases were found to be positioned with **1** in a way that is not useful for activation (Figure 7) *i.e.* the two components are positioned too far apart in solution to react. As optimisation calculations find local and not global minima, these geometries are one of many possible orientations.[109] Conformational analyses could be done to find global minima but for the purpose of this discussion, this information was not necessary.

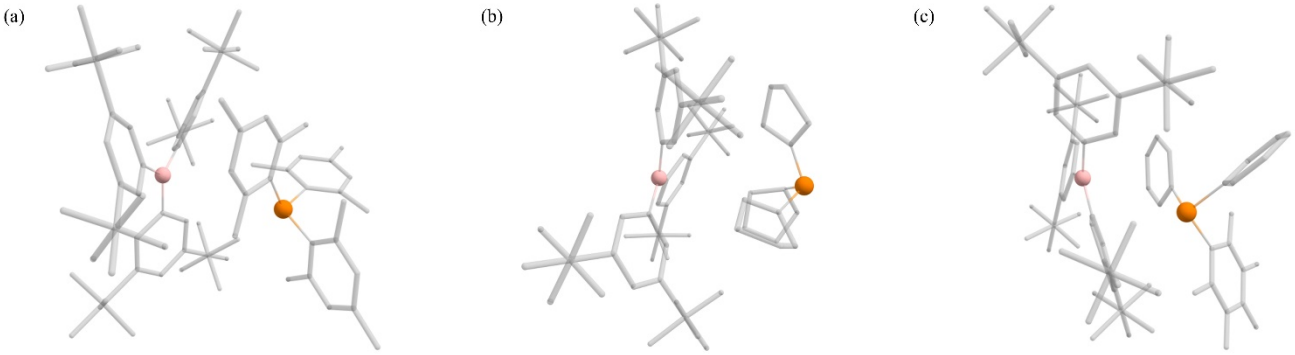

Figure 7. Selected optimised local geometries to demonstrate LB orientation. (a) **1** and **3**; (b) **1** and **6**; (c) **1** and **7**. Pink atom = B, orange atom = P. H atoms are omitted, and all other substituents represented in wireframe for clarity.

The remaining permutations between **1** and bases **2**, **5**, **11**, **13**, **14**, **16**, **18** and **20** (Figure 8) have distances of between 3.3 – 4.3 Å. These distances are too long to indicate covalent bond formation and are more typical of dispersion interactions found between FLPs. Previous solid-state multinuclear

NMR spectroscopic and DFT studies have shown that typical FLP distances are between 2.9 – 4.4 Å[110] which furthers supports the idea FLP formation would be seen if combined in solution.

Figure 8. Selected optimised local geometries to demonstrate FLP formation. (a) **1** and **2**; (b) **1** and

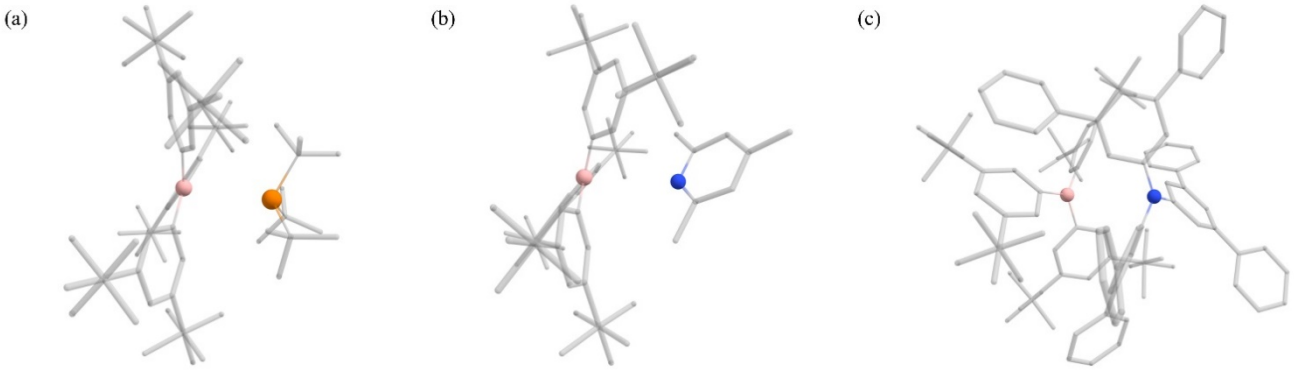

14; (c) **1** and **20**. Pink atom = B, orange atom = P, blue atom = N. H atoms are omitted, and all other substituents represented in wireframe for clarity.

3.1.2 Activation of H_2

Following from the above calculations, H_2 activation was probed. To test this, a hydride atom was added to the borane where it was then resubmitted for optimisation and single point energy calculations. The Lewis bases were also treated in the same manner except with a proton, excluding those that formed adducts with **1** or were not in chemically relevant orientations. Summarised in Table 3 are these results, calculated using Equation 7.

$$E_{Rel} = (LSAH\ G_{Corr} + LBH\ G_{Corr}) - (LSA\ G_{Corr} + LB\ G_{Corr} + H_2\ G_{Corr}) \quad (7)$$

Table 3. Relative energies for hydrogen activation between **1** and **2**-**20**.

System	ΔG (kcal/mol)
1 + 2	41.3
1 + 5	56.5
1 + 11	58.6
1 + 13	75.0
1 + 14	48.8
1 + 16	54.9
1 + 18	53.1
1 + 20	65.6

Upon initial observation, the above ΔG values do not indicate that H_2 activation would readily occur with **1**. However, computation does not always reflect experimental findings. These energies were computed in the gas phase so it may be that solvation effects play a key role in influencing activation through the favourable solvation of products. In the future, solvent phase calculations could be performed using the polarisable continuum model with an appropriate solvent such as toluene.[33] This would present a more accurate representation of how much effect solvents have. Another point for consideration is that these reactions were modelled using one mole of H_2 per association. Increasing the molar concentration of H_2 in the lab could prove useful as a driving factor in achieving activation.

It is curious that **2** does not show a favourable outcome in the activation of H_2 as this is a well-known compound that has been shown to activate H_2 with $B(C_6F_5)_3$.[35, 111, 112] In this case however, perhaps the dispersion interactions between **1** and this base are too great (and therefore the reversibility of the reaction is hindered due to the associated complex being more stable, ΔG = - 1.0 kcal/mol *vs*. 41.3 kcal/mol for H_2 splitting) whereas the tempered acidity of $B(C_6F_5)_3$ offers a balance between the two.

This could be an interesting case for further functional testing beyond the scope of what was used here to see if this changes the ΔG value. The association energy for **5** is shown to be even more favourable (ΔG = -10.3 kcal/mol) than **2** but again, the energy difference between the associated complexes and for H_2 activation may be too high (ΔG = 56.5 kcal/mol).

Lewis bases **11** and **13** are notable examples, with **13** being the phosphorus analogue of $B(C_6F_5)_3$ and a very weak Lewis base. The difference between their relative energies (ΔG = 58.6 *vs*. 75.0 kcal/mol) can be attributed to the strong electron-withdrawing effects of the pentafluorophenyl rings. Whilst this is advantageous for a Lewis acid, it is counterintuitive for a Lewis base. The removal of the fluoride groups from one of the phenyl rings does improve this slightly due to inductive and resonance effects from the phenyl ring. However, these are not substantial enough to make it a suitable candidate for this type of catalysis, even with the increased Lewis acidity of **1** compared to existing systems.

Lewis bases **14**, **16** and **18** are structurally similar as well as they all have methyl groups in both *ortho* positions. In the case of **16**, this has previously been used in a comparable manner with $B(C_6F_5)_3$ to facilitate the hydrogenation of CO_2 in the presence of a silyl halide in which the silyl halide acts as an oxophile in the presence of an FLP derived from $B(C_6F_5)_3$ and **16** with H_2 to form hydrogenation products.[113] All three are effective Lewis bases due to the inductive effects from the methyl groups around the phenyl ring and nitrogen. The ΔG values are high for all three in the context of activating H_2 (ΔG = 48.8, 54.9 and 53.1 kcal/mol respectively) when comparing these to the association energies (ΔG = 1.6, 1.2 and 4.6 kcal/mol respectively) so this reaction may not occur experimentally due to the association complexes being the more stable states. This does not entirely preclude them from synthetic consideration though as changing reaction conditions (such as the ones discussed above) could mean these are feasible choices. **20** is a moderately strong base due to the nitrogen centre not being conjugated with the terphenyl rings. This is due to the steric bulk and twisting of the terphenyl

groups forcing them out of orbital alignment with the *p*-orbitals on the nitrogen atom, thus disrupting conjugation.[114] Its bulk is advantageous for association with **1** (ΔG = -4.2 kcal/mol) however this is implied to be a hindrance when splitting H_2. Because of its size, crowding may be too great around the nitrogen atom for it to participate in bonding with H_2 which explains its high energy requirement (ΔG = 65.6 kcal/mol). With this base, it is unlikely that splitting will be seen with **1**, even with modified experimental conditions.

A different aspect to consider is the deformation energy needed for the pyramidalisation of **1**. By using a simplified method from Hamlin and co-workers,[115] a single point energy calculation of the pyramidalised structure of **1** without the hydride atom was done at the M06-2X/def2-TZVPP level of theory. Subtracting the single point energy value of **1** in its trigonal geometry from this value resulted in a pyramidalisation energy of 38.4 kcal/mol. This could contribute to high ΔG values as the bases may not be strong enough to compensate for the payoff needed to facilitate the geometry change.

4. EXPERIMENTAL RESULTS AND DISCUSSION

4.1 Precursor synthesis

Due to the limited success of this part of the project, it was decided that subsequent efforts were best spent on synthetic works for **1** as commercial precursor was available. Had the below syntheses been successful though, the next stage after producing **24** would have been to convert the di-thiol groups of **24** into SF_4Cl groups using calcium hypochlorite ($CaOCl_2$) and potassium fluoride (KF) to produce **25**. This would have enabled conversion of the resulting intermediate to **26** using silver tetrafluoroborate ($AgBF_4$) as demonstrated in Scheme 17.[116]

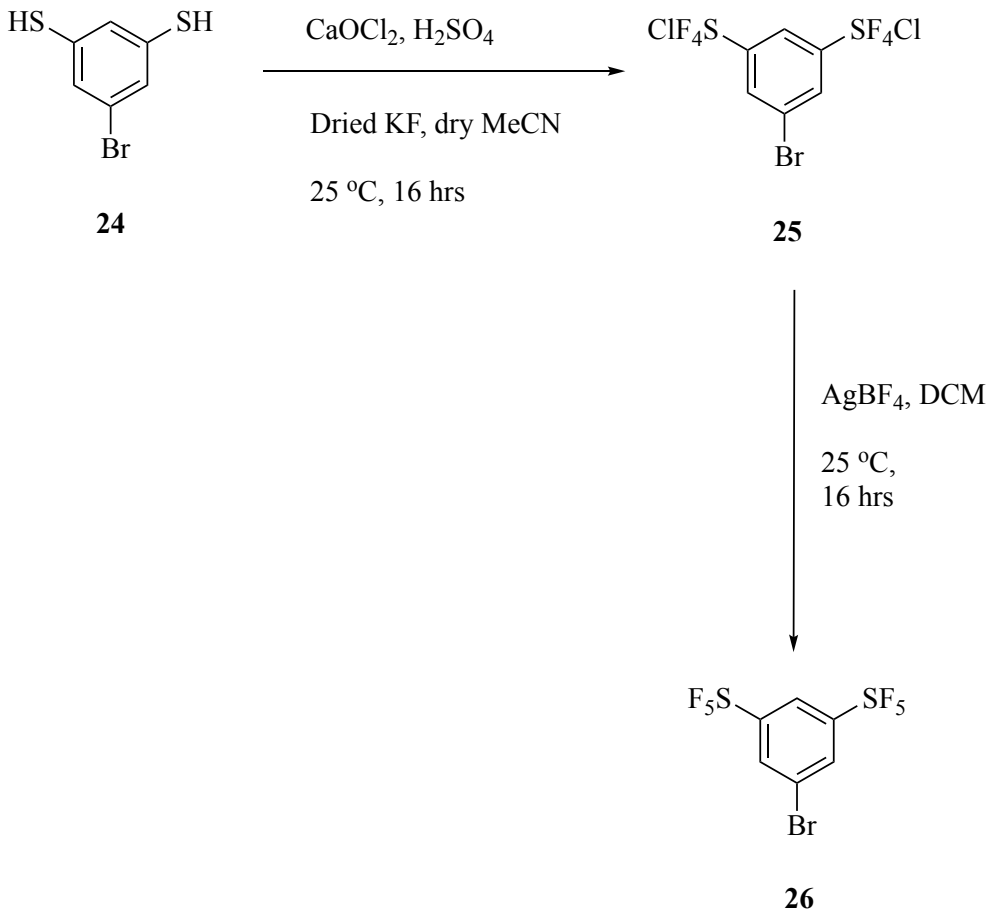

Scheme 17. Synthetic scheme to obtain 1-bromo-3,5-bis(pentafluorosulfanyl)benzene. Adapted from ref. 116.

*4.1.1 Sodium 2-methyl-2-propanethiolate (**22**)*

To access 1-bromo-3,5-bis(pentafluorosulfanyl)benzene, a multi-step synthesis is required. This begins with the deprotonation of 2-methyl-2-propanethiol with sodium hydride (Scheme 18) to produce sodium 2-methyl-2-propanethiolate (**22**).

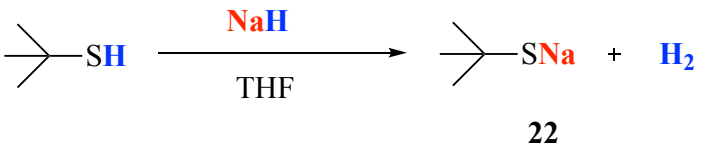

22

Scheme 18. Deprotonation of 2-methyl-2-propanethiol with sodium hydride to form **22**.

Following a protocol reported by Schoenebeck *et al*.[117] in which 2-methyl-2-propanethiol was slowly added to a suspension of sodium hydride under a nitrogen atmosphere, this was successfully isolated as a colourless solid in 80% yield. Analysis by ^{1}H NMR spectroscopy (Figure 9) showed a defined singlet at δ 1.44 ppm consistent with the *tert*-butyl group in the compound. This was used for the next step with no further purification.

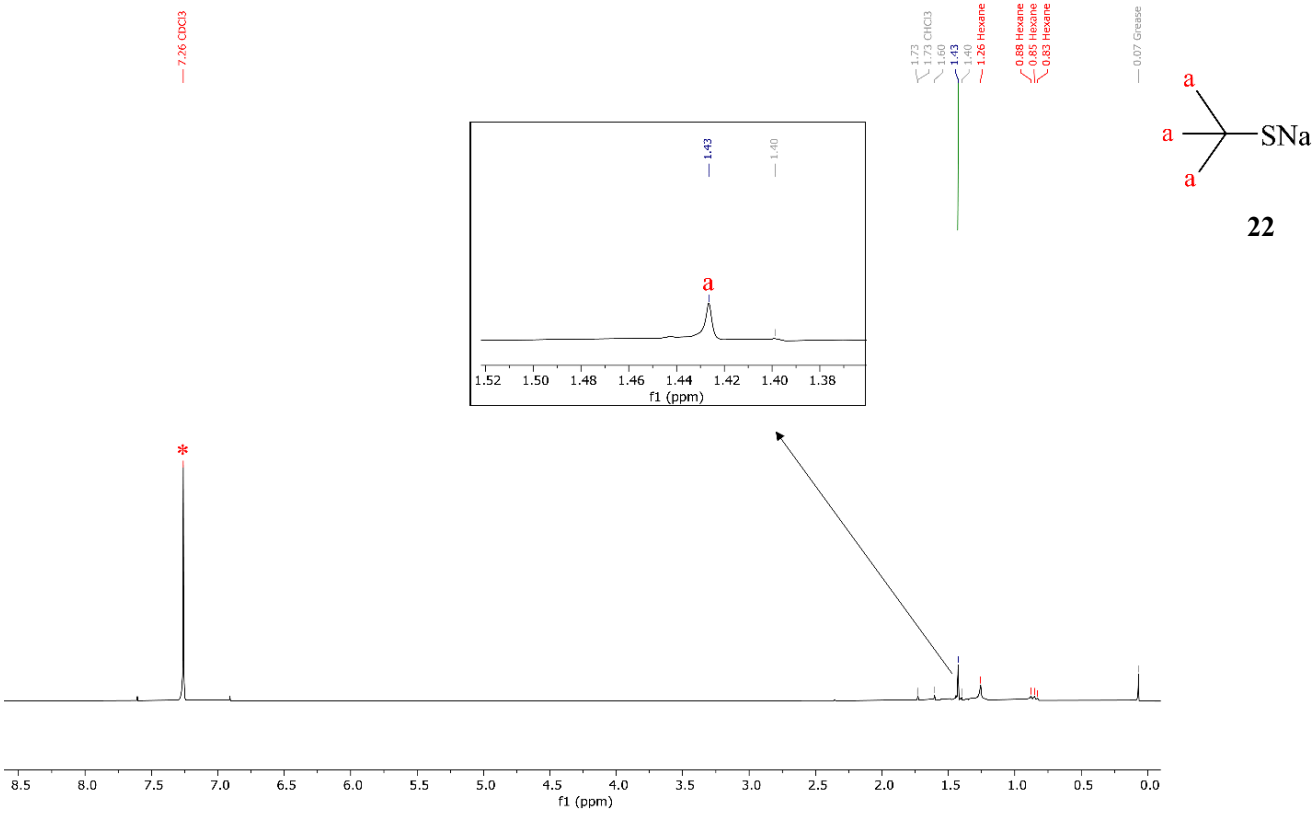

Figure 9. ^{1}H NMR (300 MHz, $CDCl_3$) spectrum of **22**. Inset shows zoomed in region between δ 1.40 – 1.44 ppm. Impurities are highlighted in grey; residual solvent is highlighted in red. * denotes deuterated solvent.

*4.1.2 1,3-bis(tert-butylthio)-5-bromobenzene (**23**)*

The next stage involved converting 1,3,5-tribromobenzene into 1,3-*bis*(tert-butylthio)-5-bromobenzene (**23**) through nucleophilic aromatic substitution using material from the previous step. Due to using a different starting material than the literature, this step took much longer because it recommended cooling the reaction to 0 °C and then allowing it to warm to room temperature. This works with near 100% conversion when using 5-bromo-1,3-difluorobenzene due to the fluorine groups being very reactive. However, because 1,3,5-tribromobenzene was readily available, this was chosen instead. This method was tried multiple times using with no success. The original solvent, *N*-methyl-2-pyrrolidone (NMP), was replaced with 1,3-dimethyl-imidazolidinone (DMI) because it was

suggested that NMP was inactivating the *tert*-butyl thiolate anion before the reaction started. Making this change however had no effect. To exclude possible errors from the previous step, sodium 2-methyl-2-propanethiolate was obtained commercially at 90% purity, again this did not change the outcome. It was only later discovered that compounds containing all bromide substituents needed heating to drive the reaction to completion. This is not a common reaction to carry out and thus the best procedure found reported a 39% yield of **23** after purification.[118] The procedure was replicated (Scheme 19), and a 19% crude yield was obtained. When column chromatography was performed, the isolated yield was a trace amount which was too little material to gain any meaningful information from NMR spectroscopy. The yield is so low due to difficulties performing the column owing to the fact the product is colourless and couldn't be seen on the silica without applying a potassium permanganate stain. When repeated, the reaction was left heating and stirring for 9 days as opposed to the 16 hours reported in an attempt to increase the crude yield. This time, the product was obtained as a brown solid in 53% yield and 90% purity (Figure 10).

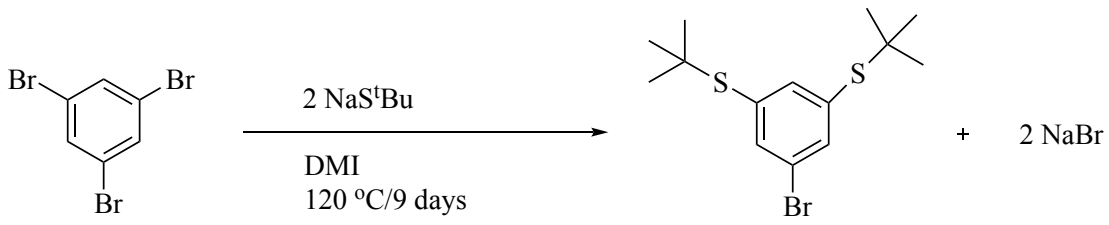

23

Scheme 19. Reaction to form **23**.

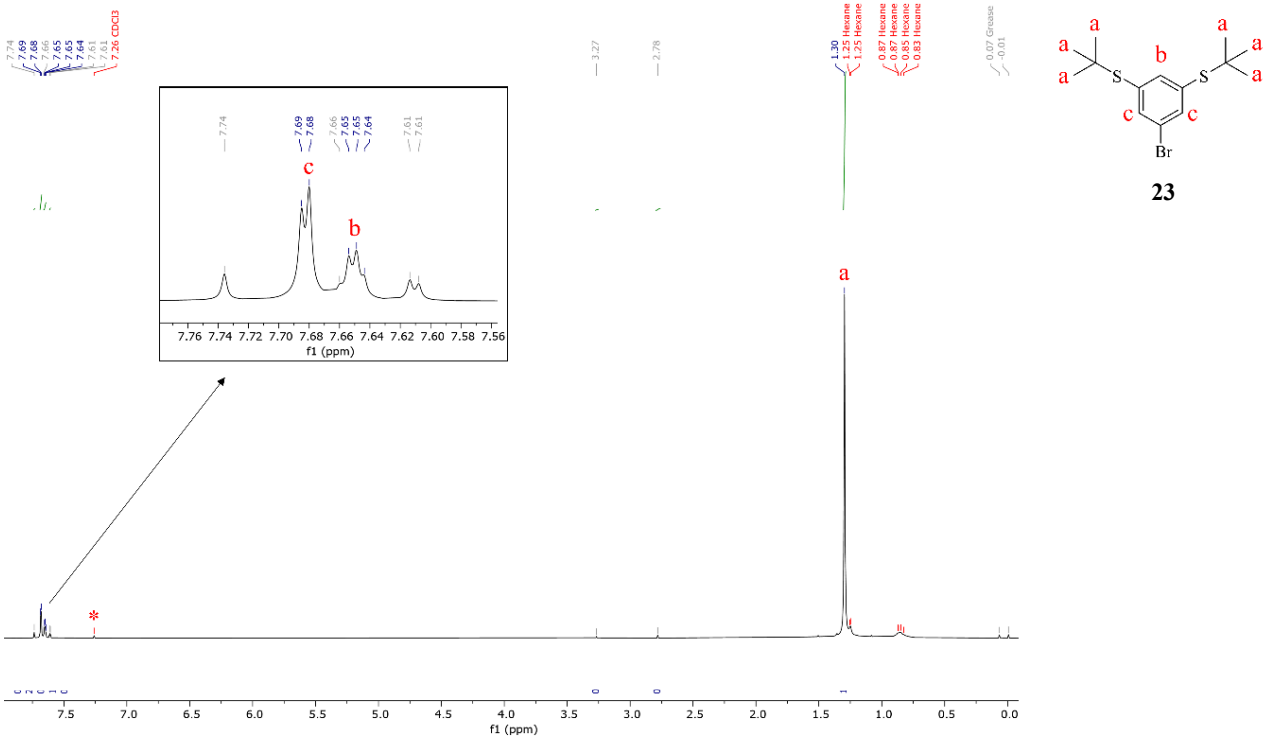

Figure 10. ^{1}H NMR (300 MHz, $CDCl_3$) spectrum of crude **23**. Inset shows zoomed in region between δ 7.61 – 7.74 ppm. Impurities are highlighted in grey; residual solvent is highlighted in red. * denotes deuterated solvent.

*4.1.3 5-bromobenzene-1,3,-dithiol (**24**)*

As a proof of concept, this reaction was carried out on a very small scale owing to the amount of pure material acquired from the last step. The reaction uses a catalytic amount of aluminium trichloride ($AlCl_3$), a known Lewis acid (Scheme 20).

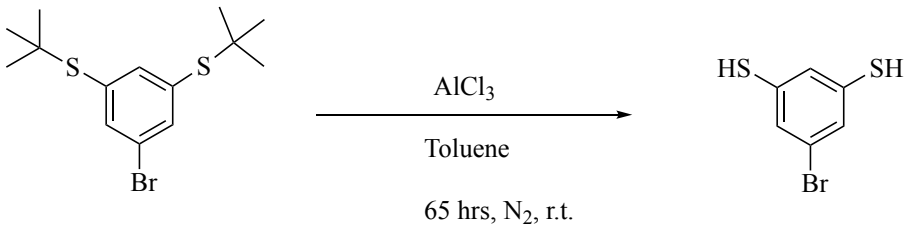

Scheme 20. Reaction of **23** with $AlCl_3$ to form **24**. Only major product shown.

The product was obtained through organic separation which yielded a colourless solid and analysed through ^{1}H NMR spectroscopy. Due to the amount of material produced (2 mg), it was not clear whether the reaction had worked as the signals were inconclusive.

4.2 Borane synthesis

To corroborate the computational data detailed in the previous chapter, we moved on to targeting the synthesis borane **1**. Preliminary efforts focused on making the analogous CF_3-containing borane (**27**) reported by Ashley *et al.*[27] and then the synthesis of **1**.

4.2.1 Solution state reaction for tris[(3,5-bis(trifluoromethyl)phenyl]borane

Generation of the Grignard reagent proceeded between isopropyl magnesium chloride (^{i}PrMgCl) and 1,3-bis(trifluoromethyl)-5-bromo-benzene. Nucleophilic attack on ethereal boron trifluoride ($BF_3.OEt_2$) with the Grignard reagent then follows to produce the neutral triaryl borane **27** (Scheme 21).

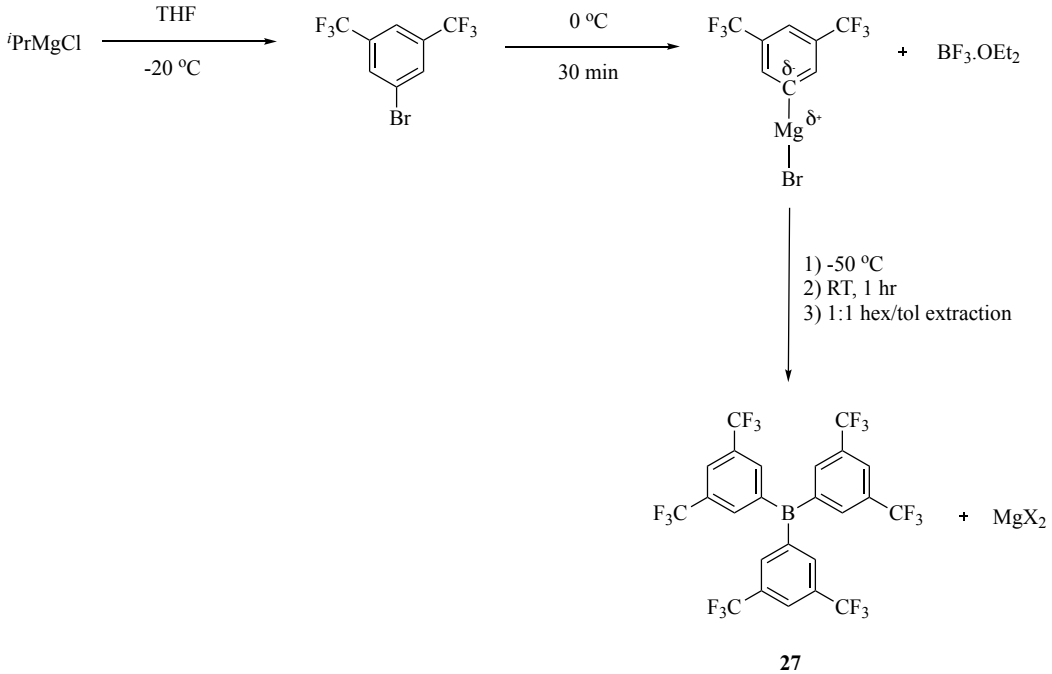

Scheme 21. Nucleophilic substitution reaction to form compound **27**. X = F, Cl, Br. Adapted from ref. 24.

The resultant white powder was isolated in 61% yield with the ^{1}H NMR spectrum confirming presence of the desired species amongst under- and over-substitution products as well as leftover starting material. Attempts to purify the crude material were made *via* sublimation at 100 °C and 2^{-2} mbar vacuum. Slow evaporation recrystallisation was also set up in toluene in the glovebox. Both methods were unsuccessful and did not yield any pure product, however, they gave good ideas for future purification.

4.2.2 Solid state reaction for tris[(3,5-bis(trifluoromethyl)phenyl]borane

After recent reports of air stable Grignard reagent formation through mechanochemistry,[119] the idea of synthesising this borane through solid state means was undertaken (Scheme 22). This would be the first time anyone has formed a borane this way as generally, solution state chemistry is a lot more viable due to being able to carefully control such as maintaining an inert atmosphere in a glove box. Nevertheless, two reactions were set up in milling jars, one with magnesium turnings and 1,3-bis(trifluoromethyl)-5-bromo-benzene and the other with commercial ^{i}PrMgCl. The idea was to compare whether Grignard formation could be seen through the well-known heterogenous route or whether it could only be done using transmetallation much like in solution state.

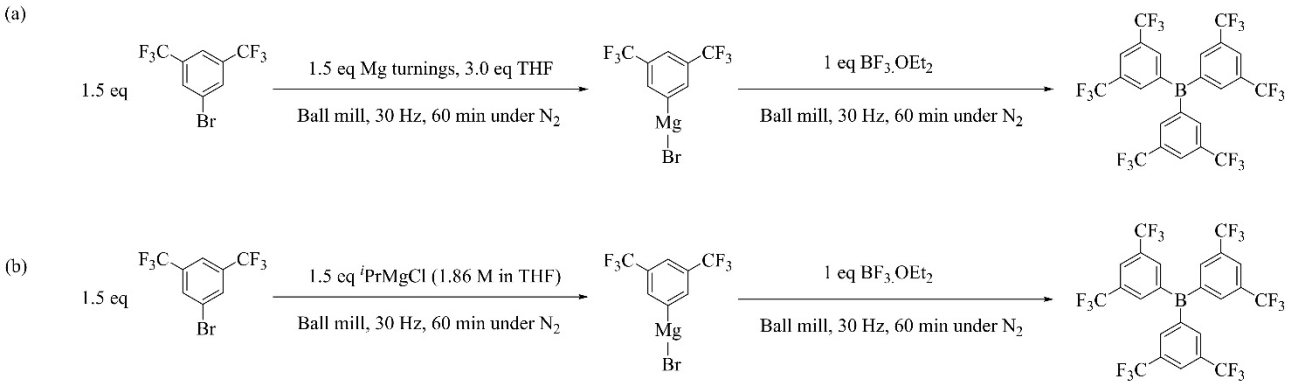

Scheme 22. (a) Formation of **27** using magnesium turnings; (b) Formation of **27** using ^{i}PrMgCl.

Set up was facile; all reagents were added to the milling jar in the glovebox and then placed in the ball mill. It is possible to track milling reactions *in situ* using Raman spectroscopy[120] but due to the nature of the reagents and the conditions needed, titanium milling jars were used which prevented this from being an option. Given this, there was no way to track formation of the Grignard reagent so it was decided that the procedure would be carried through to the next step where $BF_3.OEt_2$ was added and then was milled for 1 hour. When the reactions had finished, multinuclear NMR spectroscopy was difficult as the material formed was very viscous and did not readily dissolve in deuterated solvents. This meant it was not possible to obtain a sample of good enough quality for analysis by multinuclear NMR spectroscopy. Given these results, these reactions were not explored any further and efforts returned to solution state reactions.

*4.2.3 Tris[(3,5-bis(pentafluorosulfanyl)phenyl]borane (**1**)*

Results obtained from the previous reaction provided a foundation in which to start making **1**. Investigations began with combining 3 equivalents of 1-bromo-3,5-bis(pentafluorosulfanyl)benzene with a slight excess of ^{i}PrMgCl and 1 equivalent of $BF_3.OEt_2$ (Scheme 23). Attempts to avoid over-substitution were made through careful stoichiometric control of the aryl Grignard and $BF_3.OEt_2$. The SF_5-substituted aryl Grignard reagent was generated through transmetallation with ^{i}PrMgCl as it was noted with *tetrakis*[3,5-bis(pentafluorosulfanyl)phenyl]borate when synthesis was attempted *via* the heterogenous route with magnesium turnings, unreacted starting material was recovered.[53]

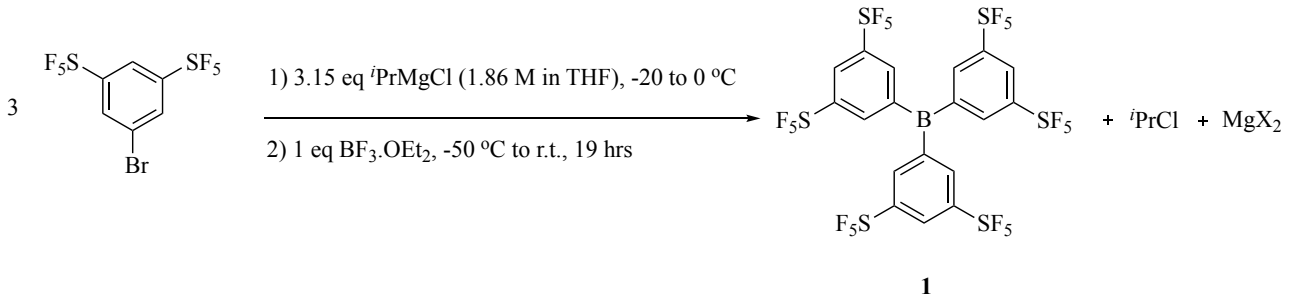

1

Scheme 23. Synthetic route for **1** using $BF_3.OEt_2$. X = F, Cl, Br. Adapted from ref. 53.

Upon completion, an amber oil was extracted with a 1:1 hexane/toluene mixture where the volatiles where then removed to yield the product as seen when analysed by multinuclear NMR spectroscopy. Unfortunately, there was also evidence of a mixture of mono- and di-substituted products. Attempts to obtain single crystals through slow evaporation recrystallisation in various solvents proved unsuccessful with precipitate being produced. It was noted that this mixture had poor solubility in hexane so vapour diffusion recrystallisation was set up with different ethereal solvents. This also yielded impure material and no crystals suitable for single crystal x-ray diffraction analysis.

Due to THF being present from the ^{i}PrMgCl solution, the complex was indicated to be present as the THF adduct. Removing the solvent through vacuum and heating over a period of time did not work with the THF adduct still being present in the ^{1}H NMR spectrum (Figure 11a). The ^{11}B NMR spectrum further confirmed presence of the adduct, evidenced by a sharp peak typical of borates at δ 0.1 ppm (Figure 11b). The tetra-aryl substituted species was ruled out as that is known to come at δ -5.8 ppm.[53] Ideally in the future, the procedure would be carried out purely in diethyl ether as this is not bound as strongly to boron. Modifying the extraction step, various solvents in increasing polarities were investigated to eliminate under-substituted by-products based on solubilities. Again, this failed to segregate the product. The reaction was heated to reflux before extraction as is common in the protocol for $B(C_6F_5)_3$[121] in hopes to drive substitution forward and reduce the quantity of side products. This was ineffective as the greatest crude yield of **1** obtained was 69% however when

analysed by ^{1}H NMR spectroscopy, still showed a mixture of mono- and di-substituted products. Subsequently, efforts moved towards trying a different boron source for a cleaner conversion.

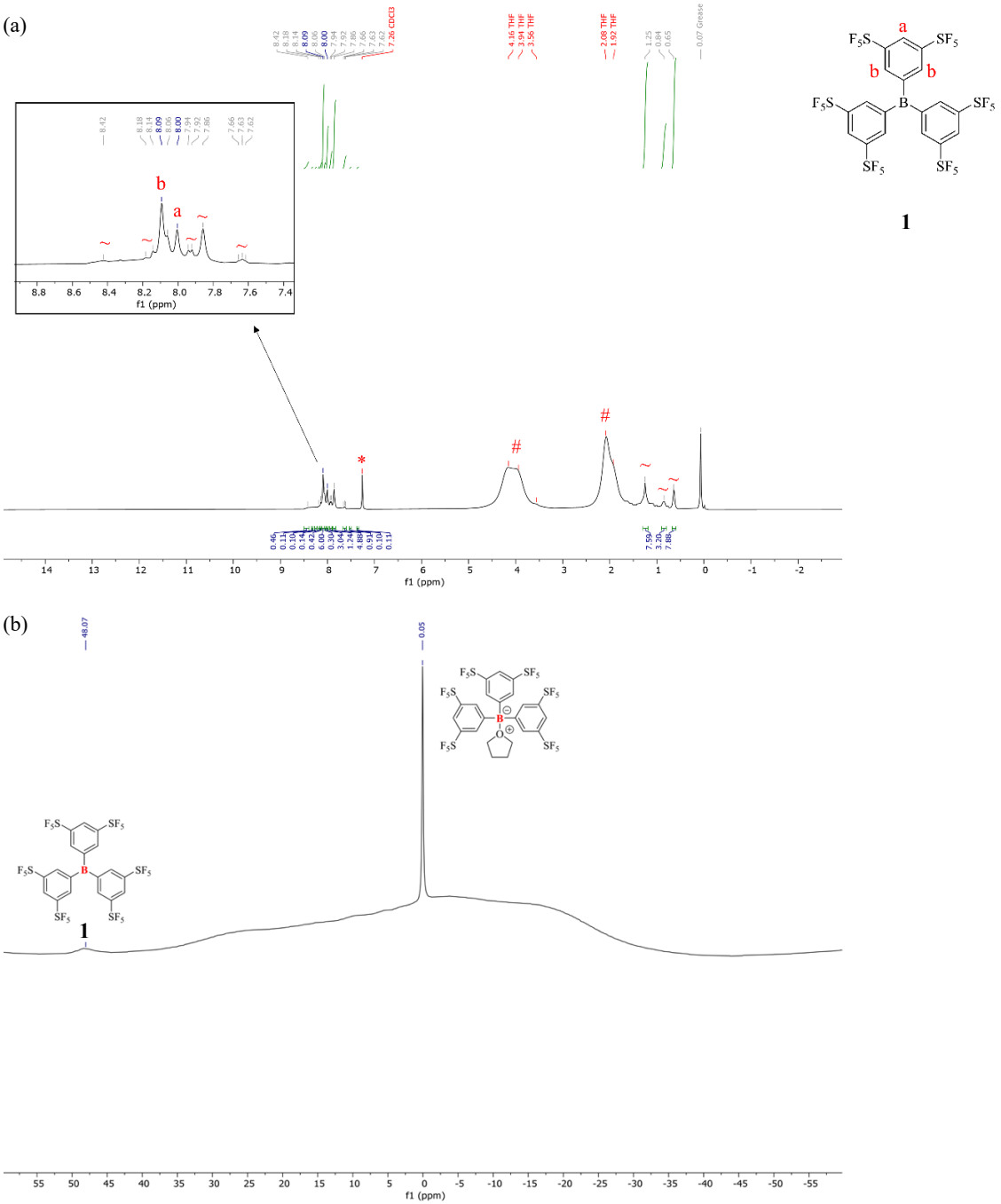

Figure 11. (a) ^{1}H NMR (300 MHz, $CDCl_3$) spectrum of **1** using $BF_3.OEt_2$. Inset shows zoomed in region between δ 7.62 – 8.42 ppm. * denotes deuterated solvent, ~ represents impurities and # is residual THF; (b) ^{11}B {^{1}H} NMR (128 MHz, $CDCl_3$) spectrum of **1** using $BF_3.OEt_2$.

Changing the boron source to BCl_3 in heptane but following the same protocol, gave a cleaner conversion with fewer side products being seen in the ^1H NMR spectrum (Figure 12). First attempts at this used DCM in the extraction step followed by a hexane wash in an endeavour to extract the product. This did not give the desired isolated product, so the reaction was repeated ensuring rigorous Schlenk conditions to eliminate any risk of contamination. Subsequent attempts also did not yield **1** in isolation.

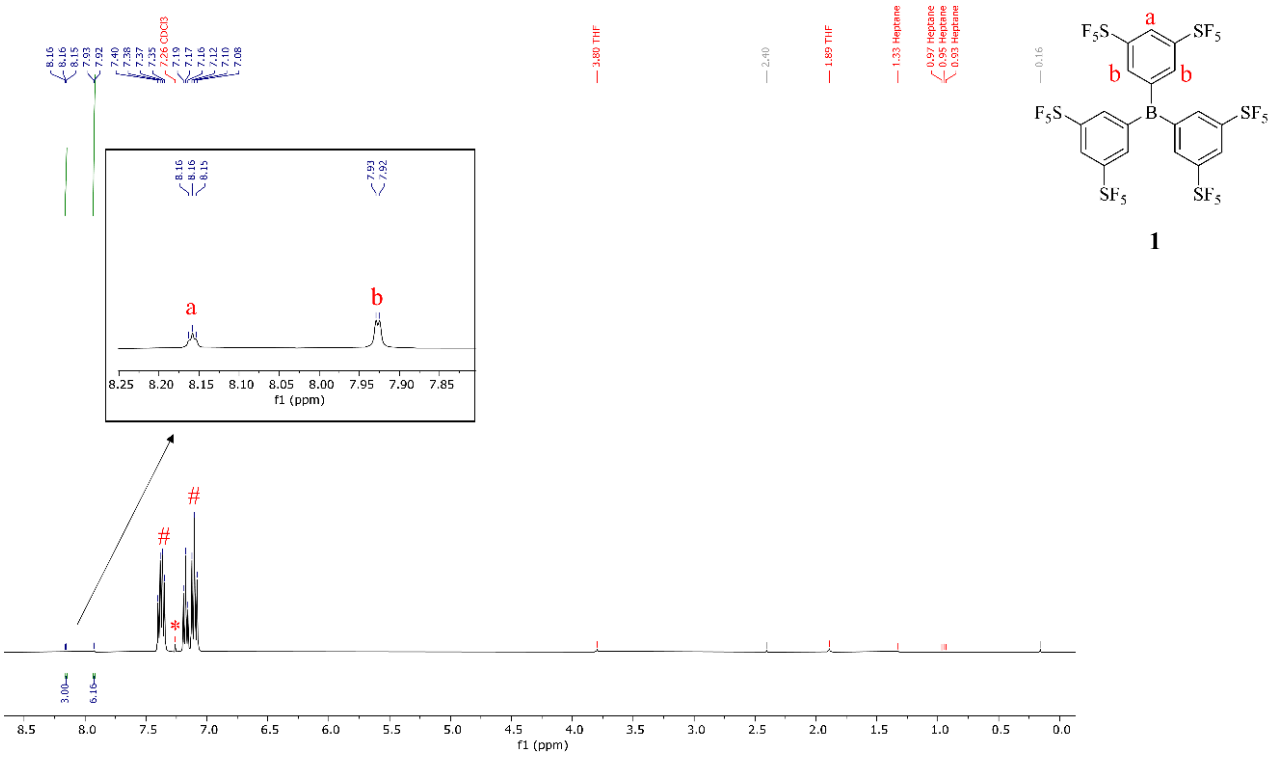

Figure 12. ^1H NMR (300 MHz, $CDCl_3$) spectrum of **1** using BCl_3 in heptane (post DCM extraction). Inset shows zoomed in region between δ 7.92 – 8.16 ppm. Impurities are highlighted in grey. # denotes fluorobenzene standard used and * denotes deuterated solvent.

5. CONCLUSIONS AND FUTURE WORK

This thesis has described the design, synthesis and applications of a novel boron-based LSA. Discussions have shown that this complex has many potential applications within Lewis acid catalysis[12, 13] and FLP chemistry.[20, 22] Preliminary experimental work started exploring various solid and solution state synthetic routes to access *tris*[(3,5-bis(pentafluorosulfanyl)phenyl]borane (Figure 13). Whilst there were difficulties obtaining it in a pure state, solution state proved to be the better route as solid state presented too many problems when trying to analyse it *via* multinuclear NMR spectroscopy. Using BCl_3 in heptane as the boron source rather than $BF_3.OEt_2$ proved to be more promising as the conversion was cleaner, however more attention is required for separating the crude mixture and obtaining a crystal suitable for x-ray crystallography. In the future, the time the crude mixture is left to stir can also be modified to see whether this yields any better results to aid separation.

Synthetic routes to access the precursor 1-bromo-3,5-bis(pentafluorosulfanyl)benzene (**26**) (Figure 13) were explored. These reactions proved to be difficult as they are not widely performed in literature and whilst it is cheaper to synthesise **26** in-house rather than purchase it, many problems were encountered which need further consideration. In the future, this could be revisited when there are less time constraints as the purification steps could be modified *e.g.* using an auto column which identifies UV-active compounds with greater accuracy than using a glass column.

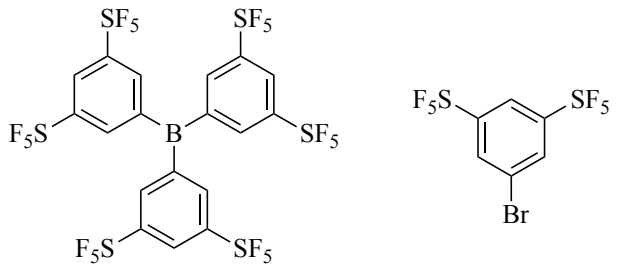

1

26

Figure 13. Structure of **1** and **26**.

The calculated FIA and HIA values of **1** show that it is much stronger than $B(C_6F_5)_3$ so this is an interesting point to explore in the context of organocatalysis as well as FLP catalysis. DFT studies aided investigations by allowing rapid screening of many Lewis bases which could save vast time when carrying out experimental work. It was shown that when **1** is combined with bases **2**, **5**, **11**, **13**, **14**, **16**, **18** and **20**, FLP formation occurs. Although H_2 activation was not shown to occur spontaneously with any of these, bases **2**, **5**, **14**, **16** and **18** could behave differently in synthesis under different conditions *e.g.* the moles of H_2 could be increased experimentally as only one mole of H_2 was used computationally, this could perhaps encourage activation.

For the continuation of this work, the next step would be to purify and test **1** in catalytic reactions against known compounds such as $B(C_6F_5)_3$ and $BArF_{18}$ *e.g.* using it as a co-catalyst in the polymerisation of olefins[12, 13] and to heterolytically split H_2[27] to see how it performs. It is hoped that it can facilitate challenging organic transformations that its predecessors cannot, allowing for the expansion of main group catalysis. Measurements such as the Gutmann-Beckett method[66] will also be done to see whether theoretical data is reflective of experimental findings.

Overall, the work carried out in this thesis has been an interesting exploration into the foundations of a novel Lewis superacid which has revealed a lot of exciting avenues for exploration in the future.

6. EXPERIMENTAL

6.1 Computational details

All DFT calculations were submitted to University of Birmingham's BlueBEAR HPC service and performed using Gaussian 09.[122] Geometry optimisations and frequency calculations were carried out at the M06-2X/def2-SVP level of theory with Grimme's D3 dispersion correction[123] and disabled symmetry. For all optimised structures, the absence of any imaginary frequencies (no negative Eigenvalues) confirmed that each structure was located at a minimum. Single point energies were performed at the M06-2X/def2-TZVPP level of theory on every atom. Visualisation of optimised structures was done using Avogadro2[124] and Chemcraft 1.8.[125]

6.2 Materials and general experimental details

Unless otherwise stated, all experiments were manipulated under an inert oxygen-free N_2 atmosphere using a standard Schlenk line and MBraun Unilab Pro SP glovebox. All glassware and Teflon-coated magnetic stirrers were dried at 80 °C overnight and further dried with a heat gun under vacuum when in use. All protiated solvents were dried and degassed using 3 Å molecular sieves (VWR chemicals, activated under vacuum at 400 °C prior to use) and the freeze-pump-thaw method. Toluene and THF were obtained from a solvent purification system with THF being refluxed over Na/benzophenone prior to drying and degassing. Hexane, DMI and NMP were obtained commercially (Sigma-Aldrich) and dried. Deuterated solvents were dried overnight with CaH_2, distilled then stored over molecular sieves for 24 hours before degassing.

1-bromo-3,5-bis(pentafluorosulfanyl)-benzene (UBE Industries – Japan) was purchased in ≥ 95% and ≥ 99% purity and used as received. ^{i}PrMgCl (1.86 M in THF) and BCl_3 (0.98 M in heptane) (Sigma-Aldrich) were used as received. BF_3 in diethyl ether (Sigma-Aldrich) was degassed prior to use. An

adaptation of the reported procedures for the synthesis of *tris*[(3,5-trifluoromethyl)phenyl]borane[27] and *tetrakis*(3,5-bis(pentafluorosulfanyl)phenyl]borate[53] were used for the synthesis of **1**. For the synthesis of 1-bromo-3,5-bis(pentafluorosulfanyl)-benzene, adapted literature procedures were used.[117] 1,3,5-tribromobenzene, sodium *tert*-butyl thiolate and aluminium trichloride were all purchased from Sigma-Aldrich and used as received.

TLC analysis was carried out on aluminium-backed silica plates (Machery-Nagel) with visualisation of spots being achieved both by the quenching of UV-light and a $KMnO_4$ stain. All column chromatography was carried out using technical grade 60 Å, 40-63 μm silica gel (Fluorochem).
NMR spectra were obtained on either a Bruker 300 MHz spectrometer fitted with a Bruker 7.04 T Ultrashield magnet, or a Bruker 400 MHz spectrometer fitted with a Bruker 9.39 T Ultrashield magnet. All spectra were carried out at 298 K with ^{1}H NMR spectra being internally referenced to residual protiated solvent. $^{11}B\{^{1}H\}$ NMR spectra are externally referenced to $BF_3.OEt_2$ and $^{19}F\{^{1}H\}$ NMR spectra are externally referenced to $CFCl_3$ unless otherwise stated.

Mass spectrometry data was collected using a Waters Atmospheric Solids Analysis Probe (ASAP) which utilises Atmospheric Pressure Ionisation (API) on a Waters Xevo G2-XS ToF spectrometer in negative ion mode.

6.3 Precursor synthesis

*6.3.1 Sodium 2-methyl-2-propanethiolate (**22**)*

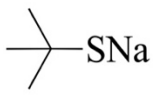

2-methyl-2-propanethiol (0.47 mL, 4.17 mmol, 1 eq) in THF (1 mL) was carefully added dropwise to a suspension of NaH (167 mg, 4.17 mmol, 1 eq) in THF (10 mL) where it was then left to stir at room temperature overnight. To the white precipitate that had formed, hexane (17 mL) was added,

and the mixture stirred for 10 minutes. The volatiles were removed under vacuum to yield sodium 2-methyl-2-propanethiolate as a white powder in 71% purity. This was used in the next step without any further purification. Isolated yield: 373 mg, 80%.

^{1}H NMR (300 MHz, $CDCl_3$): δ 1.43 (s, 9H, CH_3).

*6.3.2 1,3-bis(tert-butylthio)-5-bromobenzene (**23**)*

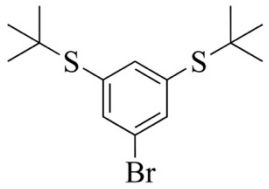

<u>*Route A:*</u>

Sodium *tert*-butylthiolate (400 mg, 3.566 mmol, 1.99 eq) was slowly added to a Schlenk flask containing 1,3,5-tribromobenzene (562 mg, 1.784 mmol, 1 eq) in DMI (4.40 mL) then heated to 120 °C for 2 days. The reaction was subsequently quenched by pouring the mixture directly into brine (20 mL) where toluene (20 mL) was added. The organic layer was separated, and the aqueous layer was extracted two further times. The combined organic layers were dried over $MgSO_4$, filtered and then dried under vacuum. Purified via column chromatography with hexane to obtain 1,3-bis(tert-butylthio)-5-bromobenzene as a white solid. Isolated yield: 8.40 mg, 1.4%.

^{1}H NMR (300 MHz, $CDCl_3$): δ 7.69 (d, J = 1.5 Hz, 2H, Ar-H), 7.66 (t, J = 1.5 Hz, 1H, Ar-H), 1.30 (s, 18H, CH_3).

<u>*Route B:*</u>

Sodium *tert*-butylthiolate (800 mg, 7.132 mmol, 1.99 eq) was slowly added to a Schlenk flask containing 1,3,5-tribromobenzene (1123 mg, 3.568 mmol, 1 eq) in DMI (8.80 mL) then heated to 120 °C for 9 days. The reaction was subsequently quenched by pouring the mixture directly into brine (20

mL) where hexane (20 mL) was added. The organic layer was separated, and the aqueous layer was extracted two further times. The combined organic layers were dried over $MgSO_4$, filtered and then dried under vacuum to obtain 1,3-bis(tert-butylthio)-5-bromobenzene as an impure brown solid. Isolated yield: 53%, 632 mg. This was used in the next step without any further purification.

^{1}H NMR (300 MHz, $CDCl_3$): δ 7.68 (d, *J* = 1.5 Hz, 2H, Ar-H), 7.65 (t, *J* = 1.5 Hz, 1H, Ar-H), 1.30 (s, 18H, CH_3).

*6.3.2 5-bromobenzene-1,3-dithiol (**24**)*

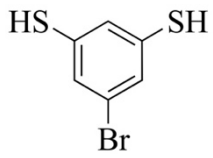

1,3-bis(tert-butylthio)-5-bromobezene (8.40 mg, 0.0252 mmol, 5.60 eq) was added to dry toluene (0.6 mL) and stirred for a couple of minutes until fully dissolved. $AlCl_3$ (0.60 mg, 0.00450 mmol, 1 eq) was then quickly added and the solution was left stirring for 3 days. After this time, the reaction was quenched and agitated with 1 M aq. HCl (10 mL), saturated brine (10 mL) and hexane (10 mL). The organic layer was separated and dried over $MgSO_4$, filtered and then dried under vacuum. Isolated yield: 36%, 2 mg.

Note: The data obtained from the ^{1}H NMR spectrum was inconclusive due to the amount of material present in the sample.

6.4 Synthesis of Tris[3,5-bis(pentafluorosulfanyl)phenyl]borane (1)

6.4.1 Using $BF_3.OEt_2$

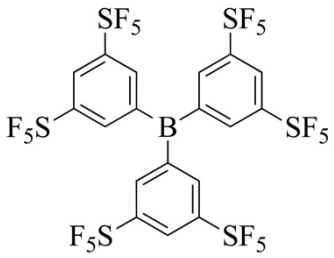

1-bromo-3,5-bis(pentafluorosulfanyl)benzene (100 mg, 0.244 mmol, 3 eq) in diethyl ether (0.98 mL) was added to an oven-dried Schlenk flask and cooled to -20 °C. ^{i}PrMgCl (1.86 M in THF, 0.137 mg, 0.14 mL, 0.257 mmol, 3.15 eq) was slowly added and the reaction mixture was allowed to warm to 0 °C. The flask was then cooled to -50 °C where $BF_3.OEt_2$ (11.50 mg, 10 mL, 0.081 mmol, 1 eq) was added dropwise where it was then warmed to room temperature and monitored to completion *via* multinuclear NMR spectroscopy. After completion, the desired product was separated from residual magnesium salts with hexane/toluene (1:1, 3 x 2 mL) to obtain *tris*(3,5-bis(pentafluorosulfanyl)phenyl]borane as a white solid. Isolated yield: 55.8 mg, 69%.

^{1}H NMR (400 MHz, $CDCl_3$): δ 8.09 (s, 6H, Ar-H), 8.00 (s, 3H, Ar-H).

^{11}B {^{1}H} NMR (128 MHz, $CDCl_3$): δ 48.1, 0.1.

^{19}F {^{1}H} NMR (377 MHz, $CDCl_3$): δ 82.7 (quint, $^{2}J_{FF}$ = 165.4 Hz, F_{ax}), 62.9 (d, $^{2}J_{FF}$ = 160 Hz, F_{eq}).

ASI – MS (negative): calcd. for $C_{18}H_9BF_{30}S_6$ = 997.8646; found = 997.8656.

6.4.2 Using BCl_3 (0.98 M in heptane)

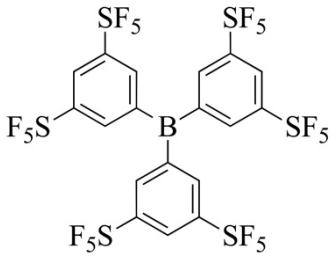

Route A:

1-bromo-3,5-bis(pentafluorosulfanyl)benzene (100 mg, 0.244 mmol, 3 eq) in diethyl ether (0.98 mL) was added to an oven-dried Schlenk flask and cooled to -20 °C. ^{i}PrMgCl (1.86 M in THF, 0.137 mg, 0.14 mL, 0.257 mmol, 3.15 eq) was slowly added and the reaction mixture was allowed to warm to 0 °C. The flask was then cooled to -50 °C and BCl_3 (0.98 M in heptane, 9.53 mg, 83 µL, 0.0815 mmol, 1 eq) was added dropwise where it was then warmed to room temperature. After completion, the desired product was separated from residual magnesium salts with DCM (3 x 2 mL) and then hexane (3 x 2 mL) to obtain *tris*(3,5-bis(pentafluorosulfanyl)phenyl]borane as an impure white solid. Isolated yield: 18%, 15 mg.

^{1}H NMR (400 MHz, $CDCl_3$): δ 8.11 (t), 7.89 (d, *J* = 1.9 Hz), 7.78 – 7.75 (m), 7.57 (d, *J* = 1.6 Hz).

^{11}B {^{1}H} NMR (128 MHz, $CDCl_3$): signal:noise ratio too great to see any peaks (see Figure A9 in appendix).

^{19}F {^{1}H} NMR (377 MHz, $CDCl_3$): δ 84.4 – 82.3 (m), 80.5 (q), 63.5 – 62.4 (m).

Route B:

1-bromo-3,5-*bis*(pentafluorosulfanyl)benzene (100 mg, 0.244 mmol, 3 eq) in diethyl ether (0.98 mL) was added to an oven-dried Schlenk flask and cooled to -78 °C. ^{i}PrMgCl (1.86 M in THF, 0.137 mg, 0.14 mL, 0.257 mmol, 3.15 eq) was then slowly added. The reaction mixture was stirred at -78 °C for 5 minutes and then at 0 °C for 25 minutes. The flask was then warmed to room temperature over the

course of an hour where it was again cooled to 0 °C for 10 minutes. BCl_3 (0.98 M in heptane, 9.53 mg, 83 µL, 0.0815 mmol, 1 eq) was added dropwise and the reaction was left to stir at room temperature for 19 hours. After completion, the product was extracted with a 1:1 hexane/toluene mixture (3 x 2 mL) to obtain *tris*[3,5-*bis*(pentafluorosulfanyl)phenyl]borane as an impure white solid. Isolated yield: 14%, 11 mg.

^{1}H NMR (400 MHz, $CDCl_3$): δ 8.14 (t, *J* = 1.9 Hz), 7.91 (d, *J* = 1.9 Hz).

^{11}B {^{1}H} NMR (128 MHz, $CDCl_3$): signal:noise ratio too great to see any peaks (see Figure A12 in appendix).

^{19}F {^{1}H} NMR (377 MHz, $CDCl_3$): δ 82.2 – 81.2 (m), 81.1 – 79.1 (m), 63.4 – 62.4 (m).

Data for leftover material post-extraction:

^{1}H NMR (400 MHz, $CDCl_3$): δ 8.16 (t, *J* = 1.9 Hz, 3H), 7.93 (d, *J* = 1.9 Hz, 6H).

^{11}B {^{1}H} NMR (128 MHz, $CDCl_3$): signal:noise ratio too great to see any peaks (see appendix).

^{19}F {^{1}H} NMR (377 MHz, $CDCl_3$): δ 80.5 (quint, $^2J_{FF}$ = 165 Hz, F_{ax}), 63.0 (d, $^2J_{FF}$ = 151.2 Hz, F_{eq}).

7. REFERENCES

1. G. N. Lewis, *J. Frank. Inst.*, 1938, **226**, 293-313.
2. T. M. Lowry, *J. Soc. Chem. Ind.* , 1924, **43**, 17.
3. P. Muller, *Pure Appl. Chem.*, 1994, **66**, 1077-1184.
4. M. Teruaki, N. Koichi and B. Kazuo, *Chem. Lett.*, 1973, **2**, 1011-1014.
5. O. Sereda, S. Tabassum and R. Wilhelm, in *Asymmetric Organocatalysis*, ed. B. List, Springer Berlin Heidelberg, Berlin, Heidelberg, 2009, pp. 86-117.
6. K. Maruoka, *J. Am. Chem. Soc.*, 2011, **133**, 8834–8837.
7. J. R. Lawson and R. L. Melen, in *Organometallic Chemistry: Volume 41*, eds. N. J. Patmore and P. Elliott, The Royal Society of Chemistry, 2017, vol. 41, pp. 1-27.
8. F. Vidal, J. McQuade, R. Lalancette and F. Jäkle, *J. Am. Chem. Soc.*, 2020, **142**, 14427-14431.
9. W. E. Piers and T. Chivers, *Chem. Soc. Rev.*, 1997, **26**, 345-354.
10. D. Naumann and W. Tyrra, *J. Chem. Soc., Chem. Comm.*, 1989, DOI: 10.1039/C39890000047, 47-50.
11. A. G. Massey and A. J. Park, *J. Organomet. Chem.*, 1964, **2**, 245-250.
12. G. Erker, G. Kehr and R. Fröhlich, *J. Organomet. Chem.*, 2005, **690**, 6254-6262.
13. X. Yang, C. L. Stern and T. J. Marks, *J. Am. Chem. Soc.*, 1991, **113**, 3623-3625.
14. D. J. Parks and W. E. Piers, *J. Am. Chem. Soc.*, 1996, **118**, 9440-9441.
15. D. J. Parks, R. E. von H. Spence and W. E. Piers, *Angew. Chem. Int. Ed.*, 1995, **34**, 809-811.
16. D. J. Parks, W. E. Piers and G. P. A. Yap, *Organometallics*, 1998, **17**, 5492-5503.
17. R. S. Phatake, A. Averdunk, C. Würtele and U. Gellrich, *ACS Catal.*, 2022, **12**, 13961-13968.
18. M. Hasenbeck, T. Müller, A. Averdunk, J. Becker and U. Gellrich, *Chem. Eur. J.*, 2022, **28**, e202104254.

19. I. Peuser, R. Fröhlich, G. Kehr and G. Erker, *Eur. J. Inorg. Chem.*, 2010, **2010**, 849-853.

20. G. C. Welch, L. Cabrera, P. A. Chase, E. Hollink, J. D. Masuda, P. Wei and D. W. Stephan, *Dalton Trans.*, 2007, 3407-3414.

21. H. C. Brown, H. I. Schlesinger and S. Z. Cardon, *J. Am. Chem. Soc.*, 1942, **64**, 325-329.

22. A. R. Jupp, *Dalton Trans.*, 2022, **51**, 10681-10689.

23. G. C. Welch, R. R. S. Juan, J. D. Masuda and D. W. Stephan, *Science*, 2006, **314**, 1124-1126.

24. T. J. Herrington, A. J. W. Thom, A. J. P. White and A. E. Ashley, *Dalton Trans.*, 2012, **41**, 9019-9022.

25. R. E. Banks, *Appl. Organomet. Chem.*, 1993, **7**, 293-294.

26. F. R. Leroux, B. Manteau, J.-P. Vors and S. Pazenok, *Beilstein J. Org. Chem.*, 2008, **4**, 13.

27. T. J. Herrington, A. J. W. Thom, A. J. P. White and A. E. Ashley, *Dalton Trans.* , 2012, **41**, 9019-9022.

28. P. A. Chase, G. C. Welch, T. Jurca and D. W. Stephan, *Angew. Chem. Int. Ed.*, 2007, **46**, 8050-8053.

29. L. Greb, P. Oña-Burgos, B. Schirmer, S. Grimme, D. W. Stephan and J. Paradies, *Angew. Chem. Int. Ed.*, 2012, **51**, 10164-10168.

30. A. E. Ashley, A. L. Thompson and D. O'Hare, *Angew. Chem. Int. Ed. Engl.*, 2009, **48**, 9839-9843.

31. R. Pal, M. Ghara and P. K. Chattaraj, *Catalysts*, 2022, **12**, 201.

32. A. Paparo, A. L. P. Nguyen, J. S. Silvia, T. P. Spaniol, L. Maron, C. C. Cummins and J. Okuda, *Dalton Trans.*, 2021, **50**, 10692-10695.

33. M. Becerra, M. Real-Enriquez, C. Espinosa-Gavilanes, C. H. Zambrano, R. Almeida, F. J. Torres and L. Rincón, *Theor. Chem. Acc.*, 2016, **135**, 77.

34. M. Heshmat and B. Ensing, *J. Phys. Chem. A.*, 2020, **124**, 6399-6410.

35. G. Skara, F. De Vleeschouwer, P. Geerlings, F. De Proft and B. Pinter, *Sci. Rep.*, 2017, **7**, 16024.

36. D. Himmel, S. K. Goll, I. Leito and I. Krossing, *Angew. Chem. Int. Ed.*, 2010, **49**, 6885-6888.

37. L. Greb, *Chem. Eur. J.*, 2018, **24**, 17881-17896.

38. R. S. Drago, presented in part at the Coordinative Interactions, Berlin, Heidelberg, 1973.

39. R. G. Pearson, *J. Am. Chem. Soc.*, 1963, **85**, 3533-3539.

40. R. S. Drago and B. B. Wayland, *J. Am. Chem. Soc.*, 1965, **87**, 3571-3577.

41. R. S. Drago, G. C. Vogel and T. E. Needham, *J. Am. Chem. Soc.*, 1971, **93**, 6014-6026.

42. G. C. Vogel and R. S. Drago, *J. Chem. Educ.*, 1996, **73**, 701.

43. G. Klopman, *J. Am. Chem. Soc.*, 1968, **90**, 223-234.

44. R. S. Mulliken, *J. Am. Chem. Soc.*, 1952, **74**, 811-824.

45. C. Hansch, A. Leo and R. W. Taft, *Chem. Rev.*, 1991, **91**, 165-195.

46. P. Das, E. Tokunaga and N. Shibata, *Tetrahedron Lett.*, 2017, **58**, 4803-4815.

47. G. Haufe, *Tetrahedron*, 2022, **109**, 132656.

48. J. T. Welch, in *Fluorine in Pharmaceutical and Medicinal Chemistry*, ed. K. M. Véronique Gouverneur, Imperial College Press, London, 2012, vol. 6, pp. 175-207.

49. M. F. Sowaileh, R. A. Hazlitt and D. A. Colby, *ChemMedChem*, 2017, **12**, 1481-1490.

50. P. R. Savoie, C. N. von Hahmann, A. Penger, Z. Wei and J. T. Welch, *Org. Biomol. Chem.*, 2018, **16**, 3151-3159.

51. R. Kordnezhadian, B.-Y. Li, A. Zogu, J. Demaerel, W. M. De Borggraeve and E. Ismalaj, *Chem. Eur. J.*, 2022, **28**, e202201491.

52. V. Debrauwer, I. Leito, M. Lõkov, S. Tshepelevitsh, M. Parmentier, N. Blanchard and V. Bizet, *ACS Org. Inorg. Au*, 2021, **1**, 43-50.

53. D. Langford, I. Göttker-Schnetmann, F. P. Wimmer, L. A. Casper, P. Kenyon, R. F. Winter and S. Mecking, *Organometallics*, 2019, **38**, 2710-2713.

54. D. L. Reger, T. D. Wright, C. A. Little, J. J. Lamba and M. D. Smith, *Inorg. Chem.*, 2001, **40**, 3810-3814.

55. J. Gaffen, *Chem*, 2019, **5**, 1355-1356.

56. P. Erdmann, J. Leitner, J. Schwarz and L. Greb, *ChemPhysChem*, 2020, **21**, 987-994.

57. J. C. Haartz and D. H. McDaniel, *J. Am. Chem. Soc.*, 1973, **95**, 8562-8565.

58. J. W. Larson and T. B. McMahon, *J. Am. Chem. Soc.*, 1985, **107**, 766-773.

59. J. W. Larson and T. B. McMahon, *Inorg. Chem.*, 1987, **26**, 4018-4023.

60. C. G. Krespan and D. A. Dixon, *J. Fluor. Chem.*, 1996, **77**, 117-126.

61. *IUPAC Compendium of Chemical Terminology*, International Union of Pure and Applied Chemistry, 3.0.1 edn., 2019, DOI: doi:10.1351/goldbook.I03272.

62. I. Krossing and I. Raabe, *Chem. Eur. J.*, 2004, **10**, 5017-5030.

63. K. L. Handoo, J. P. Cheng and V. D. Parker, *J. Am. Chem. Soc.*, 1993, **115**, 5067-5072.

64. E. R. Clark, A. Del Grosso and M. J. Ingleson, *Chem. Eur. J.*, 2013, **19**, 2462-2466.

65. D. J. Goebbert and P. G. Wenthold, *Int. J. Mass Spectrom.*, 2006, **257**, 1-11.

66. V. Gutmann, *Coord. Chem. Rev.*, 1976, **18**, 225-255.

67. I. B. Sivaev and V. I. Bregadze, *Coord. Chem. Rev.*, 2014, **270-271**, 75-88.

68. R. F. Childs, D. L. Mulholland and A. Nixon, *Can. J. Chem.*, 1982, **60**, 809-812.

69. G. Hilt and A. Nödling, *Eur. J. Org. Chem.*, 2011, **2011**, 7071-7075.

70. A. G. Pelmenschikov, R. A. van Santen, J. Janchen and E. Meijer, *J. Phys. Chem.*, 1993, **97**, 11071-11074.

71. D. F. Shriver and B. Swanson, *Inorg. Chem.*, 1971, **10**, 1354-1365.

72. D. M. Byler and D. F. Shriver, *Inorg. Chem.*, 1973, **12**, 1412-1416.

73. J. R. Gaffen, J. N. Bentley, L. C. Torres, C. Chu, T. Baumgartner and C. B. Caputo, *Chem*, 2019, **5**, 1567-1583.

74. A. R. Jupp, T. C. Johnstone and D. W. Stephan, *Dalton Trans.*, 2018, **47**, 7029-7035.

75. R. G. Parr, L. v. Szentpály and S. Liu, *J. Am. Chem. Soc.*, 1999, **121**, 1922-1924.

76. N. F. Hall and J. B. Conant, *J. Am. Chem. Soc.*, 1927, **49**, 3047-3061.

77. J. B. Conant and N. F. Hall, *J. Am. Chem. Soc.*, 1927, **49**, 3062-3070.

78. L. A. Mück, A. Y. Timoshkin and G. Frenking, *Inorg. Chem.*, 2012, **51**, 640-646.

79. G. A. Olah, G. K. S. Prakash and J. Sommer, *Science*, 1979, **206**, 13-20.

80. L. O. Müller, D. Himmel, J. Stauffer, G. Steinfeld, J. Slattery, G. Santiso-Quiñones, V. Brecht and I. Krossing, *Angew. Chem. Int. Ed.*, 2008, **47**, 7659-7663.

81. H. H. Hyman, L. A. Quarterman, M. Kilpatrick and J. J. Katz, *J. Phys. Chem.*, 1961, **65**, 123-127.

82. C. J. Hoffman, B. E. Holder and W. L. Jolly, *J. Phys. Chem.*, 1958, **62**, 364-366.

83. J. C. Culmann and J. Sommer, *J. Am. Chem. Soc.*, 1990, **112**, 4057-4058.

84. T. H. Ledford, *J. Org. Chem.*, 1979, **44**, 23-25.

85. P. J. Taylor, *Br. J. Ind. Med.*, 1966, **23**, 318-321.

86. J. F. Kögel, D. A. Sorokin, A. Khvorost, M. Scott, K. Harms, D. Himmel, I. Krossing and J. Sundermeyer, *Chem. Sci.*, 2018, **9**, 245-253.

87. E. Bernhardt, V. Bernhardt-Pitchougina, H. Willner and N. Ignatiev, *Angew. Chem. Int. Ed.*, 2011, **50**, 12085-12088.

88. G. A. Olah, K. Laali and O. Farooq, *J. Org. Chem.*, 1984, **49**, 4591-4594.

89. G. A. Olah, O. Farooq, S. M. F. Farnia and J. A. Olah, *J. Am. Chem. Soc.*, 1988, **110**, 2560-2565.

90. K. K. Laali, B. Geissler, M. Regitz and J. J. Houser, *J. Org. Chem.*, 1995, **60**, 6362-6367.

91. A. P. Davis and M. Jaspars, *Angew. Chem. Int. Ed.*, 1992, **31**, 470-471.

92. L. A. Körte, J. Schwabedissen, M. Soffner, S. Blomeyer, C. G. Reuter, Y. V. Vishnevskiy, B. Neumann, H.-G. Stammler and N. W. Mitzel, *Angew. Chem. Int. Ed.*, 2017, **56**, 8578-8582.

93. M. O. Akram, J. R. Tidwell, J. L. Dutton and C. D. Martin, *Angew. Chem. Int. Ed.*, 2022, **61**, e202212073.

94. M. O. Akram, J. R. Tidwell, J. L. Dutton and C. D. Martin, *Angew. Chem., Int. Ed.*, 2023, **62**, e202307040.

95. A. Osi, D. Mahaut, N. Tumanov, L. Fusaro, J. Wouters, B. Champagne, A. Chardon and G. Berionni, *Angew. Chem. Int. Ed.*, 2022, **61**, e202112342.

96. L. Köring, A. Stepen, B. Birenheide, S. Barth, M. Leskov, R. Schoch, F. Krämer, F. Breher and J. Paradies, *Angew. Chem. Int. Ed.*, 2023, **62**, e202216959.

97. K. Heinze and H. Lang, *Organometallics*, 2013, **32**, 5623-5625.

98. S. Peter and B. A. Aderibigbe, *Molecules*, 2019, **24**, 3604.

99. Y. Kim, H. Zhao and F. P. Gabbaï, *Angew. Chem. Int. Ed.*, 2009, **48**, 4957-4960.

100. M. M. Alharbi, Y. van Ingen, A. Roldan, T. Kaehler and R. L. Melen, *Dalton Trans.*, 2023, **52**, 1820-1825.

101. C. Becker, P. C. Trapp, B. Neumann, H.-G. Stammler and N. W. Mitzel, *Dalton Trans.*, 2022, **51**, 6565-6575.

102. H. Böhrer, N. Trapp, D. Himmel, M. Schleep and I. Krossing, *Dalton Trans.*, 2015, **44**, 7489-7499.

103. M. Akram, J. Tidwell, J. Dutton and C. D. Martin, *Angew. Chem. Int. Ed.*, e202307040.

104. J. P. Perdew and K. Schmidt, *AIP Conf. Proc.*, 2001, **577**, 1-20.

105. S. F. F. Sousa, Pedro A.; Ramos Maria J., *J. Phys. Chem. A.* , 2007, **111**, 10439–10452.

106. Y. Zhao and D. G. Truhlar, *Theor. Chem. Acc.*, 2008, **120**, 215-241.

107. I. Y. Zhang, J. Wu and X. Xu, *Chem. Commun.*, 2010, **46**, 3057-3070.

108. A. I. Briceno-Strocchia, T. C. Johnstone and D. W. Stephan, *Dalton Trans.*, 2020, **49**, 1319-1324.

109. M. Bursch, J.-M. Mewes, A. Hansen and S. Grimme, *Angew. Chem. Int. Ed.*, 2022, **61**, e202205735.

110. T. Wiegand, H. Eckert, O. Ekkert, R. Fröhlich, G. Kehr, G. Erker and S. Grimme, *J. Am. Chem. Soc.*, 2012, **134**, 4236-4249.

111. F. G. Fontaine and D. W. Stephan, *Philos. Trans. R. Soc., A.*, 2017, **375**.

112. R. Gupta, D. Csókás, K. Lye and R. D. Young, *Chem. Sci.*, 2023, **14**, 1291-1300.

113. T. Wang, M. Xu, A. R. Jupp, Z.-W. Qu, S. Grimme and D. W. Stephan, *Angew. Chem. Int. Ed.*, 2021, **60**, 25771-25775.

114. M.-J. Kim, M. Ahn, M. Chae, S. Kim, D. Kim and K.-R. Wee, *RSC Adv.*, 2021, **11**, 34945-34954.

115. D. Rodrigues Silva, L. de Azevedo Santos, M. P. Freitas, C. F. Guerra and T. A. Hamlin, *Chem. Asian J.*, 2020, **15**, 4043-4054.

116. T. Umemoto, L. M. Garrick and N. Saito, *Beilstein J. Org. Chem.*, 2012, **8**, 461-471.

117. T. Scattolin, E. Senol, G. Yin, Q. Guo and F. Schoenebeck, *Angew. Chem. Int. Ed.*, 2018, **57**, 12425-12429.

118. A. Błaszczyk, M. Elbing and M. Mayor, *Org. Biomol. Chem.*, 2004, **2**, 2722-2724.

119. R. Takahashi, A. Hu, P. Gao, Y. Gao, Y. Pang, T. Seo, J. Jiang, S. Maeda, H. Takaya, K. Kubota and H. Ito, *Nat. Commun.*, 2021, **12**, 6691.

120. L. Batzdorf, F. Fischer, M. Wilke, K.-J. Wenzel and F. Emmerling, *Angew. Chem. Int. Ed.*, 2015, **54**, 1799-1802.

121. T. A. Gazis, B. A. J. Mohajeri Thaker, D. Willcox, D. M. C. Ould, J. Wenz, J. M. Rawson, M. S. Hill, T. Wirth and R. L. Melen, *Chem. Commun.*, 2020, **56**, 3345-3348.

122. M. J. Frisch, G. W. Trucks, H. B. Schlegel, G. E. Scuseria, M. A. Robb, J. R. Cheeseman, G. Scalmani, V. Barone, G. A. Petersson, H. Nakatsuji, X. Li, M. Caricato, A. V. Marenich, J. Bloino, B. G. Janesko, R. Gomperts, B. Mennucci, H. P. Hratchian, J. V. Ortiz, A. F. Izmaylov, J. L. Sonnenberg, Williams, F. Ding, F. Lipparini, F. Egidi, J. Goings, B. Peng, A. Petrone, T. Henderson, D. Ranasinghe, V. G. Zakrzewski, J. Gao, N. Rega, G. Zheng, W. Liang, M. Hada, M. Ehara, K. Toyota, R. Fukuda, J. Hasegawa, M. Ishida, T. Nakajima, Y. Honda, O. Kitao, H. Nakai, T. Vreven, K. Throssell, J. A. Montgomery Jr., J. E. Peralta, F. Ogliaro, M. J. Bearpark, J. J. Heyd, E. N. Brothers, K. N. Kudin, V. N. Staroverov, T. A. Keith, R. Kobayashi, J. Normand, K. Raghavachari, A. P. Rendell, J. C. Burant, S. S. Iyengar, J. Tomasi, M. Cossi, J. M. Millam, M. Klene, C. Adamo, R. Cammi, J. W. Ochterski, R. L. Martin, K. Morokuma, O. Farkas, J. B. Foresman and D. J. Fox, *Gaussian 09*, *Revision A.02*, Gaussian Inc., Wallingford CT, 2016.

123. S. Grimme, *WIREs Comput. Mol. Sci.*, 2011, **1**, 211-228.

124. M. D. Hanwell, D. E. Curtis, D. C. Lonie, T. Vandermeersch, E. Zurek and G. R. Hutchison, *J. Cheminf.*, 2012, **4**, 17.

125. G. A. Zhurko, *ChemCraft v1.8 (build 682)*, www.chemcraftprog.com.

8. APPENDIX

8.1 Computational data

Table A1. Thermodynamic data for **1** – **21**.

Table A2. Thermodynamic data for association energy calculations for systems **1** and **2** – **21**.

Table A3. Thermodynamic data for hydrogen activation energies for systems **1** and **2** – **21**.

Table A1. Thermodynamic data for **1** – **21**.

System	E (Ha)	H (Ha)	G (Ha)	G_{BB} (Ha)	G_{corr} (Ha)	G_{corr} (kcal/mol)
1	-6095.0	-6094.6	-6094.7	-6100.6	-6100.3	-3828015.5
2	-814.2	-813.8	-813.8	-814.8	-814.5	-511096.8
3	-1388.8	-1388.2	-1388.3	-1390.0	-1389.6	-871972.6
4	-1035.4	-1035.1	-1035.1	-1036.3	-1036.0	-650113.9
5	-1495.8	-1495.3	-1495.4	-1497.2	-1496.8	-939253.8
6	-976.5	-976.1	-976.1	-977.3	-977.0	-613063.8
7	-1531.0	-1530.7	-1530.8	-1532.5	-1532.3	-961530.9
8	-1260.1	-1259.6	-1259.6	-1261.3	-1260.8	-791172.5
9	-1977.7	-1976.7	-1976.9	-1979.7	-1978.8	-1241725.9
10	-887.9	-887.5	-887.6	-888.6	-888.3	-557441.2
11	-1153.2	-1152.8	-1152.9	-1154.2	-1153.9	-724071.1

12	-2522.3	-2522.1	-2522.2	-2524.9	-2524.8	-1584363.5
13	-2026.6	-2026.4	-2026.5	-2028.7	-2028.6	-1272946.8
14	-365.8	-365.6	-365.7	-366.2	-366.1	-229713.3
15	-344.9	-344.7	-344.8	-345.3	-345.2	-216585.2
16	-326.5	-326.4	-326.4	-326.9	-326.8	-205060.3
17	-408.7	-408.4	-408.4	-409.1	-408.9	-256577.9
18	-444.3	-444.1	-444.1	-444.8	-444.6	-278994.5
19	-328.9	-328.7	-328.7	-329.3	-329.1	-206522.2
20	-2133.6	-2132.8	-2132.9	-2135.9	-2135.2	-1339887.8
21	-381.8	-381.6	-381.7	-382.2	-382.1	-239772.2

Table A2. Thermodynamic data for association energy calculations for systems **1** and **2** – **21**.

System	E (Ha)	H (Ha)	G (Ha)	G_{BB} (Ha)	G_{corr} (Ha)	G_{corr} (kcal/mol)	E_{rel} (kcal/mol)
1 + 2	-6909.2	-6908.4	-6908.6	-6915.4	-6914.8	-4339113.3	-1.0
1 + 3	-7483.8	-7482.9	-7483.1	-7490.6	-7489.9	-4699985.7	2.3
1 + 4	-7130.4	-7129.8	-7129.9	-7136.9	-7136.4	-4478144.1	-14.8
1 + 5	-7590.9	-7590.0	-7590.2	-7597.8	-7597.1	-4767279.5	-10.3
1 + 6	-7071.5	-7070.7	-7070.9	-7077.9	-7077.3	-4441075.0	4.2
1 + 7	-7626.0	-7625.4	-7625.6	-7633.1	-7632.6	-4789543.8	2.5
1 + 8	-7355.2	-7354.3	-7354.4	-7361.9	-7361.2	-4619208.6	-20.7
1 + 9	-8072.8	-8071.4	-8071.7	-8080.3	-8079.2	-5069766.6	-25.3
1 + 10	-6982.9	-6982.2	-6982.4	-6989.2	-6988.7	-4385451.8	4.8
1 + 11	-7248.2	-7247.4	-7247.6	-7254.8	-7254.2	-4552078.7	7.9
1 + 12	-8617.3	-8616.7	-8616.9	-8625.5	-8625.2	-5412370.9	8.1
1 + 13	-8120.8	-8121.1	-8121.2	-8129.3	-8129.7	-5101482.2	-5.2
1 + 14	-6460.8	-6460.2	-6460.4	-6466.8	-6466.4	-4057727.1	1.6
1 + 15	-6440.0	-6439.4	-6439.5	-6445.9	-6445.5	-4044611.6	-10.9
1 + 16	-6421.5	-6421.0	-6421.2	-6427.5	-6427.1	-4033074.5	1.2
1 + 17	-6503.7	-6503.0	-6503.2	-6509.7	-6509.2	-4084587.5	5.8
1 + 18	-6539.3	-6538.7	-6538.8	-6545.4	-6544.9	-4107005.4	4.6
1 + 19	-6424.0	-6423.4	-6423.5	-6429.9	-6429.5	-4034551.5	-13.9
1 + 20	-8228.7	-8227.5	-8227.7	-8236.6	-8235.6	-5167907.5	-4.2
1 + 21	-6476.9	-6476.3	-6476.5	-6482.9	-6482.5	-4067813.2	-25.5

Table A3. Thermodynamic data for hydrogen activation energies for systems **1** and **2** – **21**.

System	E (Ha)	H (Ha)	G (Ha)	G_{BB} (Ha)	G_{corr} (Ha)	G_{corr} (kcal/mol)	E_{rel} (kcal/mol)
1 + 2	-814.5	-814.1	-814.2	-815.2	-814.9	-511339.5	41.3
1 + 3	-1389.2	-1388.6	-1388.7	-1390.4	-1390.0	-872218.7	34.5
1 + 4	-1035.8	-1035.4	-1035.5	-1036.6	-1036.4	-650345.4	66.2
1 + 5	-1496.2	-1495.7	-1495.8	-1497.5	-1497.2	-939490.5	56.5
1 + 6	-976.9	-976.5	-976.5	-977.7	-977.4	-613312.9	29.6
1 + 7	-1260.5	-1260.0	-1260.0	-1261.7	-1261.2	-791418.7	57.4
1 + 8	-1978.1	-1977.1	-1977.3	-1980.1	-1979.2	-1241966.9	67.2
1 + 9	-888.3	-887.9	-888.0	-889.0	-888.7	-557681.3	38.0
1 + 10	-1153.6	-1153.2	-1153.2	-1154.6	-1154.3	-724306.0	40.1
1 + 11	-1531.4	-1531.1	-1531.2	-1532.8	-1532.7	-961752.7	58.6
1 + 12	-2027.0	-2026.7	-2026.8	-2029.1	-2028.9	-1273158.9	68.9
1 + 13	-2522.6	-2522.4	-2522.5	-2525.3	-2525.7	-1584563.4	75.0
1 + 14	-366.2	-366.0	-366.0	-366.6	-366.4	-229945.8	48.8
1 + 15	-345.3	-345.1	-345.1	-345.7	-345.5	-216814.4	64.6
1 + 16	-326.9	-326.7	-326.8	-327.3	-327.1	-205287.1	54.9
1 + 17	-409.0	-408.7	-408.8	-409.5	-409.3	-256811.4	43.6
1 + 18	-444.7	-444.4	-444.5	-445.2	-445.0	-279219.8	53.1
1 + 19	-329.3	-329.1	-329.1	-329.7	-329.5	-206754.8	64.2
1 + 20	-2134.0	-2133.1	-2133.3	-2136.3	-2135.6	-1340109.4	65.6
1 + 21	-382.2	-382.0	-382.1	-382.6	-382.5	-240010.3	70.4

8.2 Experimental data

Figure A1 ^{1}H NMR (400 MHz, $CDCl_3$) spectrum of **22**

Figure A2 ^{1}H NMR (400 MHz, $CDCl_3$) spectrum of **23**

Figure A3 ^{1}H NMR (400 MHz, $CDCl_3$) spectrum of **1** using $BF_3.OEt_2$ as boron source

Figure A4 ^{11}B $\{^{1}H\}$ NMR (128 MHz, $CDCl_3$) spectrum of **1** using $BF_3.OEt_2$ as boron source

Figure A5 ^{19}F $\{^{1}H\}$ NMR (377 MHz, $CDCl_3$) spectrum of **1** using $BF_3.OEt_2$ as boron source

Figure A6 ^{1}H NMR (400 MHz, $CDCl_3$) spectrum of **1** post extraction (1:1 hex/tol system)

Figure A7 ASI-MS (negative) spectrum of **1** using $BF_3.OEt_2$ as boron source

Figure A8 ^{1}H NMR (400 MHz, $CDCl_3$) spectrum of **1** using BCl_3 in heptane as boron source

Figure A9 ^{11}B $\{^{1}H\}$ NMR (128 MHz, $CDCl_3$) spectrum of **1** using BCl_3 in heptane as boron source

Figure A10 ^{19}F $\{^{1}H\}$ NMR (377 MHz, $CDCl_3$) spectrum of **1** using BCl_3 in heptane as boron source

Figure A11 ^{1}H NMR (400 MHz, $CDCl_3$) spectrum of **1** using BCl_3 in heptane as boron source

Figure A12 ^{11}B $\{^{1}H\}$ NMR (128 MHz, $CDCl_3$) spectrum of **1** using BCl_3 in heptane as boron source

Figure A13 ^{19}F $\{^{1}H\}$ NMR (377 MHz, $CDCl_3$) spectrum of **1** using BCl_3 in heptane as boron source

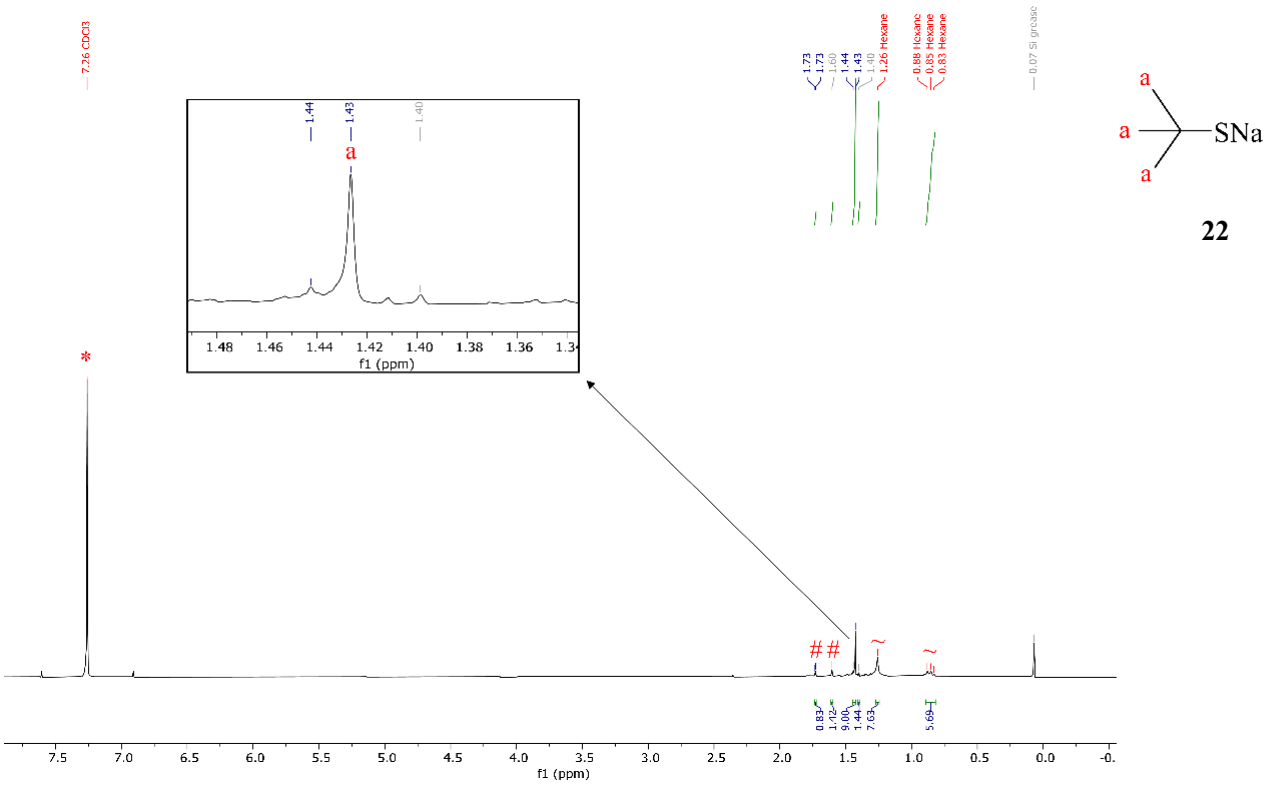

Figure A1. ^{1}H NMR (400 MHz, $CDCl_3$) spectrum of **22**. Inset shows zoomed in region between δ 1.40 – 1.44 ppm. * denotes solvent peak, ~ is residual solvent and # represents impurities.

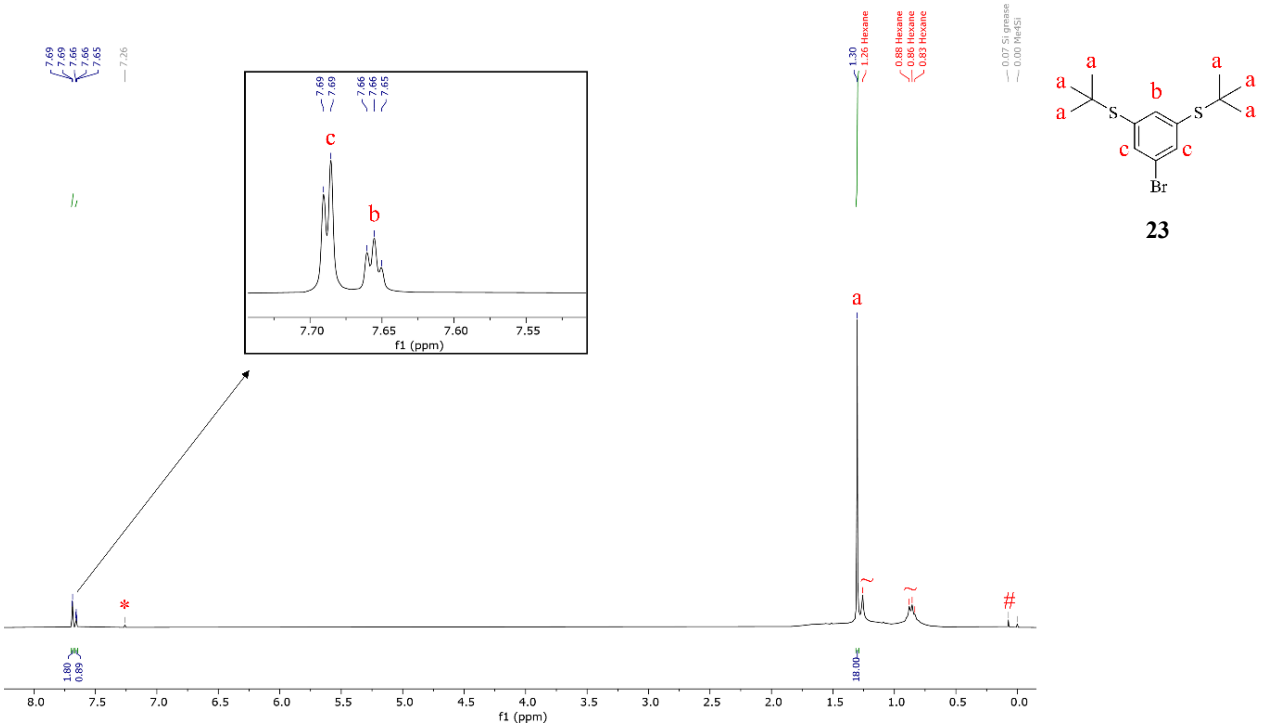

Figure A2. ^{1}H NMR (400 MHz, $CDCl_3$) spectrum of **23**. Inset shows zoomed in region between δ 7.65 – 7.69 ppm. * denotes deuterated solvent, ~ is residual hexane and # represents Si grease/TMS.

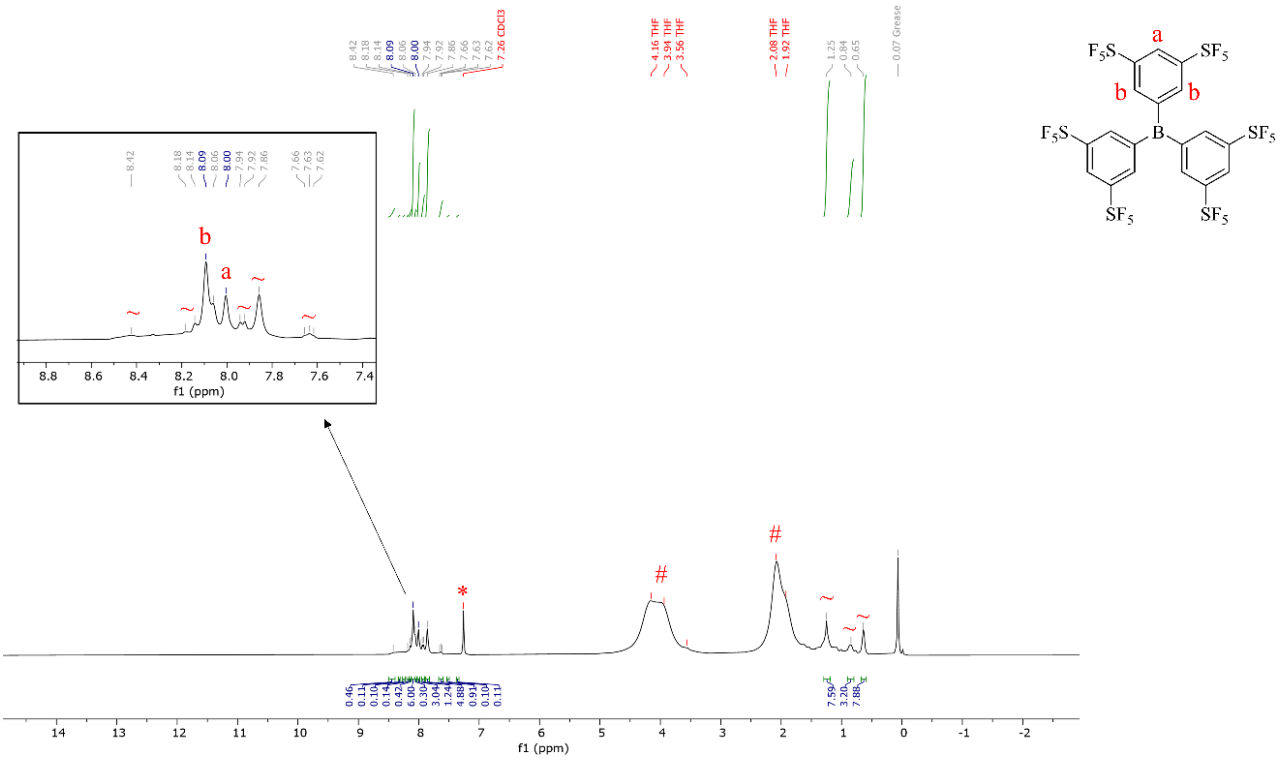

Figure A3. ^{1}H NMR (400 MHz, $CDCl_3$) spectrum of **1** using $BF_3.OEt_2$ as boron source. Inset shows zoomed in region between δ 7.62 – 8.42 ppm. * denotes deuterated solvent, ~ represents impurities and # is residual THF.

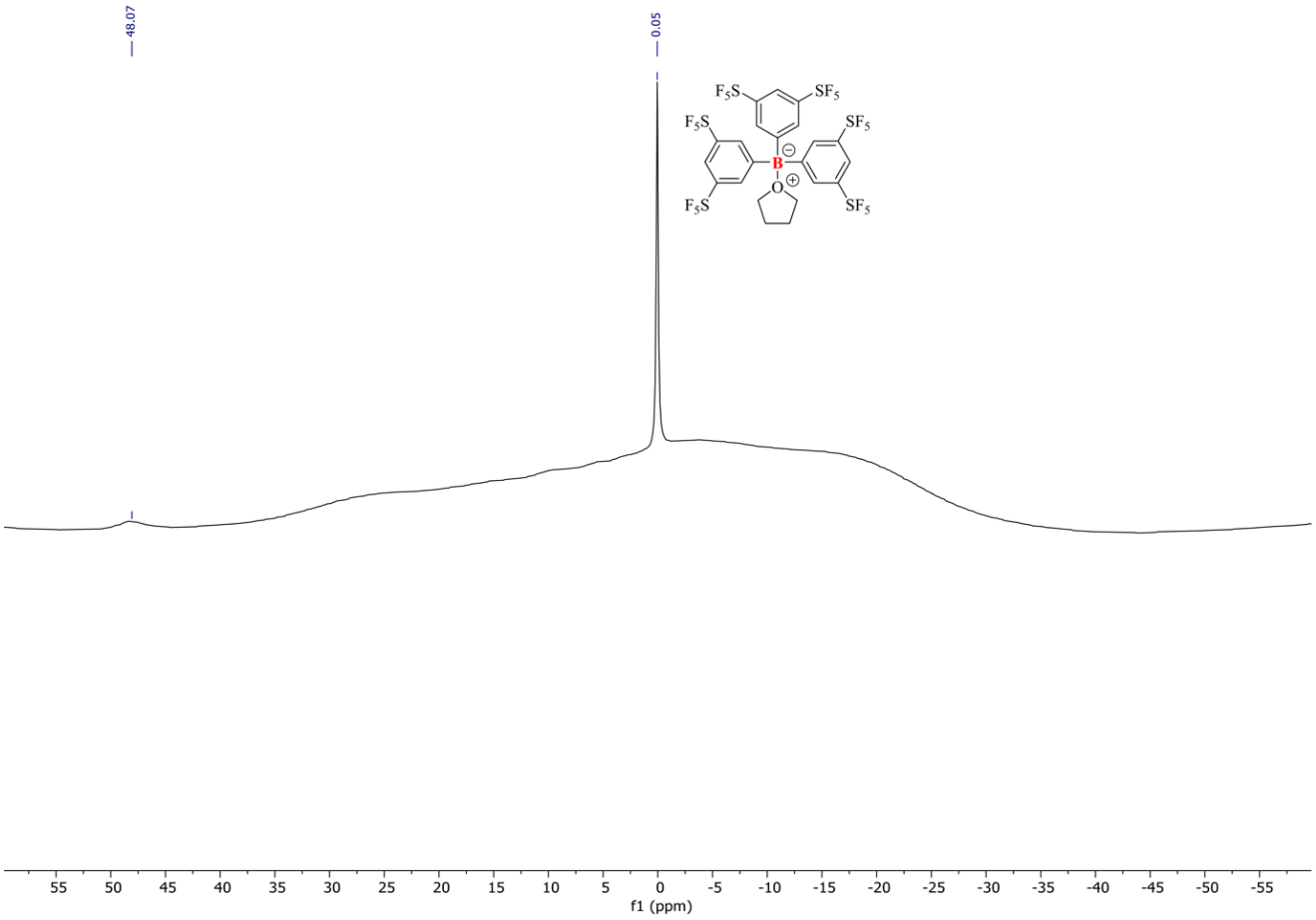

Figure A4. ^{11}B $\{^{1}H\}$ NMR (128 MHz, $CDCl_3$) spectrum of **1** using $BF_3.OEt_2$ as boron source.

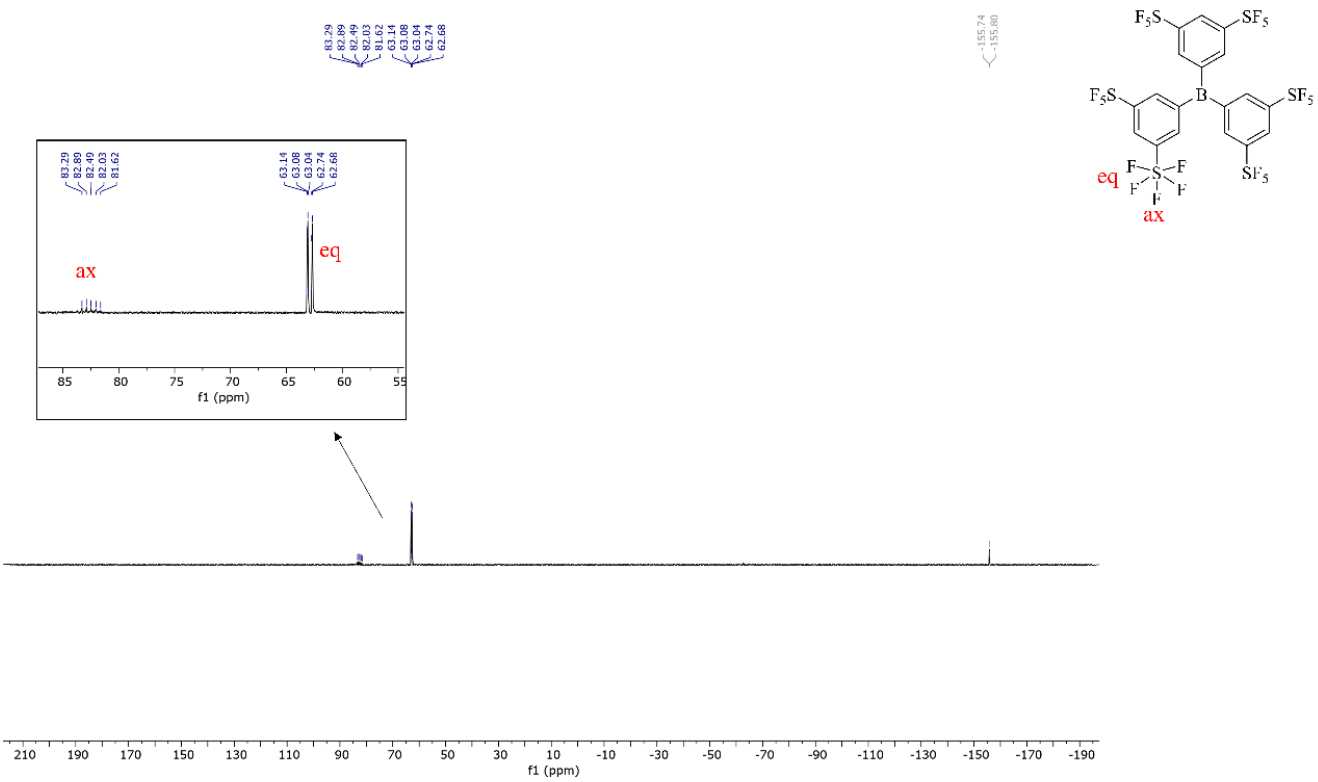

Figure A5. ^{19}F $\{^{1}H\}$ NMR (377 MHz, $CDCl_3$) spectrum of **1** using $BF_3.OEt_2$ as boron source. Inset shows zoomed in region between δ 62.7 – 83.3 ppm. Impurities are highlighted in grey.

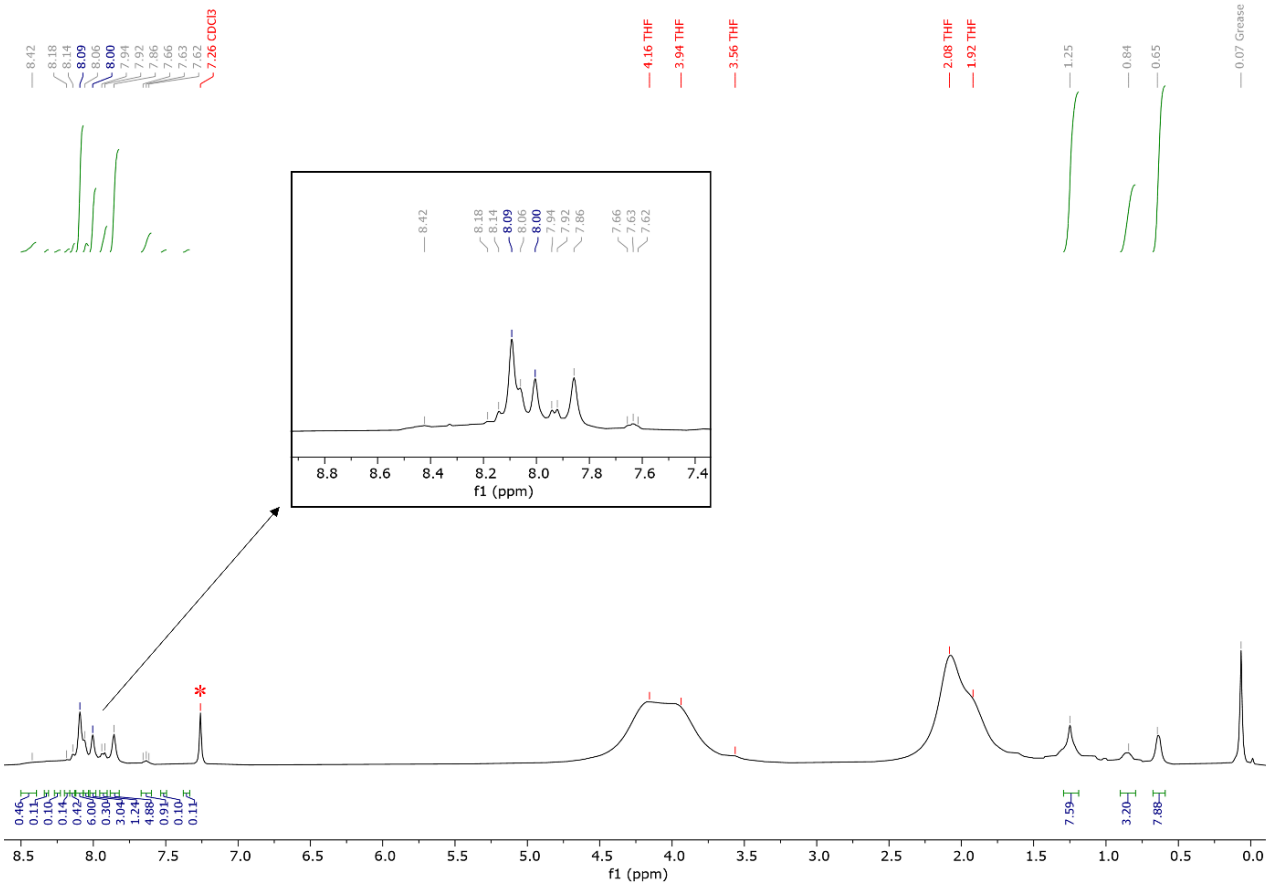

Figure A6. ^{1}H NMR (400 MHz, $CDCl_3$) spectrum of **1** after extraction using 1:1 hexane/toluene solvent system. Inset shows zoomed in region between δ 7.62 – 8.42 ppm. Impurities are highlighted in grey, residual solvent is highlighted in red. * denotes deuterated solvent.

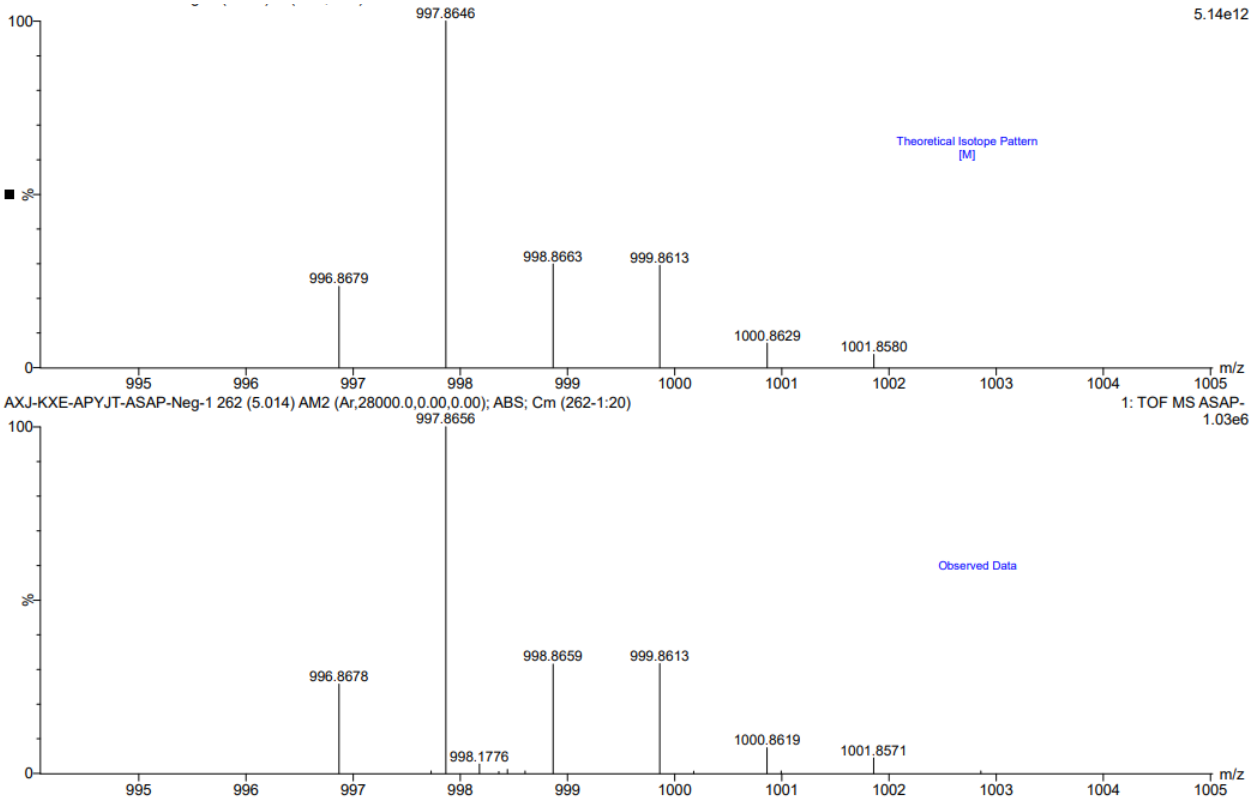

Figure A7. ASI-MS (negative) spectrum of **1** using $BF_3.OEt_2$ as boron source.

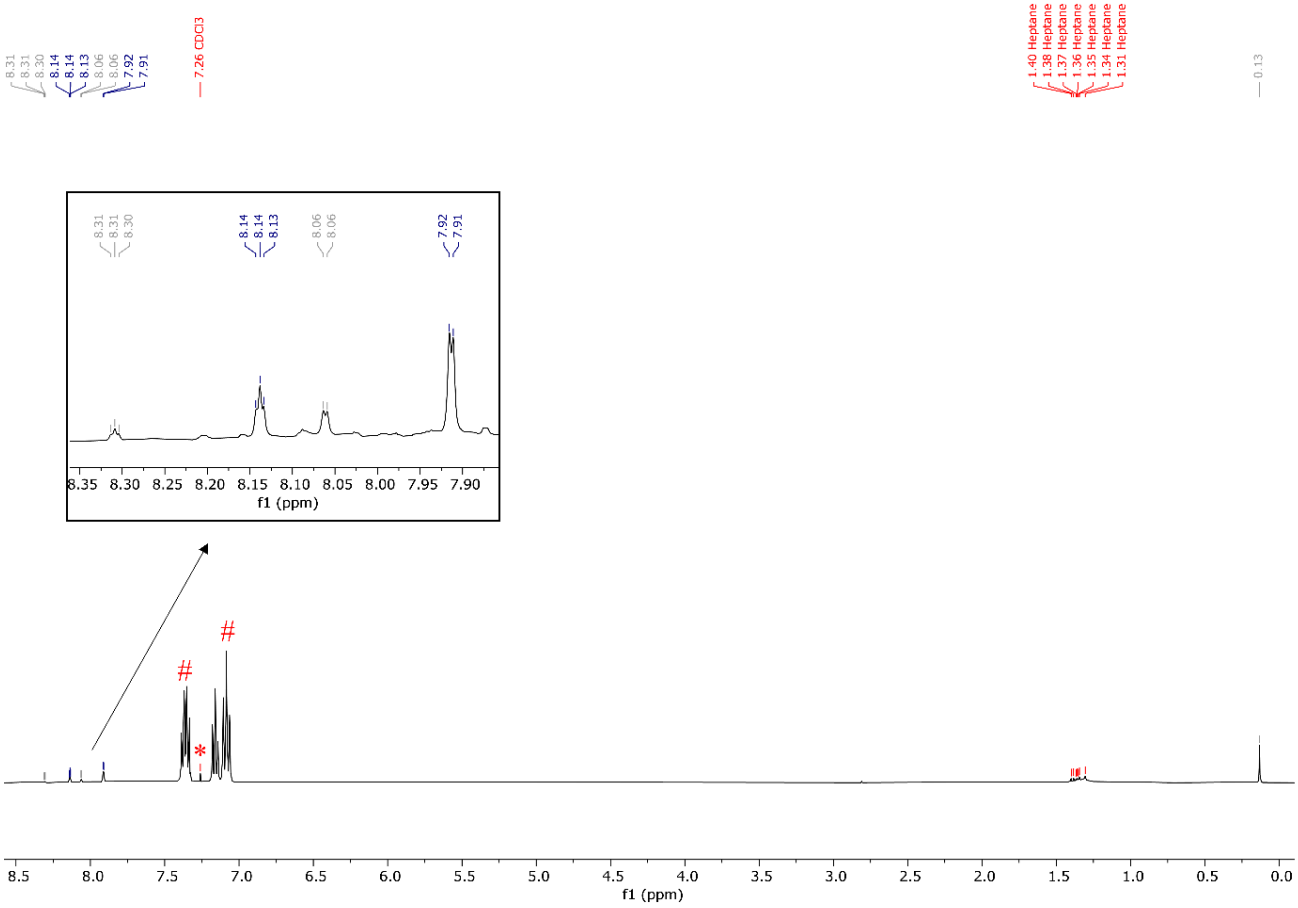

Figure A8. ^{1}H NMR (400 MHz, $CDCl_3$) spectrum of crude mixture of **1** using BCl_3 in heptane as boron source. Inset shows zoomed in region between δ 7.91 – 8.31 ppm. Impurities are highlighted in grey, residual solvent is highlighted in red. # denotes fluorobenzene standard used and * denotes deuterated solvent.

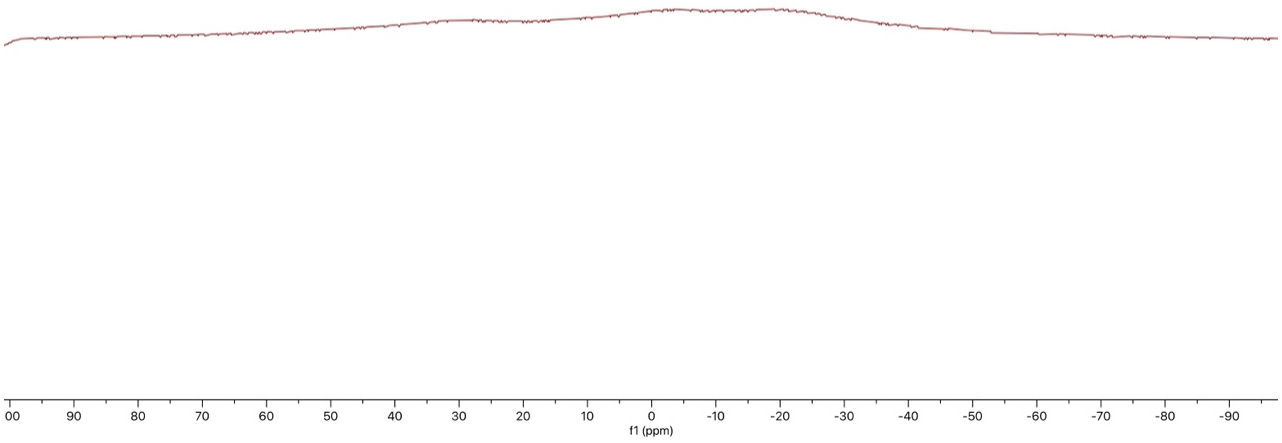

Figure A9. ^{11}B $\{^{1}H\}$ NMR (128 MHz, $CDCl_3$) spectrum of **1** using BCl_3 in heptane as boron source. Signal:noise ratio too great to see any resonances.

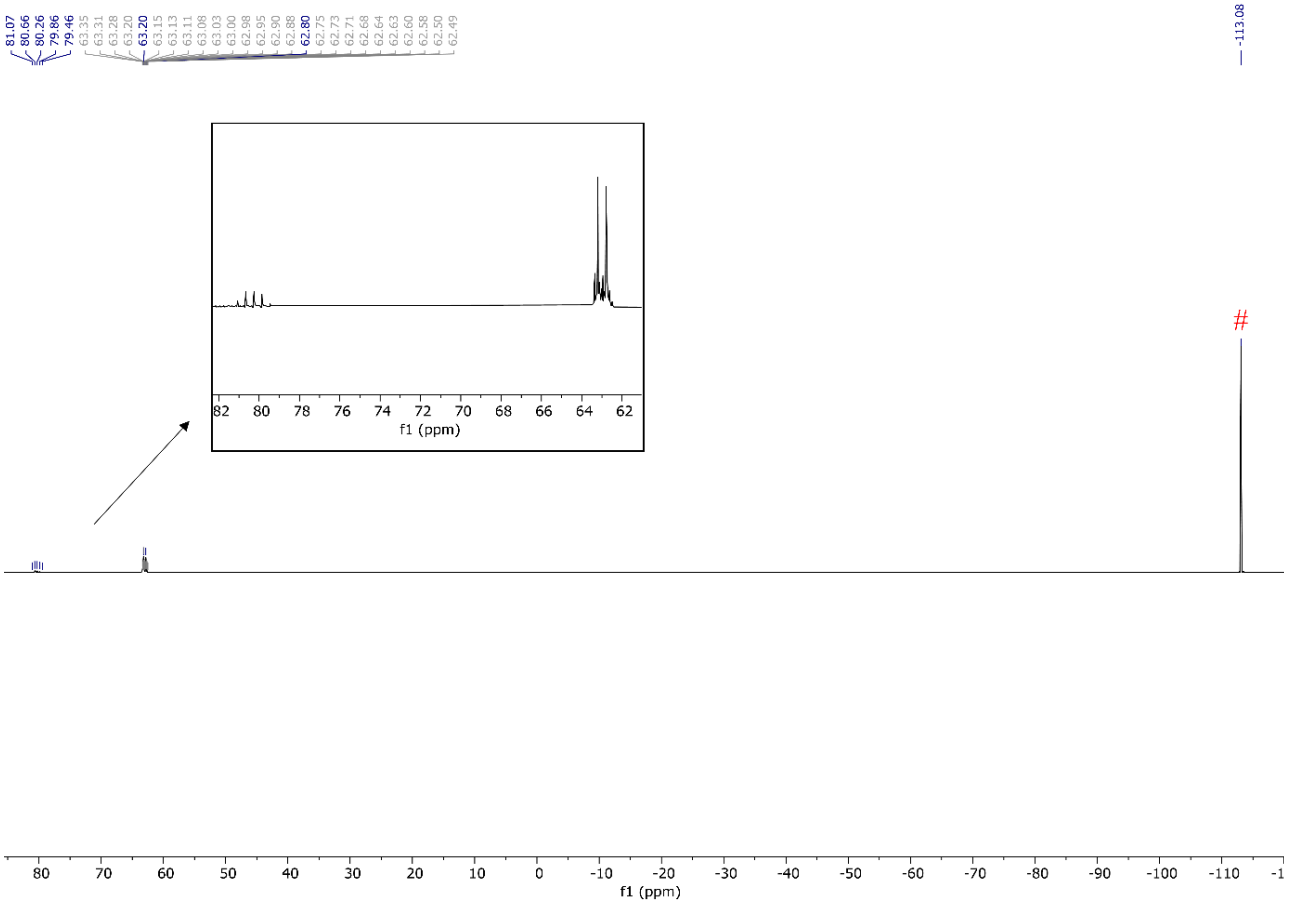

Figure A10. ^{19}F $\{^{1}H\}$ NMR (377 MHz, $CDCl_3$) spectrum of **1** using BCl_3 in heptane as boron source. Inset shows zoomed in region between δ 62.4 – 81.1 ppm. Impurities are highlighted in grey, residual solvent is highlighted in red. # denotes fluorobenzene standard used.

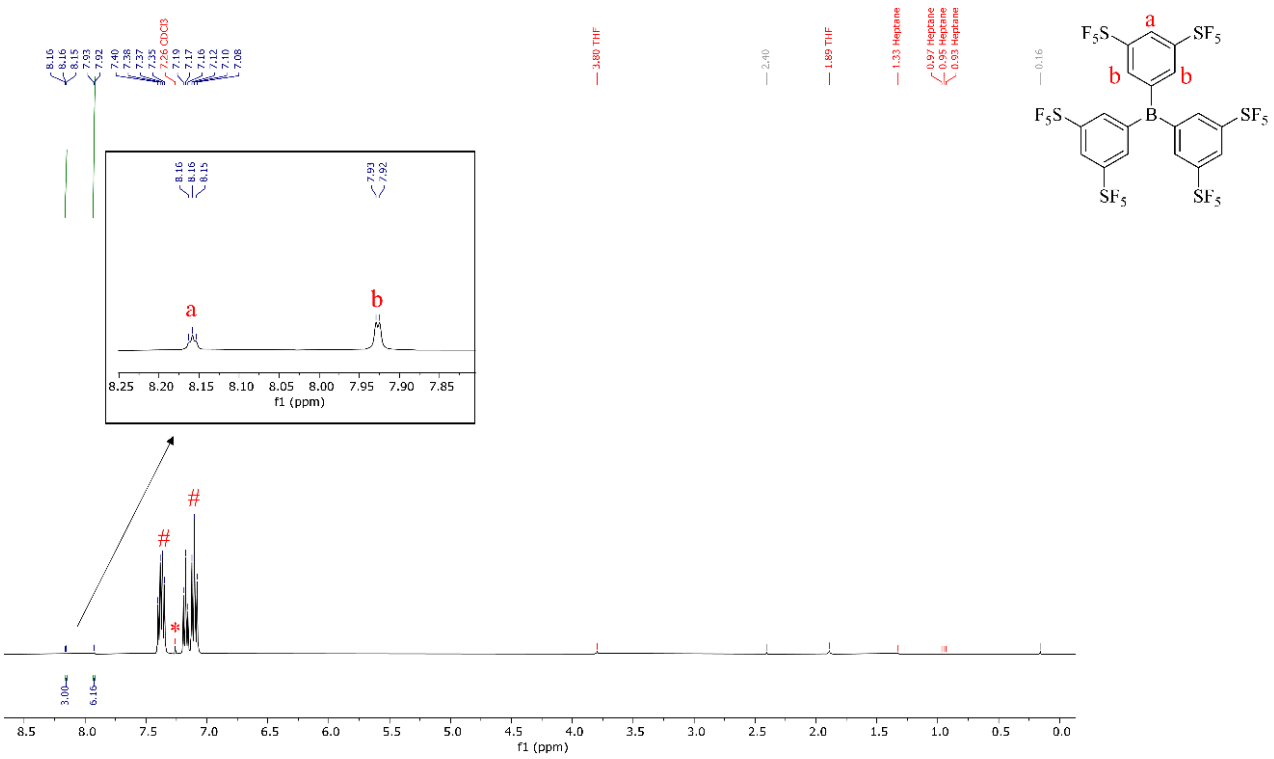

Figure A11. ^{1}H NMR (400 MHz, $CDCl_3$) spectrum of **1** using BCl_3 in heptane as boron source (post extraction). Inset shows zoomed in region between δ 7.92 – 8.16 ppm. Impurities are highlighted in grey. # denotes fluorobenzene standard used and * denotes deuterated solvent.

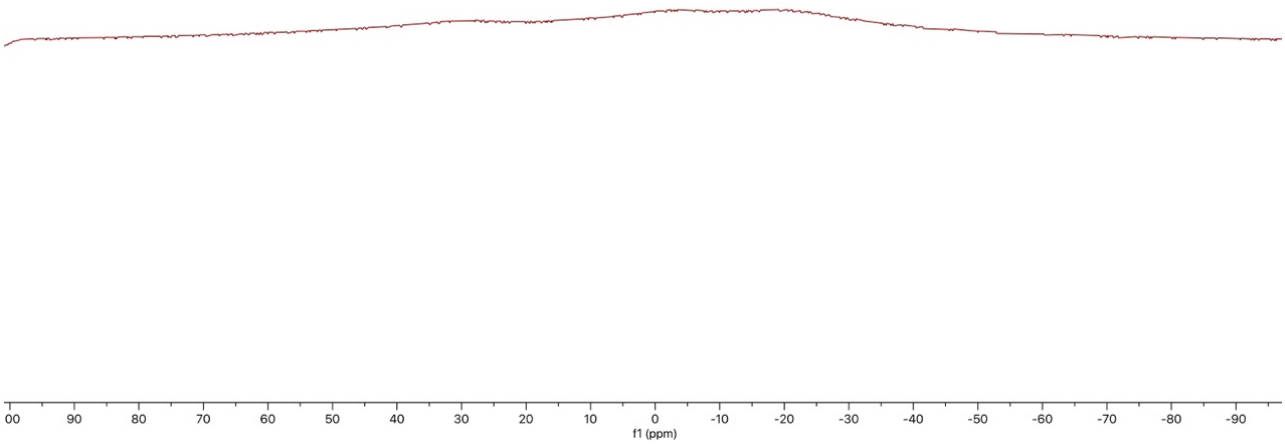

Figure A12. ^{11}B $\{^{1}H\}$ NMR (128 MHz, $CDCl_3$) spectrum of **1** using BCl_3 in heptane as boron source (post extraction). Signal:noise too great to see resonances clearly.

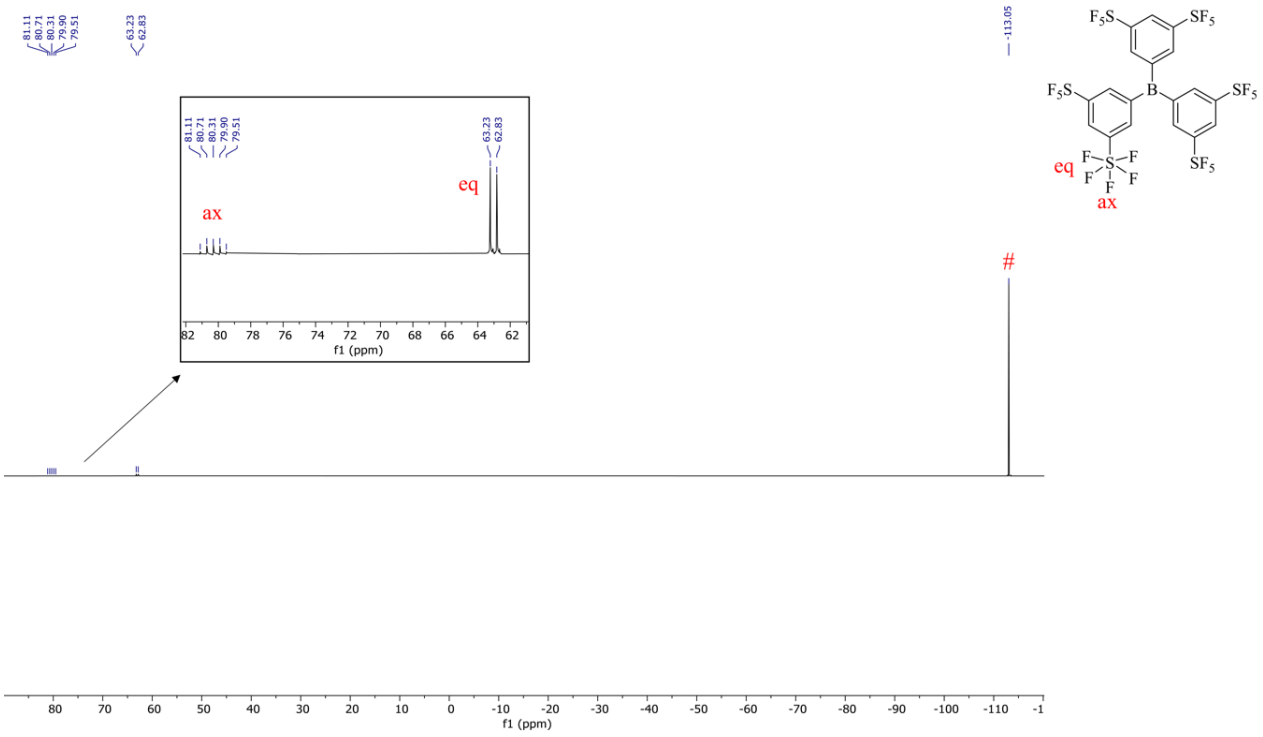

Figure A13. ^{19}F $\{^{1}H\}$ NMR (377 MHz, $CDCl_3$) spectrum of **1** using BCl_3 in heptane as boron source (post extraction). Inset shows zoomed in region between δ 62.8 – 81.1 ppm. # denotes fluorobenzene standard used.